CONSOLIDATION CHARACTERISTICS OF SOFT SEDIMENTS BY SEEPAGE INDUCED CONSOLIDATION TEST

By

MASOUD JANBAZ

A dissertation submitted to the

Graduate School-New Brunswick

Rutgers, the State University of New Jersey

In partial fulfillment of the requirements

For the degree of

Doctor of Philosophy

Graduate Program in Civil and Environmental Engineering

Written under the direction of

Professor Ali Maher

And approved by

_____

_____

_____

_____

New Brunswick, New Jersey

October, 2016

ABSTRACT OF THE DISSERATION

Consolidation Characteristics of Soft Sediments by Seepage Induced Consolidation Test

MASOUD JANBAZ

Dissertation Director:

Ali Maher

The thesis presented herein outlines the seepage-induced consolidation test (SICT) results of soft sediments dredged from Newark bay, NJ, for the determination of consolidation characteristics. The Seepage induced consolidation testing device was constructed based on the original version (SICT) presented by Dr. Prof. Dobroslav Znidarcic at the University of Colorado Boulder (CU).

The author traveled to CU and consulted Dr. Znidarcic for recommendations on the device design and construction, preferred manufacturers, and sample testing procedures. A SICT device was then designed and constructed for Rutgers University in New Brunswick, with some modifications like deadweight loading system for easier troubleshooting. The SICT results for kaolinite clay, performed by Dr. Znidarcic at the CU laboratory, were compared with the author's test results from the Rutgers Soil and Soft Sediment Laboratory. The comparison served to assess the reliability and repeatability of the Rutgers University SICT device.

Following the collection of dredged sediment samples from the Newark bay area, five different clays were purchased and their consolidation characteristics were tested. In

addition, the tests sought to determine a correlation between sediment index properties and consolidation model parameters. Index property determination is less time consuming and cumbersome than consolidation testing under seepage force, which is more technical and can take up to two weeks for a single test. Therefore, there is inherent merit in gaining insight into consolidation behavior without running the seepage tests.

A total of sixteen tests were performed. Eleven tests were conducted on the Newark soft sediments, and the remaining five on the clay samples. The results have been partially published via the 15th Asian Regional Conference in Japan, the International Conference on Civil Engineering in Iran, and the Journal of Geotechnical Engineering. The consolidation model parameters were correlated with the samples' index properties and the resulting equations satisfactorily approximated the reality.

Contents

List of Figures

List of Tables

Chapter 1 Background & Problem Identification

1. Problem Identification:

The consolidation of soft to very soft sediments is a complex process because it does not readily follow the common one-dimensional model proposed by Terzaghi, whereby the coefficient of permeability and the coefficient of volume compressibility remain constant throughout the consolidation process. In most soft to very soft sediments, permeability and volume compressibility change with time during the consolidation process. The estimated settlement of such materials under stress differs significantly from those determined by the one-dimensional Terzaghi model. This change in consolidation characteristics is important for cases in which soft to very soft sediments are being considered for reclamation, beneficial use, and navigational harbor deepening projects.

In the Port of NY/NJ, which is the third largest port in the United States and a major freight and goods movement hub, more than approximately 4 million cubic yards of sediments have to be dredged annually for maintenance purposes. Many of the dredged sediments are soft to very soft silty clay, which require special considerations for handling and potential beneficial use or reclamation applications. For instance, many reclamation projects involve the hydraulic dredging of bottom sediments and the pumping of soil-water mixtures into diked ponds located near the shore. The importance of effective dredging techniques is manifested in the millions of dollars spent annually on the disposal of dredged materials. Soft, contaminated or uncontaminated sediments dredged from rivers and harbors pose an ever-increasing number of challenges to geotechnical engineering firms every year. In general, any soft, low-density material that is deposited hydraulically in confined retention ponds and left for some time to consolidate under its own weight can be challenging for reclamation purposes. Increasing environmental concerns, reductions in the number of available placement areas, and the delay for sediment preparation for reclamation to be initiated have created the need for maximum utilization of existing and planned containment areas. The accurate design of catchment ponds and dikes for the vast amount of dredge work can reduce its material footprint. However, this requires knowledge of the materials' consolidation characteristics. The

economics of the operation dictate that each catchment area be designed and used to its fullest potential; therefore, understanding the settlement-time, or consolidation, of the materials is a prerequisite for the design.

Soft to very soft sediment material can be defined as a wide range of low-density material, from fine sands to very fine-grained silt and clay, with a very high water content of saturated state or above. The pumping of soil slurries into diked areas results in the formation of landfills with very high initial void ratios, which must be allowed to settle down for some time. Due to the high void ratio and the evaporation of free water from the surface, significant settlement is expected to take place as time passes. Low material density causes self-weight settlement to play an important role in the sediment's consolidation. Since the consolidation process is very time consuming, it strongly influences the planning of reclamation projects, future landfill utilization, and vegetation. It is very important to precisely evaluate the time-settlement behavior and final density of the landfill in order to best estimate the useful life of the disposal area and the time required to achieve reclamation.

The actual capacity of the disposal area (design life), availability of the disposal area, required time for consolidation, seepage potential, and embankment stability for reclamation purposes are just some of the issues related to the disposal of soft sediments. It should be noted that one of the disadvantages of disposing the soft sediments with high water content into confined disposal facilities is to tie up huge amount of water, which is trapped inside of the sediments, which prevents land development for agricultural, residential, or commercial purposes for many years.

In practice, waste slurry with solid content on the order of 30-50% (comparatively equal to moisture content of 100-230%) is pumped into a containment area and then allowed to settle under its own weight. During this time, excess water either seeps downward into a porous layer underneath the pond or is decanted from the top. However, dredged slurries usually contain a significant fraction of clay. The presence of clay can result in large volume change in case of application of surcharge because of

roads, buildings or any type of other loads. In Figure 1.1 the typical schematic of an impoundment dike is presented.

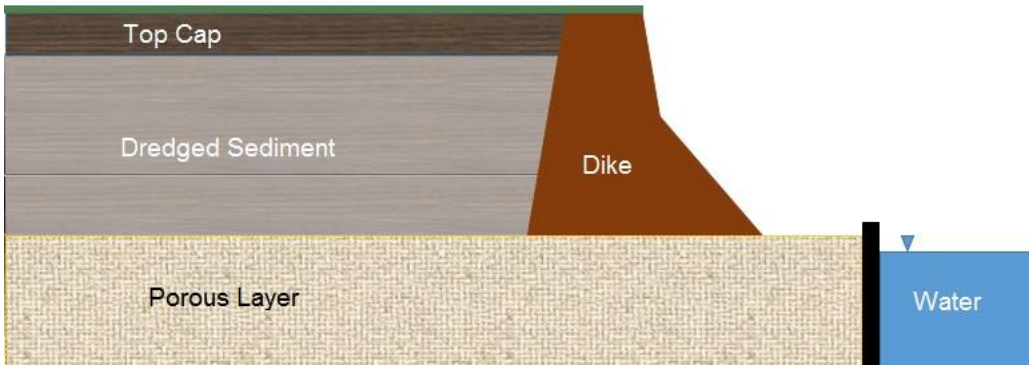

Figure 1.1. Schematic of impoundment dike

When diluted slurries are pumped into a containment area, soil particles generally settle by forming flocs. These flocs are formed as a result of physicochemical interactions between the particles and the water surrounding them. The flocs settle down to the bottom and compress underlying flocs, initiating settlement by increasing the effective stress between particles. Consolidation characteristics govern the subsequent behavior of the deposit. Since the specific gravity and buoyant weight of flocs are very small, self-weight consolidation will start from very low effective stresses (usually less than 0.1 kPa). Due to the very low effective stresses needed to compress the sample, and the requirement of specimens in the form of slurries, the conventional odometer test is not effective (initial stress is about 50 kPa). Due to the loose nature of the deposit, the resulting vertical deformations attributed to self-weight and consolidation are usually beyond the range that can be handled by classical small-strain Terzaghi consolidation theory. Instead, it is essential that finite strain nonlinear consolidation theory be developed.

A decrease in the volume of dredged fill may result from four different processes: sedimentation (self-weight effect), consolidation, secondary compression (creep), and desiccation. The processes of sedimentation and consolidation may exist at different stages of development throughout the deposit at any given time, and the deposit is

heterogeneous in nature in the vertical direction. However, for mathematical modeling purposes, it is often assumed that, at any point in time and at any point in the deposit, sedimentation is finished and consolidation is instantaneously initiated.

In fact, consolidation and desiccation are two of the most important natural processes affecting the long-term height of dredged material. These two processes can induce large axial strains in fine-grained dredged material, sometimes on the order of 50% of the total settlement (Cargill, 1981).

In order to accurately design dredged material containment areas for service life, the increase in storage capacity resulting from the settlement of confined dredged material must be accounted for. Many efforts have been made to find the most precise solutions for accurately predicting the consolidation characteristics and final elevations of slurries in containment areas. Predictions of the consolidation rate and final material height dictate the ultimate storage capacity and the time required to achieve it. Overall slurry retention consists of two different processes: the sedimentation of fine particles (self-weight consolidation) and the consolidation of the sediment layer by both seepage force (water moving downward through the sediments) and surcharge load (capping the containment area).

Sedimentation in this context refers to the downward movement of soil particles due to their own weight, i.e. gravity force, until the point at which they come to a halt and form a layer of soil. The speed of this movement varies based on the size and specific gravity of the particles, the viscosity of the fluid, and the operating temperature. Since the speed of sedimentation is typically low due to the low specific gravity of particles, the rate of settlement at this stage is also very low. As a result, the sedimentation process can take a significant amount of time (10-100 years) to produce any significant change in the degree of consolidation, and is dependent on material characteristics and containment area's depth. Once deposition has taken place, soil particles come into contact with one other, creating effective stresses between particles. At this point of the process, pore pressures are generated and consolidation begins. Self-weight consolidation is driven by

the buoyant weights of particles. During this stage, very small amounts of pore pressures develop and consolidation is governed by the low density of the sediment. The subsequent application of surcharge increases the contact stresses between particles, resulting in a decrease in void spaces. Settlement occurs as the void spaces are reduced by the application of surcharge load atop the sediment. Overall settlement thus includes settlement due to sedimentation, self-weight consolidation, and consolidation under surcharge load.

In order to characterize the consolidation behavior of sediments, the following one-dimensional finite strain consolidation theories have been published:

1. The conventional theory of Terzaghi (1923), in which the permeability and compressibility of the soil skeleton are assumed to be constant throughout the consolidation (Znidarcic, 1982).

2. Mikasa (1963, 1965) theory and Gibson et al. (1967), which were developed primarily for rapidly-deposited dredged fills but still apply for slow sedimentation. Both theories cast in terms of logarithmic constitutive relationships (Pane, 1981).

3. Koppula (1970) and Koppula and Morgenstern (1982) theory, based on Gibson's theory, which uses excess pore-water pressure as the dependent variable. In this theory, the constitutive relationships are based on power functions.

4. The works of Raymond (1969), Berry (1972) and Mesri (1974), which implement the finite strain theory for weightless material. In this case, the constitutive relationships are based on the log-linear function.

5. The work of Monte and Krizek (1976), based on the Gibson's theory, which introduces the "fluid limit" as the void ratio above which the "soil" behaves as a heavy fluid and the effective stress principle does not apply. This theory was initially developed to account for the sedimentation processes of soil formation.

It should be noted that the general approach of theories following the Gibson, England and Hussey theory remains constant, thus all of the above finite strain theories can be considered special cases of this theory (Schiffman, 1980).

A variety of analytical and numerical solutions based upon the monotonic consolidation of normally consolidated, homogeneous layers have been developed. The works by Somogyi (1980, 1981), Pane (1981), and Znidarcic (1982) make additional assumptions regarding a particular relationship between parameters, initial and boundary conditions, and applications. These assumptions are intended to eliminate any restricting conditions and form a more generalized consolidation theory.

2. Objective and Scope of Research

The primary objectives of this research are:

- To accurately characterize the consolidation behavior of soft to very soft sediments dredged from the NY/NJ harbor system, with the goal of assisting geotechnical engineers in developing better designs for navigational deepening/reclamation projects and potential beneficial use applications.
- To design and build a new consolidometer, capable of inducing low amount of stresses based on seepage force, in order to investigate the consolidation process of low density, high water content soft sediments and allow for changes in permeability and volume compressibility.
- To develop an empirical correlation between index properties and sediment consolidation characteristics.
- To develop site-specific constitutive relationships (void ratio-permeability and void ratio-effective stress relationships) for the NY/NJ harbor system using the data obtained from the refined consolidation. Such relationships can assist geotechnical engineers in the handling of navigational dredged materials for both disposal and beneficial use applications.

The objectives of this research are met through the construction of the seepage induced consolidation tester in the Richard N. Weeks soil and sediment management laboratory, the sampling of sediment from dredging barges in Newark Bay, the testing of index properties and consolidation, and the acquisition of the required relationships.

3. Research Approach

A dual experimental/analytical program is proposed to achieve the objectives of the research. The primary purpose of the experimental program is to design and build a new consolidation device, which takes into account the unique permeability and compressibility characteristics of soft to very soft sediments during the consolidating process. The material to be tested will be sampled from the NY/NJ harbor (Newark Bay) and characterized according to geotechnical index properties. The analytical phase of the study uses the data from the experimental program to build constitutive relationships between void ratio and permeability and effective stress, respectively. Such site-specific relationships can aid geotechnical engineers in sediment disposal, reclamation and beneficial use applications and also help plan recurring navigational dredging programs.

4. Outline of Thesis

The thesis is comprised of five chapters. A brief description of each chapter is provided below.

The remainder of the current chapter provides general information about Newark Bay. Resource-based physical properties and a brief introduction to consolidation theories are presented.

Chapter 2 presents detailed information regarding the principles, procedures, and development of the governing equation.

Chapter 3 is devoted to the literature review of the best consolidation theory for this application. It focuses on the seepage-induced consolidation concept and its model, which is used throughout this thesis.

Chapter 4 discusses the construction of the apparatus and provides a detailed description of the device, the results of the index properties and seepage-induced consolidation tests. The results are discussed thoroughly, then the thesis is concluded by a summary of major outcomes and recommendations for future research.

5. Newark Bay

In New Jersey, three management regions geographically divide the general physical properties of the sediment into estuarine, coastal, and riverine sediments, respectively. In general, estuarine sediments are comprised of fine-grained silts and clays that are typically found in the Harbor region; coastal sediments are primarily sand from the Shore region; and riverine sediments are a combination of all grain sizes, sorted by hydrologic condition, and found in the Delaware region (see Figure 1.2).

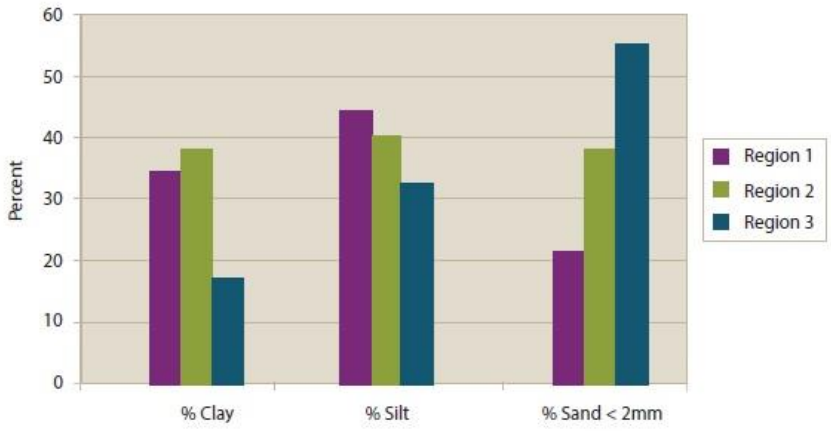

Figure 1.2. Soil type in geographical regions in New Jersey (Region 1: Harbor region, Region 2: Shore region, and Region 3: Delaware region) (Maher et al., 2013)

Understanding the geotechnical behavior of sediment requires the identification of key geotechnical traits, including the material's index properties, permeability, and strength. The geotechnical experimental plan can change based on the type of application and project specifications.

In general, a wide variety of sediment types are dredged from the Newark Bay every year due to construction or navigation channel maintenance. A general overview of the

material includes fine-grained silt, pre-industrial red clay, glacial till, and sand (Maher et al, 2013).

Dredged material from the maintenance of waterways and navigation channels in New Jersey harbor tends to be highly organic mud with a very high water content, making it very difficult to handle. In order to use it in more practical and beneficial ways, such as for reclamation purposes, consolidation of this material is of interest. However, due to the low density and high water content of the material, there is a need to develop a procedure and apparatus for the acquisition of time-settlement characteristics. Increasing the potential for utilization of the high volume (approximately two million cubic yards/year) of dredged sediments in beneficial use applications is a priority for maritime transportation planners. Examples of beneficial use include landfill caps, fill, and roadway embankments. Assessing the adequate placement capacity of dredged sediment is a crucial management decision. As a result, geotechnical data must be obtained and analyzed based on the type of beneficial application.

The general soil classification of Newark bay is high plasticity silt (MH) or organic silt (OH) depending on the organic content of the sample. Organic content can be as high as 10%, with the rest of the soil consisting of mostly silt and up to 20 percent of clayey material. The water content varies depending on the sampling method and location but ranges between 70 to 180 percent. Some of the physical properties of Newark Bay sediments are presented in Table 1.1 (Maher et al. 2013).

Table 1.1. Index properties of Newark bay silt sediment (Maher et al. 2013)

Location	USCS Classification	Sand (%)	Silt (%)	Clay (%)	Moisture Content (%)	LL-PL	Permeability (cm/Sec)
Newark Bay, Port Elizabeth	OH	19	72	9	480	94-54	3.8×10^{-8}
Newark Bay, Port Elizabeth	OH	22	70	8	175	88-52	3.8×10^{-8}
Newark Bay, Port Elizabeth	OH	14	80	6	146	100-64	3.8×10^{-8}
Newark Bay, Lower Channel	OH	40	50	2	70	54-30	5.5×10^{-8}
Newark Bay	CH	6.5	33	60.5	35	39-26	1×10^{-7}
Arthur Kill	OH	10	78	12	181	113-70	-
Lower Passaic	OH	4	74	22	144	108-60	2.9×10^{-8}

As can be seen from the table, the overall physical properties of the soft sediment in Newark Bay, center around organic silts with high water contents. Figure 1.3 shows the overall map of the bay. The high water content and organic type of the sediments indicate that the bay is comprised of mostly low-density sediment types prone to high compressibility and low hydraulic conductivity. It should be noted that there is not a definite definition for soft sediments, but that low density and high water content are typical characteristics of soft sediments.

On the other hand, simplifying assumptions in traditional consolidation theories may cause discrepancies in observations and calculations. This research aims to further investigate Newark Bay sediments' consolidation characteristics.

Figure 1.3. Newark bay map (Shrestha et al., 2014)

6. One-Dimensional Consolidation theories

The first theory predicting one-dimensional soil consolidation was published by Karl Terzaghi in 1924. This theory is one of the fundamental theories in soil mechanics due to its simplicity in assumptions. Though it is considered the mathematical base for soil mechanics, the consolidation theory consistently provides large discrepancies between predictions and observations. Because the theory considers relatively thin, stiff clay layers at large depths, the simplifying assumptions of the theory are believed to be only approximately satisfied in practice. For example, the assumptions of a constant void ratio along the sample thickness, or constant permeability in a particular load step, are valid only when the ultimate change in effective stress is small in comparison to the pre-consolidation stress. In addition, due to the low density of soft sediments, changes in void ratio due to self-weight consolidation are dramatic and will certainly affect the sample's permeability. The magnitude of error arising from the assumed linearity in compressibility and void ratio depends on the magnitude of changes in the void ratio during the consolidation process. This relationship, when dealing with highly compressible soft sediments, can produce discrepancies between calculations and field observations. Overall, it is believed that the void ratio changes significantly in soft sediments; even a very small amount of stresses can cause a lot of settlement to occur.

As mentioned earlier, great strains occur very prevalently in dredged fills, contrasting Terzaghi's assumption of small strains. Moreover, the softer the soil is, the greater the non-linearity of the behavior. Finally, the effect of self-weight is generally neglected by conventional analysis. It should be included in the analysis of 'thick' clay layers, as it can produce considerable stresses.

Thus the consolidation theory of Terzaghi is not effective in dealing with the consolidation of fine-grained dredged materials. The usual form of Terzaghi's governing equation (Terzaghi and Peck 1967) is presented in

$$\frac{du}{dt} = C_v \frac{d_u^2}{d_x^2} \tag{1.1}$$

Where *u* represents the excess pore water pressure and *x* is the vertical space coordinate. C_v is the coefficient of consolidation and *t* is the independent variable representing time.

Despite its limited applicability to generalized soil consolidation, Terzaghi's equation is the most popular choice among geotechnical engineers because it is the simplest equation and is taught in all basic soil mechanics courses. However, much effort in the field of soil mechanics has been devoted to improving upon this basic theory. The first approach addresses its use of a one-dimensional base to represent a three-dimensional phenomenon. Authors like Biot (1941, 1956) attempt to introduce dimensions to the one-dimensional Terzaghi theory.

The various resulting theories of consolidation can be categorized into one of two broad types: infinitesimal strain theories and finite strain theories. Both types of theories can include linear and nonlinear soil properties, as well as stress-strain relationships that is either dependent or independent of time.

Infinitesimal strain theories consider the thickness of the soil layer to be constant during consolidation. Finite strain theories, on the other hand, include this parameter as one of the variables of the problem. Infinitesimal strain theory uses the Eulerian coordinate system for governing balance equations and is therefore fixed in space and time. Finite strain theory uses the convective coordinate system, in which the movements of particles are functions of time, to follow the motion of a soil particle in a mathematically reasonable manner. The material coordinate system is the simplified form of the convective coordinate system and is based upon the volume of soil particles lying between a datum plane and the point being analyzed. This concept will be explained thoroughly in subsequent chapters.

The second approach tries to improve the constitutive relationships in Terzaghi theory, i.e. compressibility and permeability relationships. Under Terzaghi theory, the void ratio-compressibility and void ratio-permeability relationships remain constant during consolidation under a particular load increment. This set of improvements tries to account for variations in permeability and compressibility during consolidation (Richart, 1957; Schiffman and Gibson, 1964). However, the assumption of small strain remains, causing errors when dealing with large strains in dredged material consolidation.

According to Cargill (1982), Schiffman and Gibson (1964) assume that the variations of permeability and the coefficient of volume with depth are known, thus derived the following governing equation (**Error! Reference source not found.**):

$$\frac{\partial_{\mathrm{u}}^2}{\partial_{\mathrm{x}}^2}+\frac{1}{\mathrm{k}}\frac{\mathrm{d_k}}{\mathrm{d_x}}\frac{\partial_{\mathrm{u}}}{\partial_{\mathrm{x}}}=\frac{\gamma_{\mathrm{w}}\mathrm{m_{v(x)}}}{\mathrm{k(x)}}\frac{\partial_{\mathrm{u}}}{\partial_{\mathrm{t}}} \tag{1.2}$$

Where k is permeability, γ_w is unit weight of water, m_v is coefficient of volume change, and other terms remain as previously defined.

The third approach introduces improvements on the magnitudes of strain and flow velocities. From this point on, non-linear constitutive relationships are introduced into consolidation theories. The softer the media is, the greater the non-linearity of the constitutive relationships.

Although the early works by McNabb (1960) and Mikasa (1963) provided a framework for rigorous formulations for consolidation, the many variations of Terzaghi's equation have their own limitations and are not quite useful for applications with large deposits of soft dredged sediments.

While the equation by McNabb and Mikasa is capable of considering large strains, the first general finite strain theory of one-dimensional soil consolidation was published by Gibson, England and Hussey in 1967. This theory constitutes a breakthrough, as it can be well-suited for the behavior of soft sediments. Gibson's theory is very similar to Mikasa

theory; the difference is in the initial condition (Pane and Schiffman, 1981) and Gibson's consideration of self-weight effect. The effect of self-weight is one of the important aspects of Gibson's theory and is neglected in the conventional theory of Terzaghi, especially when dealing with thick natural layers of clayey soil. The weight of these layers may produce considerable stresses, affecting the soil's consolidation behavior by way of rapid sedimentation (Pane and Schiffman, 1981), slow sedimentation (Schiffman and Cargill, 1981) and the consolidation of loaded clay layers (Gibson, Schiffman and Cargill, 1981).

Gibson's governing equation, which will be fully developed in subsequent sections, is described mathematically as**Error! Reference source not found.**:

$$\left(\frac{\gamma_s}{\gamma_w}-1\right)\frac{d}{de}\left[\frac{k(e)}{1+e}\right]\frac{\partial e}{\partial z}+\frac{\partial}{\partial z}\left[\frac{k(e)}{\gamma_w(1+e)}\frac{d\sigma'}{de}\frac{\partial e}{\partial z}\right]+\frac{\partial e}{\partial t}=0 \qquad (1.3)$$

where γ_s is the unit weight of solids, e is the void ratio, z is a material coordinate and other terms remain as previously defined. The equation considers:

- The effect of self-weight,
- Variation of permeability with void ratio,
- Variation of effective stress with void ratio, and
- Independence from magnitude of strain.

Therefore, this governing equation is suitable for applications in thick soft clayey layers. As shown by Schiffman (1980), all other theories of consolidation are special cases of this equation, and can be concluded by applying their simplifying assumptions to the governing equation.

The general solution to the Gibson, England, and Hussey (1967) equation, which will be referred as the finite strain consolidation equation from this point on, leads to a non-linear differential equation. There is thus no analytical solution for this equation, and it

can be solved by numerical analysis. However, by assuming linear relationships between the logarithm of vertical effective stress and logarithm of vertical hydraulic conductivity and ignoring the effect of self-weight on the total stress distribution, Fox (1997) presented an analytical solution with limited applications for the differential equation. It should be noted that because it ignores the self-weight effect, Fox's solution is not suitable for soft sediment consolidation applications.

The basic assumptions of finite strain consolidation are similar to the Terzaghi infinitesimal strain theory, with the exception of limitations on the magnitude of the strains. These assumptions are:

1. The soil consists of soil particles, soil skeleton and pore fluid and the soil system is saturated.
2. The flow of fluid is governed by Darcy's law.
3. The effective stress principle is valid.
4. The soil is considered to be incompressible.
5. The fluid is incompressible and isotropic.

The governing equation is developed from the constitutive relationships and balance laws. Since the fluid and soil are considered to be incompressible, the balance relationship, in between, is already satisfied. The details of deriving the governing equation will be presented later.

Some numerical solutions have been developed (Gibson, England and Hussey, 1967; Monte and Krizek, 1976), but all assume that the governing equation's nonlinear term has little effect on consolidation behavior and that the linear term dominates the solution. Later works by Abu-hejleh and Znidarcic (1994), based on the inverse solution of the governing equation proposed by Huerta et al. (1988) led to the numerical solution of the finite strain consolidation equation. The numerical solution is then programmable into spreadsheets for calculation purposes. This method is based on seepage-induced consolidation, which results in relationships between compressibility, permeability, and

void ratio. Using this method, two constitutive relationships will be obtained from laboratory tests and used to solve the governing equation to determine the settlement time relationship.

The model and required procedure will be fully described later. This method and its testing procedures will be the base concepts of this thesis for the determination of consolidation characteristics of Newark Bay sediments.

Chapter 2 Development of governing equation of finite strain consolidation

The traditional consolidation theory developed by Terzaghi (1942) is based on infinitesimal strain and will be referred to as small strain consolidation theory. The compressibility and permeability relationships are summarized as the coefficient of consolidation (*Cv*), which is assumed to be constant during consolidation.

Mikasa (1965) and Gibson et al. (1967) developed the one dimensional finite strain consolidation theory to remove the restriction on the strain magnitude. The compressibility and permeability relationships vary with the void ratio as single-valued functions. Mikasa sought to improve the Terzaghi formulation based on the coefficient of consolidation. Gibson's approach, however, was based on changes in compressibility and permeability with the void ratio. The void ratio, or the ratio of the volume of voids over the volume of solids, is thus considered to be the dependent variable in the consolidation equation.

The governing equation of finite strain consolidation theory is based on the work of Gibson, England, and Hussey (1967). The theory of consolidation is designed to predict the progress of deformation of an element in a saturated porous medium that is subjected to an imposed stress. In general, a porous material can be considered to be a system of interacting components. Each component is governed by its constitutive relationships; namely, stress-strain and flow.

Traditional geotechnical engineering applications of porous media consist of two phases: a deformable mineral skeleton (soil) and an incompressible Newtonian fluid (water). Consolidation refers to the deformation caused by the outflow of pore water from a saturated soil skeleton. Since the system is considered to be saturated at all times, the outflow of pore water is equal to the deformation of the soil, or the increase in effective stress in the soil skeleton. In this case, the water flow is stimulated by any change

in imposed stress on the soil skeleton. For example, it may be produced by a difference in hydraulic head between the top and bottom of the soil layer, or by a surcharge load.

If the only surcharge applied to the soil skeleton is the buoyant weight of the solid particles, then it is referred to as self-weight consolidation.

1. Coordinate system

The description of the flow of a fluid, in fluid mechanics, requires the identification of a coordinate system upon which the flow can be characterized. Two main approaches exist: Eulerian and Lagrangian (Material). The coordinate system typically used in geotechnical engineering is the Eulerian system. In this system, fluid properties are determined as a function of time and space. Attention is focused on fixed points of space and properties are measured within that specific point or boundary. It is helpful to imagine a container (boundary) through which fluid particles can go in and out, but only the properties of those particles inside of the container (boundary) are determined. This system only requires the identification of a fixed boundary for the determination of fluid properties (like velocity) at any time. From a physical point of view, it is more convenient to express dependent variables, like stress or pore-water pressure, in terms of the Eulerian coordinate system. This is due to the ability to pick a point of interest and measure or calculate the water pressure or stress at that point. Any response within the Eulerian system is related to a fixed point in the space. For example, the infinitesimal strain theories of consolidation assume that the deformation of the layer at any time during the consolidation process is negligible compared to the initial thickness of the layer; therefore, the Eulerian coordinate of a particle remains the same throughout the consolidation in this coordinate system.

The second coordinate system is the Lagrangian system, in which the history of an individual particle is described by attaching the coordinate system to the particle itself. In this case, the particle is followed by the domain and the fluid properties are determined

at any time as particle moves about. Information is readily obtained in the Lagrangian system by just following the particle movement.

During consolidation, the sediment surface drops and the position of the associated spatial coordinate system must drop too. Due to the relatively large movement of the top boundary of the consolidating layer, using a fixed coordinate system (Eulerian) to account for unlimited strain is impractical. In other words, the moving surface of the sediment will result in a moving boundary problem, which is mathematically difficult to solve. The simplest coordinate system for developing the governing equation is therefore the one that can be attached to a volume of solid particles and can produce results at any time: i.e. the Lagrangian coordinate system. Defining the Lagrangian coordinate in the form of the volume of solid particles in the layer, which is a constant quantity, produces the properties at any time for that volume of particles. This is referred to as the Material coordinate system. The coordinate system can now move with top boundary of the consolidating layer and becomes much simpler to deal with it mathematically, since at each point in time the amount of solid particles is constant. It is also independent of time and strain amount, making it a unique tool for the time-dependent consolidation problem.

The Eulerian system is much simpler for use in the mathematical development of equations, but it is complicated when dealing with moving boundary problems. On the other hand, the Lagrangian/Material coordinate system is complicated in equation development but is simpler in application. Therefore, it is simplest to derive everything mathematically in the Eulerian coordinate system and then convert it to the Material coordinates. For this purpose, a set of relationships must be established between the different coordinate systems.

Consider the soil element shown within the consolidating layer in Figure 2.1. At $t = 0$, all of the material is under the sediment surface and therefore $z = 1$ (z represents the material coordinate system). At this point in time, the datum plane does not have any material underneath it, therefore $z = 0$. After some time, the sediment surface will drop

but the total volume of sediment is still underneath the surface and none of the sediment particles will pass over each other, therefore the z is still equal to 1. The datum does not have any material underneath and remains at 0. However, in Lagrangian and Eulerian coordinate systems, the spatial coordinate x(0) and the element's thickness dx(0) at initial time (t=0), and x(t) and dx(t) for later time (t) will change.

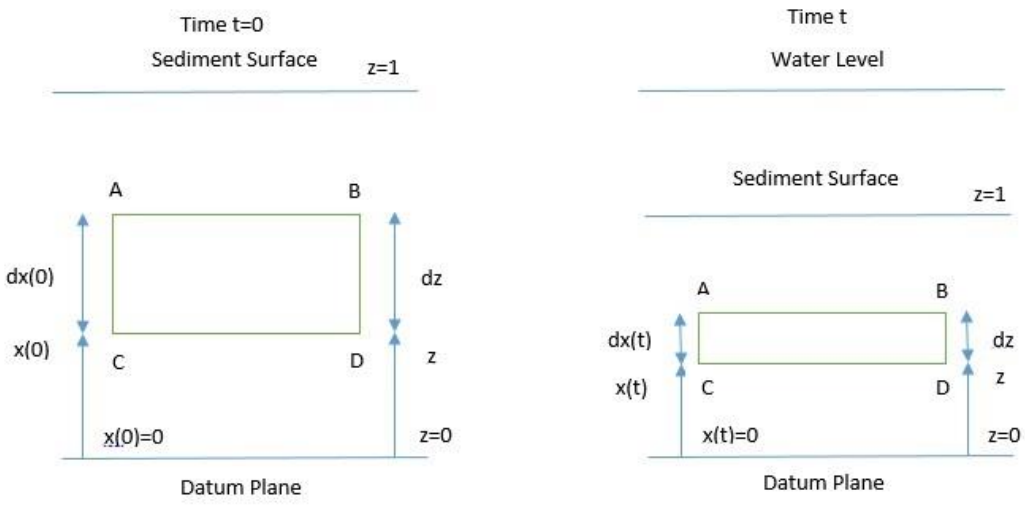

Figure 2.1.Material coordinate system (Bartholomeeusen, 2003)

In the Material coordinate system, the label of a point at the initial state does not change with time. The boundaries remain constant throughout the consolidation.

In the Eulerian coordinate system, the sptial domain is fixed and the parameter of interest is measured at a special point within that domain. Interest is focused on one particular point in the fixed space and measurements are taken at that point through time. Therefore, the boundaries will have different values at different times.

As previously stated, the Material coordinate system measures the volume of solid particles only. As an example a comparison of the coordinate systems (Material, Eulerian, and Lagrangian) is illustrated in Figure 2.2. Based on the work by Cargill (1982), as shown in the illustration, only the Lagrangian and Material coordinates are constant at all times

for particular points in the soil layer and the Eulerian coordinates will change as the top boundary of the sediment moves.

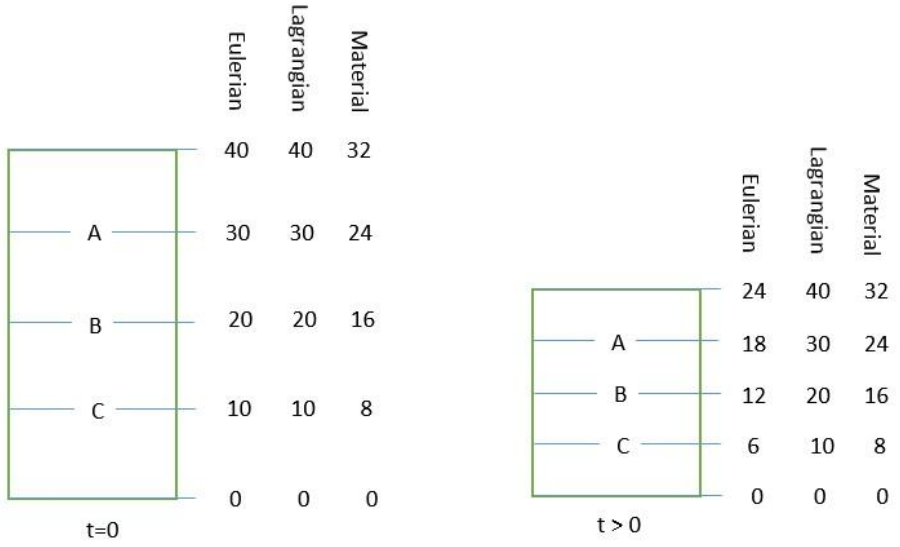

Figure 2.2. Different coordinate systems

Since Material coordinates are not measurable in the usual sense, it is necessary to develop a method of conversion from one coordinate system to another so that the layer thickness can be expressed in understandable conventional units at any time. Consider the differential elements of soil, shown in Figure 2.3, which have a unit volume of solid particles:

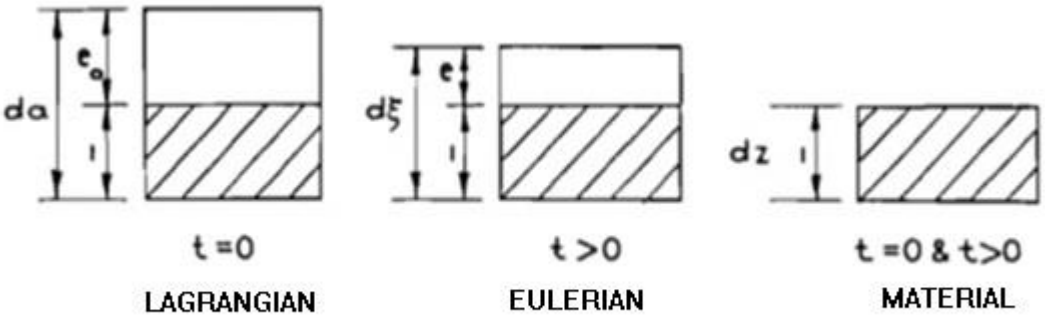

Figure 2.3. Soil Elements

Based on Figure 2.3, we have:

$$da = 1 + e_0 \tag{2.1}$$

$$d\varepsilon = 1 + e \tag{2.2}$$

$$dz = 1 \tag{2.3}$$

Where e_0 is the initial void ratio and e is the void ratio at some later time during consolidation. By simple mathematics we will have:

$$\frac{dz}{da} = \frac{1}{1 + e_0} \tag{2.4}$$

$$\frac{d\varepsilon}{dz} = 1 + e \tag{2.5}$$

$$\frac{d\varepsilon}{da} = \frac{1 + e}{1 + e_0} \tag{2.6}$$

Thus conversion from one coordinate system to another can be accomplished by simple integration. Equation 2.7 is the conversion between Material and Lagrangian coordinates and Equation 2.8 is the conversion between Eulerian and Material coordinates.

$$z = \int_0^a \frac{da}{1 + e(a, 0)} \tag{2.7}$$

$$\varepsilon = \int_0^z [1 + e(z, t)]\, dz \tag{2.8}$$

These relationships will be used throughout the remainder of this chapter for equilibrium and continuity conditions. They allow balance laws to be expressed in an easily understood manner, and enable transformation into the Material coordinate system for the development of the governing equation. Some principles must be satisfied in order to derive the governing equation. They are illustrated in Figure 2.4:

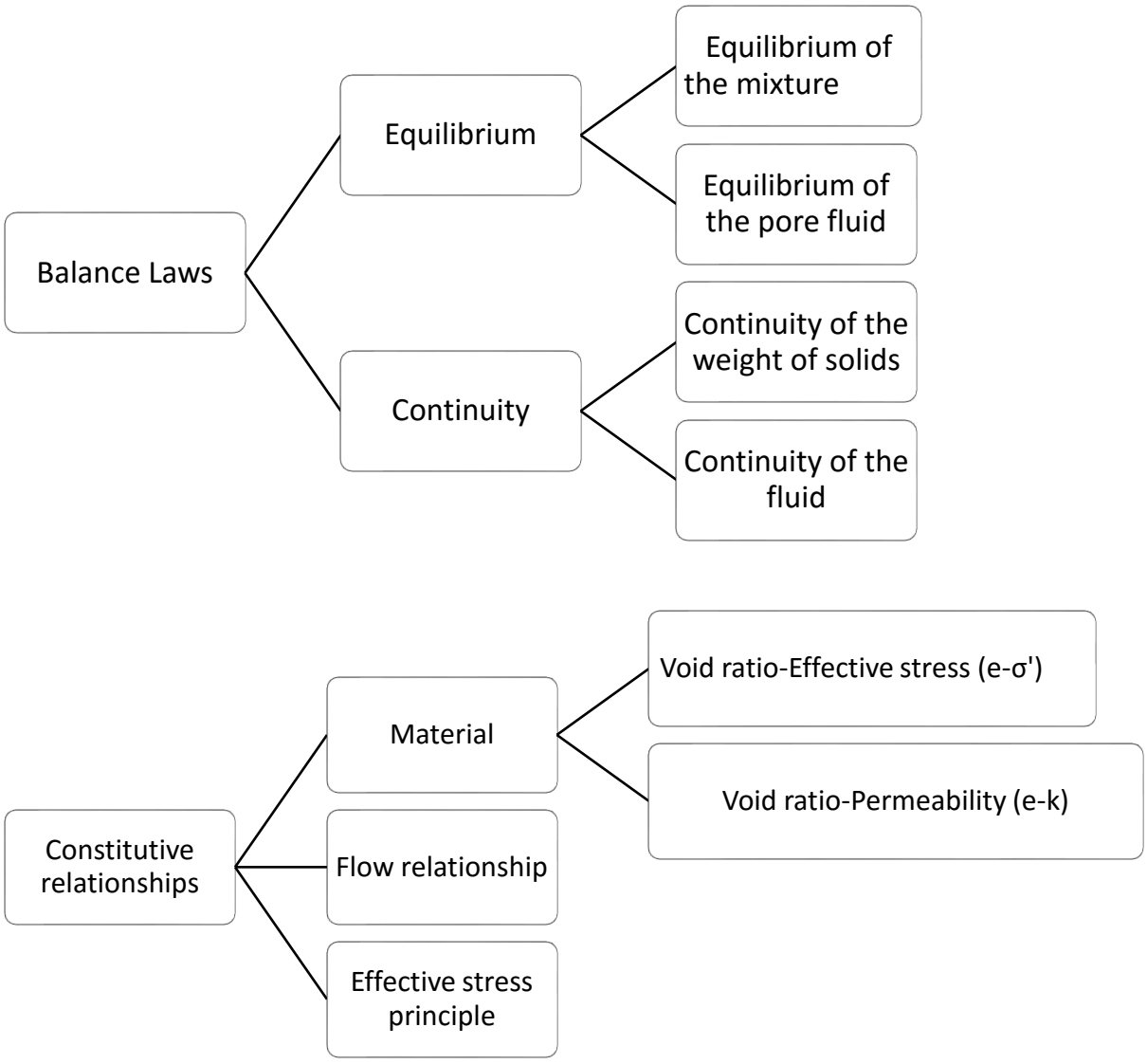

Figure 2.4. Governing equation principles

2. Equilibrium of the mixture

A soil element in equilibrium condition with unit area, oriented perpendicular to the page with a unit volume of solid particles, is illustrated in Figure 2.5. The weight, *W*, of the element is the sum of the weights of the pore fluid and solid particles:

$$W = V \times \gamma = (V \times \gamma)_w + (V \times \gamma)_s \tag{2.9}$$

Based on the Eulerian coordinate system (Figure 2.5) we have:

$$W = e\gamma_w + \gamma_s \tag{2.10}$$

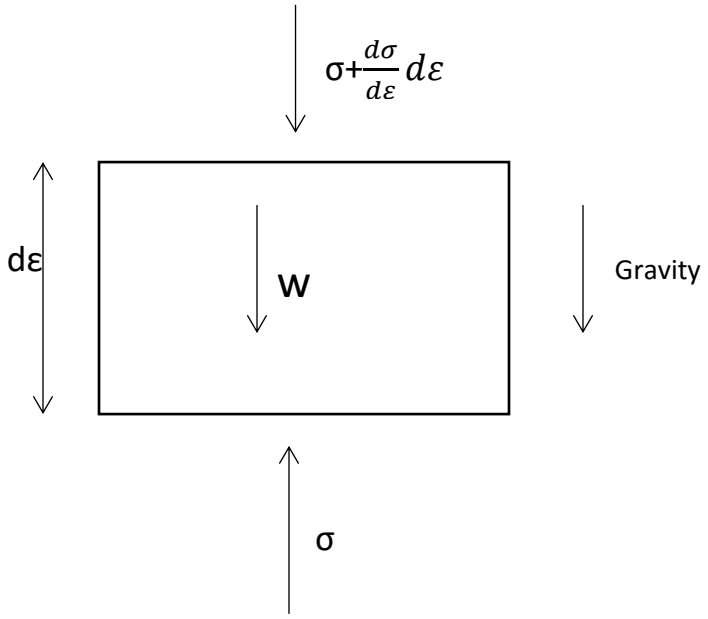

Figure 2.5. Soil element in equilibrium

Therefore, equilibrium of the soil mixture is given by:

$$\sigma + \frac{\partial \sigma}{\partial \varepsilon} d\varepsilon + (e\gamma_w + \gamma_s) - \sigma = 0 \tag{2.11}$$

Where σ is the total stress and e is the void ratio. By simplifying and applying Equation 2.10, the spatial rate of change in total stress to the void ratio (e), unit weight of solids (γ_s), and unit weight of fluid (γ_w) is obtained:

$$\frac{\partial \sigma}{\partial \varepsilon} + \frac{e\gamma_w + \gamma_s}{1 + e} = 0 \tag{2.12}$$

Multiplying by $\frac{d\varepsilon}{dz}$ and using Equation 2.5 gives the equilibrium equation in terms of Material coordinates:

$$\frac{\partial \sigma}{\partial z} + e\gamma_w + \gamma_s = 0 \tag{2.13}$$

3. Equilibrium of Pore Fluid

It is worth noting that the equilibrium of pore fluid should be derived as well. Considering the total fluid pressure at any time to be composed of both static and excess pressure gives:

$$u_w = u_s + u_e \tag{2.14}$$

Where u_w, u_s, and u_e are total, static, and excess pore water pressures, respectively. Static pressure equilibrium is ensured if:

$$\frac{\partial u_s}{\partial \varepsilon} + \gamma_w = 0 \tag{2.15}$$

Therefore, by differentiating Equation 2.14:

$$\frac{\partial u_w}{\partial \varepsilon} - \frac{\partial u_e}{\partial \varepsilon} + \gamma_w = 0 \tag{2.16}$$

or in Material coordinates:

$$\frac{\partial u_w}{\partial z} - \frac{\partial u_e}{\partial z} + \gamma_w(1 + e) = 0 \tag{2.17}$$

4. Fluid Continuity

The equation of continuity for the fluid phase of the soil element can be derived by the weight of fluid inflow minus the weight of fluid outflow, equated to the time rate of change of the weight of fluid stored in the element. As shown in Figure 2.6, the mass flow rate, or the rate at which mass flows past a given point, of fluid flowing into the volume is; $n.v.\gamma_w$, which is given per unit area (dot product), where *n* is porosity and *v* is the velocity of flow. Since the soil's solid particles are also in motion during consolidation, the actual velocity of the flow will be:

$$v = v_f - v_s \tag{2.18}$$

Where subscripts *f* and *s* represent the fluid and solids, respectively.

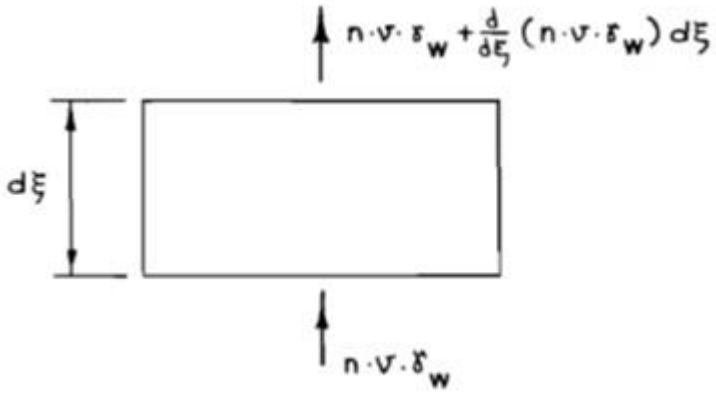

Figure 2.6. Fluid flow through soil element

The weight of fluid outflow is

$$W\ outflow = n.v.\gamma_w + \frac{\partial}{\partial \varepsilon}(n.v.\gamma_w)d\varepsilon \tag{2.19}$$

Since the soil element has a unit volume of solid particles, the weight of fluid contained within the element is:

$$V_S = 1 = \frac{V_V}{e},\ V_V = V_W,\ \ W_{fluid} = V_V\gamma_w = e\gamma_w \tag{2.20}$$

And its time rate of change will be: $\frac{\partial}{\partial t}(e\gamma_w)$

Equating the time rate of change of the weight of fluid within an element to inflow minus outflow results in:

$$\frac{\partial}{\partial \varepsilon}\left[n(v_f - v_s)\right]d\varepsilon + \frac{\partial e}{\partial t} = 0 \tag{2.21}$$

Since the fluid is assumed to be incompressible, it has a constant unit weight, which is cancelled in Equation 2.21.

Equation 2.21 is the equation of continuity expressed in terms of the Eulerian coordinate system. Utilizing the chain rule for differentiation, as below:

$$\frac{\partial F}{\partial z} = \frac{\partial F}{\partial \varepsilon}\frac{d\varepsilon}{dz} \tag{2.22}$$

Equations 2.2, 2.5, and 2.22 can be applied, and Equation 2.21 can be rewritten as:

$$\frac{\partial}{\partial z}\left[n(v_f - v_s)\right]d\varepsilon + \frac{\partial e}{\partial t} = 0 \tag{2.23}$$

Or:

$$\frac{\partial}{\partial z}\left[(v_f - v_s)\frac{e}{1+e}\right] + \frac{\partial e}{\partial t} = 0 \tag{2.24}$$

Since:

$$n = \frac{e}{1+e} \tag{2.25}$$

5. Governing Equation

Derivation of the governing equation requires the use of two other relationships. The first is the well-known effective stress principle:

$$\sigma = \sigma' + u_w \tag{2.26}$$

Where, σ is the total stress, σ' is effective stress and u_w is pore water pressure. The next is Darcy's, law which is usually written in the form:

$$n\left(v_f - v_s\right) = -\frac{k}{\gamma_w}\frac{\partial u_e}{\partial \varepsilon} \tag{2.27}$$

Where *k* is the hydraulic conductivity and u_e is excess pore water pressure. Equations 2.16 and 2.25 can be used to write Equation 2.27 in terms of total fluid pressure and the void ratio:

$$(v_f - v_s)\frac{e}{1+e} = -\frac{k}{\gamma_w}(\frac{\partial u_w}{\partial \varepsilon} + \gamma_w) \tag{2.28}$$

By inserting Equations 2.22 and 2.5 into Equation 2.28, this becomes:

$$e(v_f - v_s) = -\frac{k}{\gamma_w}[\frac{\partial u_w}{\partial z} + \gamma_w(1+e)] \tag{2.29}$$

The governing equation can now be produced by combining Equations 2.13, 2.24, 2.26, and 2.29.

First, Equation 2.29 is substituted into Equation 2.21 to eliminate the velocity terms. Thus:

$$\frac{\partial}{\partial z}\left[-\frac{k}{\gamma_w(1+e)}[\frac{\partial u_w}{\partial z} + \gamma_w(1+e)]\right] + \frac{\partial e}{\partial t} = 0 \tag{2.30}$$

Next, Equation 2.26 is substituted into Equation 2.30 to eliminate u_w :

$$\frac{\partial}{\partial z}\left[-\frac{k}{\gamma_w(1+e)}[\frac{\partial \sigma}{\partial z} - \frac{\partial \sigma'}{\partial z} + \gamma_w(1+e)]\right] + \frac{\partial e}{\partial t} = 0 \tag{2.31}$$

Then Equation 2.13 is substituted into Equation 2.31 to eliminate σ:

$$\frac{\partial}{\partial z}\left[-\frac{k}{\gamma_w(1+e)}[-\gamma_s - \frac{\partial \sigma'}{\partial z} + \gamma_w]\right] + \frac{\partial e}{\partial t} = 0 \tag{2.32}$$

Or

$$(\gamma_s - \gamma_w)\frac{\partial}{\partial z}\left(\frac{k}{(1+e)}\right) + \frac{\partial}{\partial z}\left[\frac{k}{\gamma_w(1+e)}\frac{\partial \sigma'}{\partial z}\right] + \frac{\partial e}{\partial t} = 0 \qquad (2.33)$$

Again, by the chain rule of differentiation (Equation 2.22), Equation 2.33 can be written as:

$$\left(\frac{\gamma_s}{\gamma_w} - 1\right)\frac{d}{de}\left[\frac{k(e)}{(1+e)}\right]\frac{\partial e}{\partial z} + \frac{\partial}{\partial z}\left[\frac{k(e)}{\gamma_w(1+e)}\frac{d\sigma'}{de}\frac{\partial e}{\partial z}\right] + \frac{\partial e}{\partial t} = 0 \qquad (2.34)$$

This is the same equation as proposed by Gibson et al. (1967) for one-dimensional finite strain consolidation of soft soils. It will be known as the governing equation in terms of the void ratio, e, and the functions k (e) and σ' (e).

An analytical solution to Equation 2.34 is not possible, but once appropriate boundary conditions are specified, its numerical solution is possible with the aid of a computer. The constitutive relationships or material functions govern the behavior of the soil during the consolidation. The relationships are based on physical properties of the material and are not time dependent. Also, the material functions do not depend on the spatial coordinate system. Traditional forms of these functions are logarithmic, exponential and power functions that relate the void ratio to effective stress and permeability. The constitutive relationships are needed for the solution of governing equation.

6. Boundary Conditions

Three types of boundary conditions are possible for a soft clay deposit undergoing consolidation. They are shown in Figure 2.7 with possible combinations at the top and bottom of the layer.

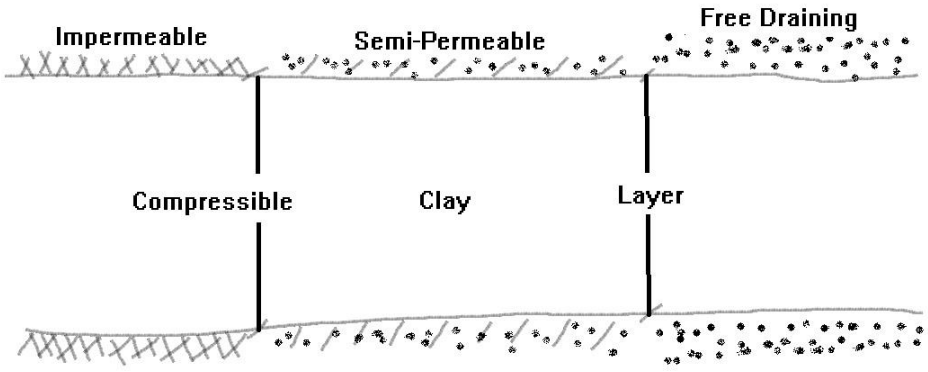

Figure 2.7. Boundary Conditions

The semipermeable condition represents the state at which a compressible layer is in contact with a different compressible layer or when a compressible layer is in contact with an incompressible layer, which has neither the characteristics of a free draining layer nor those of an impermeable layer, but something in between.

6.1. Boundary Condition for Free Drainage

For the case of a free-draining boundary, there is no excess fluid pressure at the boundary and the total fluid pressure is equal to the static pressure:

$$u_w = u_s = h_w \gamma_w \tag{2.35}$$

Where h_w is the height of the free water table above the boundary. Total stress may be calculated if the total weight of material above the boundary is known, and effective stress can be calculated by the effective stress principle. The void ratio is then deduced from the known or assumed relationship between the void ratio and effective stress.

6.2. Boundary Condition for Impermeable Layer

At an impermeable boundary, there is no fluid flow, thus:

$$v_f = v_s \tag{2.36}$$

Applying this assumption to Equation 2.29 results in:

$$\frac{\partial u_w}{\partial z} + \gamma_w(1+e) = 0 \tag{2.37}$$

By considering Equation 2.26, the effective stress equation, gives:

$$\frac{\partial \sigma}{\partial z} - \frac{\partial \sigma'}{\partial z} + \gamma_w(1+e) = 0 \tag{2.38}$$

If Equation 2.13 is used to replace the total stress term and the chain rule of differentiation is used to express the effective stress in terms of the void ratio, Equation 2.38 can be written as:

$$\frac{\partial e}{\partial z} + \frac{\gamma_s - \gamma_w}{\frac{d\sigma'}{de}} = 0 \tag{2.39}$$

This equation is the boundary condition where the compressible layer meets an impermeable layer.

6.3. Boundary Condition for Semipermeable Layer

The boundary condition for a semipermeable layer is based on the fact that the quantity of fluid flowing out of one layer must equal the quantity of fluid flowing into the other layer across their common boundary.

The quantity of fluid flowing across a boundary of unit area is:

$$n(v_f - v_s) \tag{2.40}$$

Therefore,

$$[n(v_f - v_s)]_{Upper} = [n(v_f - v_s)]_{Lower} \tag{2.41}$$

The subscripts indicate upper and lower layers. Then, from Equation 2.27 and the relationship between Equations 2.22 and 2.5:

$$(\frac{k}{(1+e)}\frac{\partial u}{\partial z})_{Upper} = (\frac{k}{(1+e)}\frac{\partial u}{\partial z})_{Lower} \tag{2.42}$$

Where, γ_w is eliminated because the same fluid is in both layers. It should also be noted that the total, static, and therefore excess fluid pressures must be equal in the two layers at their common boundary:

$$(u_e)_{upper} = (u_e)_{Lower} \tag{2.43}$$

And from the effective stress principle,

$$\frac{\partial \sigma}{\partial z} - \frac{\partial u_w}{\partial z} = \frac{\partial \sigma'}{\partial z} \tag{2.44}$$

By use of the Equations 2.13 and 2.17, Equation 2.44 can be rewritten as:

$$\frac{\partial \sigma'}{\partial z} = \gamma_w - \gamma_s - \frac{\partial u}{\partial z} \tag{2.45}$$

which can also be written as:

$$\frac{\partial e}{\partial z} = (\gamma_w - \gamma_s - \frac{\partial u}{\partial z}) \frac{de}{d\sigma'} \tag{2.46}$$

The conditions expressed by Equations 2.42, 2.43, and 2.46 may be used to numerically solve the problem of semipermeable boundaries.

Chapter 3 Seepage-induced Consolidation

1. Background

Consolidation is a deformation caused by imposing a stress on a porous media in saturated state. Any disturbance in the stress levels within the saturated porous material will cause excess pore water pressure to build up. Since the material is porous, the excess pore water pressure will dissipate over time, and soil grains will tolerate the stress. In other words, in geotechnical engineering, consolidation is always associated with the outflow of pore water because of the change in stress levels. In seepage-induced consolidation, the disturbance happens by way of a difference in the hydraulic head between the top and the bottom of the soil sample or by applying surcharge. If no surcharge is applied on the sample and the buoyant weight of the solid particles is the only source of stress, then it is called self-weight consolidation.

The idea of consolidation under seepage force was first proposed by Imai in 1979. He proposed a new method for the prediction of consolidation constants for fine grained sediments by applying seepage force on a sample in a consolidometer. His observations showed that, by knowing the distribution of pore water pressure, the water content profile, and the velocity of flow, all of the consolidation constants and the compression curve could be determined. The only restriction is that the abovementioned achievements occur when the steady-state seepage flow happens within the sample. Since the consolidation of soft sediments can occur from very small stresses, Imai's apparatus was capable of running tests in very low stress ranges of 0.01 to 50 kN/m^2. This test method is the basis for later improvements in seepage-induced consolidation testing devices. However, it was not as commonly used as Terzaghi's test method for consolidation. The focus of most researchers was on the modification of the traditional consolidometer or on improving the finite strain consolidation theory.

Works by Cargill in 1982 resulted in development of a new computer program, named CSLFS (Consolidation of Soft Layers by Finite Strain analysis), as an alternative to the conventional methods of calculating one-dimensional consolidation. The program was

based on the explicit finite difference technique, which had the capability of considering multiple dredged fill layers deposited on a compressible foundation. Cargill used small strain theory in developing void ratio-permeability and void ratio-effective stress relationships. Later in 1984, he applied linear terms to the Gibson's equation for soil permeability and compressibility and developed consolidation calculations charts. These charts related improvement of consolidation by percent (with 100% representing fully consolidated) to a time factor for initial and boundary conditions commonly encountered in the field.

In 1982, Schiffman worked on the slow deposition of Holocene sediments from Gulf of Mexico. He showed that by using finite strain consolidation theory, the states of effective stress and excess pore water pressure are very different from those calculated by conventional Terzaghi theory. He concluded that the conventional theory of consolidation seriously underestimates the effective stress profile at any time during consolidation, leading to serious errors in the deposit's shear strength calculations. Some concerns proposed by Schiffman, regarding the non-homogeneity of the deposits, effect of gas bubbles in the deposits, and skeleton creep of the soil, should have been addressed in the theory development. Ultimately, Schiffman concluded the applicability of finite strain theory, rather than traditional Terzaghi theory, in soft sediments.

In 1983, Carrier et al. studied the consolidation properties of fine-grained waste materials using the finite strain consolidation theory. They used field and laboratory tests to develop a general relationship between Atterberg limits and consolidation properties. They proposed a correlation between the liquidity index and the effective stress and permeability characteristics of fine-grained waste material and believed that there was a direct relationship between the plasticity index and compressibility and permeability parameters. Carrier et al. used the Constant Rate of Strain Consolidometer (CRSC) as a laboratory testing device, but the lack of accurate permeability measurements caused them to emphasize the need for improvement in permeability measurements. The CRSC

is similar to the constant rate of strain oedometers proposed by Smith et al (1969) and Wissa et al (1971). Carrier proposed constitutive relationships in the form of:

$$e = A\sigma'^{B} \tag{3.1}$$

$$k = E\frac{e^{f}}{1+e} \tag{3.2}$$

where *e* is the void ratio, σ' is effective stress, *k* is permeability and *A, B, E,* and *f* are model constants. This is the first expression of constitutive relationships in the form of power functions to be used with finite strain consolidation theory.

Znidarcic (1984) summarized all of the methods for the determination of the consolidation properties in the laboratory. He considered the step loading test, constant rate of deformation test, controlled gradient test, constant rate of loading test, continuous loading test, seepage test, and relaxation test. He states that some of the methods are better than others, but none of them is theoretically complete and without restrictive assumptions. All methods besides the seepage test try to obtain material properties from the differential equation solution and implement simplifying assumptions in their consolidation theory. However, their inherent simplifying assumptions limit their applicability. In the case of constant or linear material properties, all of the methods are in good agreement and result in a good approximation of real behavior. Since the consequences of the restrictive assumptions are not critically evaluated, their influences on constitutive relationships (void ratio-effective stress and void ratio-permeability) cannot be quantified. Therefore, Znidarcic states that there is a need to develop a new testing procedure with less restrictive assumptions that can solve the finite strain consolidation problem.

McVay et al. (1986) asserted that, although linearization of the original theory may work in some special cases, the most appropriate usage form of the nonlinear formulation

of Gibson's theory is the complete one, without restrictions. They found that assumptions like the rigidity of soil skeleton in Terzaghi's infinitesimal theory can cause the overestimation of settling rate. They also emphasized the inadequacy of the void ratio-permeability relationship, which must be improved in test procedures to obtain better results. McVay et al. suggested the use of the constant rate of deformation test over standard oedometers in order to produce better outcomes for void ratio-effective stress and void ratio-permeability of fine grained materials. They proposed constitutive relationships in the form of:

$$e = A\sigma'^{B} \tag{3.1}$$

$$k = Ee^{f} \tag{3.4}$$

As mentioned previously, Carrier et al. (1983) used a strain-controlled rate device for testing the consolidation of soft materials. In 1986, Cargill devised a new apparatus for consolidation testing of fine grained soils based on Carrier's concepts. Large Strain, controlled Rate of Strain Consolidation (LSRSC) was proposed, with the ability to measure both the self-weight consolidation and small range of stress for surcharge application. The apparatus was capable of monitoring the excess pore water pressure during consolidation by using special ports along the sample chamber. Cargill used the Controlled Rate of Strain Test (CRST) computer program, which was based on the explicit finite difference scheme, to solve the governing differential equation numerically. Using the pore water pressure profile of the sample throughout consolidation over time, he tried to directly solve the governing equation and produce functions for void ratio-permeability and void ratio-effective stress.

One of the major problems with the Controlled Rate of Strain Test (CRST) is the time requirement. Self-weight consolidation is a very time-consuming process because it involves the sedimentation of very fine, low density, and dust-like particles. In addition, excess pore water pressure must be dissipated at each loading step when the surcharge

is applied on the sample, signifying another time-consuming process. For these reasons, running a test with this method may take as long as 6 months!

Scott et al. also introduced a new testing device in 1986. They built a 10-meter high, 1-meter diameter slurry consolidometer as part of a research program to investigate self-weight consolidation. They first used sand-sludge samples in 2-meter high cylinders. If the consolidation results looked promising, they would consider the use of 10-meter high cylinders. Scott et al. noticed the development of thixotropic strength during the consolidation, affecting consolidation in the upper part of the cylinder. In low solid content samples, this could result in initial consolidation rates lower than those predicted from incrementally-loaded consolidation tests. One of the difficulties of this method involved the measurement of low excess pore water pressure during long testing periods (up to 550 days). The 10-meter high cylinders posed a challenge for density sampling along the specimen, therefore Scott et al. suggested the indirect measurement of sample density to overcome disturbance effects on the samples.

In 1988, Huerta et al. used a one dimensional mathematical model based on finite strain theory to solve the seepage-induced consolidation problem originally proposed by Imai (1979). He proposed an inverse solution that uses the final settlement of sample and steady state flow through the sample to deduce permeability and compressibility relationships for soft sediments. Before this, researchers tried to come up with void ratio profile by either measuring density through slicing the sample or by monitoring pore water pressure during consolidation. Then they used the information to find the best fit to solve the governing equation, i.e. finding an equation which can relate void ratio to permeability, time and effective stress.

In Imai's consolidation setup, consolidation happens by the force of seeping water through the sample. He showed that the permeability influences both the time to reach steady-state condition and also the steady state itself. In other words, the final height of the deposit depends on the variation of permeability with the void ratio.

Huerta used the final settlement and steady state condition to come up with model parameters that fit into the governing equation. The use of seepage force to induce consolidation and measurement of the sample's permeability during the test removed all of the permeability measurement problems associated with previous test methods. His way of solving the governing equation was a major breakthrough in the study of soft sediment consolidation.

In 1989, Znidarcic et al. introduced a new testing technique for the consolidation of soft soils based on the seepage-induced consolidation test. They also implemented the inverse solution procedure for parameter estimation. Their procedure seemed to be well suited for soft soils. It had a rational approach for parameter estimation, and the test analysis was in complete agreement with the nonlinear theory of consolidation, for which the parameters would be used.

In other words, Znidarcic et al. used Imai's approach in building the testing apparatus and Huerta's approach in obtaining the constitutive relationships. Therefore, their method had no restricting assumptions for the implementation of nonlinear Gibson's consolidation theory. Since seepage-induced consolidation is based on seepage forces, it provides a suitable method for permeability determination. Another advantage of this method, which made it superior to other methods, is its reasonable time frame for running a test, between two and seven days. Therefore, it is not only based on the theory, but it also provides better quality data in a timely fashion.

Until 1994, Znidarcic mostly worked on parameter estimation algorithms for the determination of the nonlinear consolidation compressibility and permeability relationships from the seepage-induced consolidation test results at steady-state. He rewrote the governing equation in the form of an integral and used the numerical solution for it. He proposed constitutive relationships in the form of:

$$e = A(\sigma' + Z)^B \tag{3.5}$$

$$k = Ce^{D} \tag{3.6}$$

The estimation of parameters was based on Newton's estimation method for finding the coefficients of constitutive relationships, i.e. *A, B*, and *Z* are for void ratio-effective stress, and *C* and *D* are for void ratio-permeability.

In the following years, researchers focused more on how to easily and efficiently implement this approach and proposed more practical and alternative solutions. In 1996, Abu-Hejleh et al. used the seepage-induced consolidation test to confirm the method for very soft Phosphatic clays. Based on their measurements, the final height and bottom effective stress are measured as the sample reaches steady state under downward seepage flow through it. These two measurements and the measured zero effective stress void ratio, based on the sedimentation test, represent three experimental data in the low effective stress range, where the constitutive relations are highly nonlinear. They employed a parameter estimation scheme for the steady-state condition in order to determine the soil consolidation parameters. This was a complete testing and analysis of very soft soils based on seepage-induced consolidation and it confirmed its effectiveness and precision.

Fox et al. (1997) proposed closed-form equations for discharge velocity, as well as the distribution of pore pressure and effective stress at steady-state flow conditions, for the seepage-induced consolidation test. This avoids the use of numerical solutions to obtain constitutive relationships. They considered two assumptions: first, that a one-to-one linear relationship exists between the logarithm of effective stress and the logarithm of permeability; and second, that the contribution of side friction and self-weight to the distribution of vertical total stress is small compared to the applied pressure difference. These two assumptions were based on reported lab results of various previous published data. Fox et al. tried to use the test procedure and direct solution of Imai (1979) than the test procedure and inverse solution of Znidarcic (1994). Therefore, the void ratio distribution was obtained by slicing the sample, bringing into question how precisely one

can slice a soft soil sample. The analysis is based on closed-form equations, which are relatively simple to approach when all parameters are available. The advantage of this method is that there is no need for specialized numerical procedures to calculate the desired constitutive relationships for the sample. However, the procedure cannot be used for tests in which the top effective stress is zero. Fox et al. noted that the required time to perform the seepage-induced consolidation test is 75% less than that needed for the step-loading consolidation test, confirming the time effectiveness of the seepage test. In 1999, Fox presented graphical solution charts for one-dimensional finite strain consolidation of a single homogeneous layer of normally consolidated clay. The charts included the effects of vertical strain, self-weight, and decreasing compressibility and permeability during consolidation process. The purpose of presenting these types of solutions with restrictive assumptions is to avoid using computer programs for solutions of finite strain consolidation theory. However, the charts lack accounting for any time effect on the parameters, such as pore pressure or settlement as a function of time. As a design tool, the charts can be used to make preliminary estimates of settlement and excess pore water pressure, but it should be noted that the estimates are only good for middle stages of consolidation and that they are in lesser agreement during the early and later stages. In 2000, Fox et al. proposed a computer program named CS4, based on a piecewise-linear model for the consolidation of an accreting soil layer that accounted for self-weight, large strains, and variable permeability and compressibility during consolidation. The program was based on the Eulerian coordinate system and it was demonstrated that the program result was identical to its Material coordinate equivalent. The disadvantage of the program is that it lacks in accurately modeling the behavior of high void ratio materials during the early stages of deposition. This is a result of assuming linear consolidation behavior for these types of material. Overall, the charts are only good for preliminary design purposes.

Yao et al. (2001) proposed his software, based on early work of Abu-Hejleh and Znidarcic (1995), named CONDES. CONDES was based on a semi-implicit time integration

scheme that is numerically convergent. Yao et al. used a centrifuge test to validate their software outputs and found promising results.

Luca (2002) used seepage-induced consolidation setups for the determination of consolidation behavior of dredged materials of mineral origin. Their device was an automated version of original seepage-induced consolidation device introduced by Znidarcic in 1994. They also used SICTA program that was developed in 1992 by Abu-Hejleh and Znidarcic for the derivation of constitutive relationships. It should be noted that the capability of seepage-induced consolidation setups for very low effective stress ranges was also reapproved. Overall, this method seems to be the best method, procedure and time-wise, to determination the consolidation of fine-grained materials.

Xie and Leo (2004) compared their solution to the one-dimensional consolidation of saturated homogeneous clay with the infinitesimal strain theory. Their solution is based on Lagrangian coordinates, in explicit form. It should be noted that the explicit numerical solution refers to the direct computation of the dependent variable in terms of known quantities, while the implicit form refers to a situation in which the dependent variable is defined by set of equations. Usually, an iterative technique is needed to obtain the solution. They stated that as the compressibility of the soil increased, the discrepancy between the infinitesimal theory and large strain theory decreased. In addition, although the dissipation of excess pore water pressure in small strain consolidation is slower than in large strain, they found the settlement predicted by small strain theory to be larger than that predicted by large strain theory. Another analytical solution was proposed by Morris in 2005 which linearized Gibson's finite strain theory of consolidation, and preserved the non-linearity of the soil permeability and compressibility by assuming two new variables.

The attempt for avoiding numerical solution by these authors and efforts to find an analytical solution for finite strain consolidation theory simply reflects the simplicity of Terzaghi's solution which is analytically available. They try to connect the Gibson's theory of consolidation for large strain to the infinitesimal strain theory of Terzaghi. Morris

mentions that his solution is only applicable for the analysis of first stage of low-stress one-dimensional consolidation tests of fine-grained soils and similar materials. In addition, since the new solution is based on the linear form of the finite strain consolidation theory, it is valid for a limited range of effective stress and void ratios and it is not applicable to many large strain consolidation problems, as was stated earlier by Fox (1997, 1999).

Berilgen et al. (2006) used the seepage-induced consolidation test procedure to investigate the consolidation characteristics of Golden Horn dredged materials. They used the setup proposed by Znidarcic for their research to obtain realistic relationships between void ratio and effective stress and permeability. They tried this system for three different clays and the results were very satisfying. Empirical correlations were also presented between liquidity index (I_L) and plasticity index (PI) with unknown consolidation parameters, describing the constitutive relationships (e-σ' and e-k). They also concluded that these empirical relationships are useful for practical applications but further studies are needed to validate their general applicability.

Pedroni and Aubertin (2008) also investigated the consolidation behavior of sludge produced by an acid mine drainage treatment plant based on the simplified seepage-induced consolidation setup proposed by Sridharan and Prakash (2001). Their general concept is based on seepage-induced consolidation; however the testing procedure is simpler and is only good for limited low effective stress ranges.

Gan et al. (2011) introduced a new prototype apparatus for large strain consolidation and hydraulic conductivity testing of slurried materials. Their device can measure pore water pressure along the sample height for monitoring the consolidation process. The permeability testing concept is very similar to the seepage-induced consolidation test but this test is useful for high effective stress ranges. The test is mostly based on the step loading test, which is very time-consuming. One loaded step can take up to almost two weeks to be completed, which is three times more time-consuming than the full testing period for the seepage-induced consolidation test.

Znidarcic et al. continued their studies in 2011, investigating the consolidation properties of mature fine tailings (MFT) via the seepage-induced consolidation test to obtain constitutive relationships. They also compared their results with centrifuge tests to independently verify the obtained properties. The presented results confirmed that seepage-induced consolidation is applicable in the testing of oil sand mature fine tailings and can produce repeatable datasets. This is very useful in understanding the behavior of such high void ratio materials.

Finally, in 2014, Estepho worked on the consolidation characteristics of oil sand slurry tailing waste based on the seepage-induced consolidation concept. He also used Znidarcic's setup and concluded that the method results in repeatable and comparable results. He proved again that the results are in good agreement with other published data on similar type of materials. He noted that the test data, combined with the CONDES0 program for processing the results, can be used in the design of waste disposal facilities in mining projects.

This review of the history of methods and approaches for solving the finite strain consolidation of soft soils concludes that the Znidarcic seepage-induced consolidation setup is the best way to investigate the consolidation behavior of low density slurry type soils. Znidarcic's method proves to provide repeatable and reliable test data in a timely manner. The remainder of this chapter is devoted to describing the seepage-induced consolidation device constructed in the soil and sediment management laboratory of Rutgers University.

2. Seepage-induced consolidation Tester at Rutgers

The schematic of Rutgers University's seepage-induced consolidation device is shown in Figure 3.1. The device consists of the different components:

- Triaxial chamber for sample placement
- Syringe pump to provide water withdraw/infuse
- Water flow tubing system

- Dead weight or pneumatic loading system
- Axial deformation measurement system (LVDT)
- Differential pressure transducer
- Data acquisition system

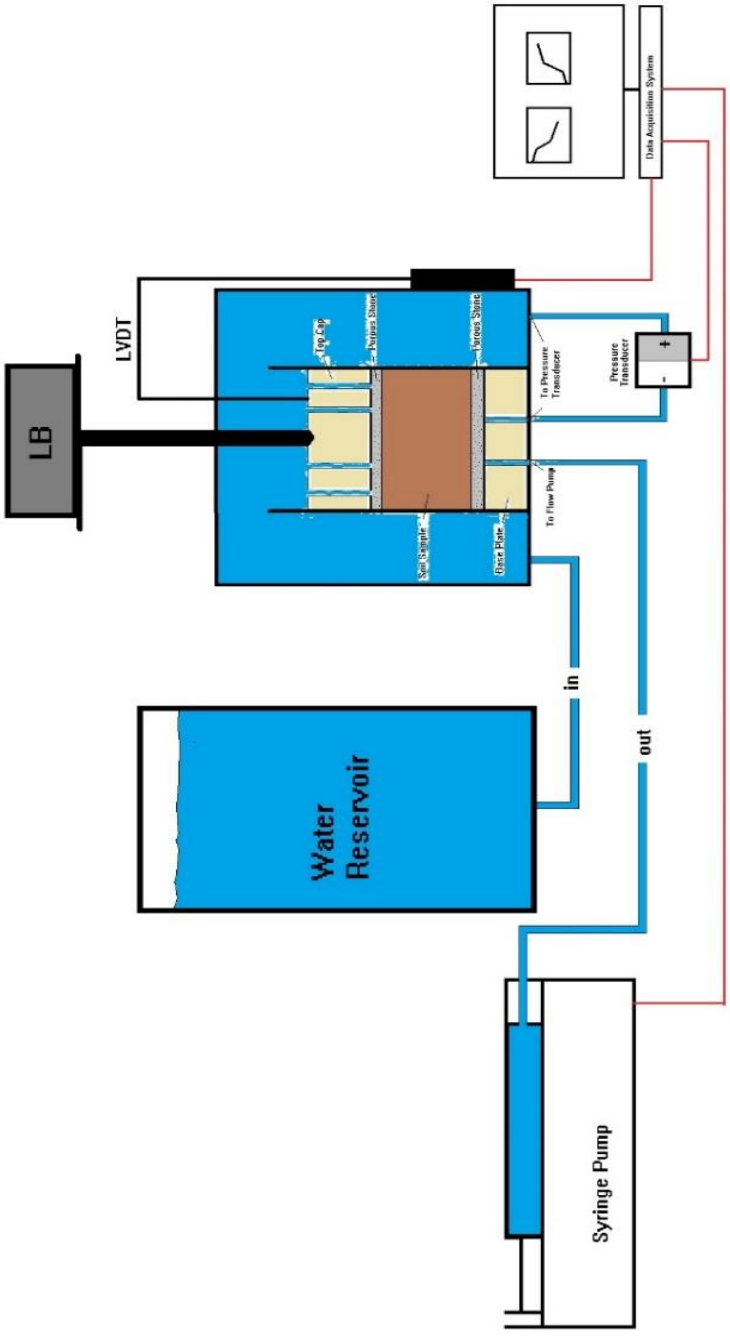

Figure 3.1. Schematic of Seepage-induced consolidation Apparatus

2.1. Triaxial Chamber for Sample Placement

The soil sample is placed inside of a Triaxial chamber which has an outer chamber and an inner cell. The inner cell is where the sample is placed, atop a base plate. On top of the base plate, the sample is confined by two porous stones and filter paper. Finally, the top cap is placed atop this setup, inside of the inner cell. The inside diameter of the inner cell (Figure 3.2) is 3 inches (7.62 cm), which is the same as the diameter of the base plate and sample. A customized piece of Plexiglas is used to fabricate the base plate and the inside of the cell to this exact diameter. The base plate is mounted on the Triaxial chamber by bolts (Figure 3.3). It has two ports for water withdrawal, one for differential pressure transducer, and one for the flow pump to withdraw water from underneath the sample. As mentioned earlier, the sample sits between two porous stones and filter paper, one at the bottom of sample and one on top. These serve to separate the base plate, sample and top cap. The top cap is manufactured to the exact diameter and has 4 holes to ensure that water passes easily through it (Figure 3.2, Figure 3.3, and Figure 3.4).

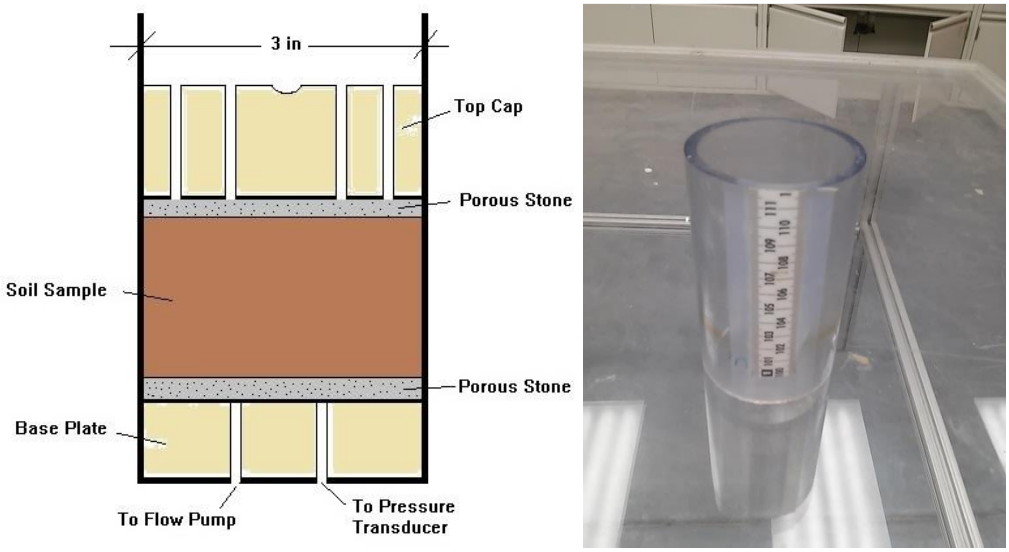

Figure 3.2. Inside Cell

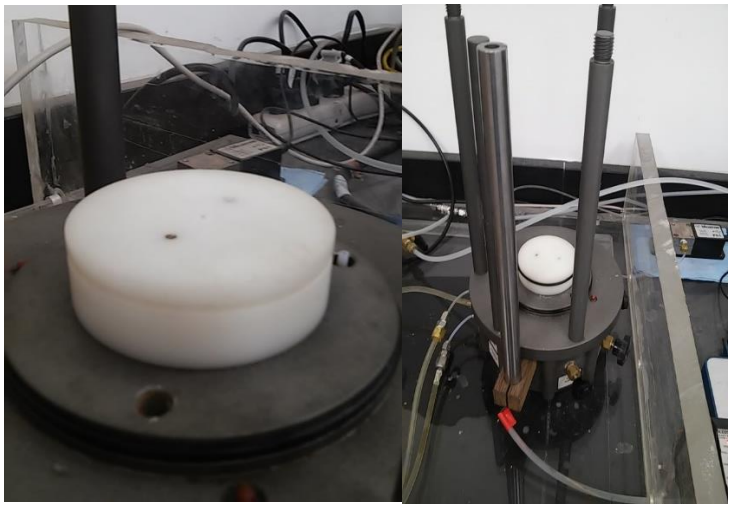

Figure 3.3. Base plate

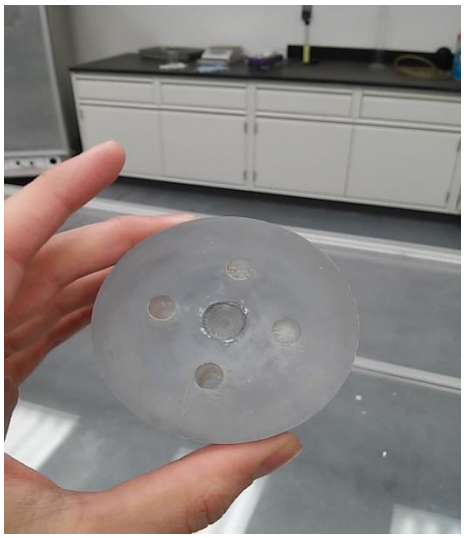

Figure 3.4. Top Cap, Inner Cell, Porous Stones

As shown in Figure 3.4, there are four water ports on the top cap to provide water flow through the sample. There is also a groove for when the Triaxial cell is filled with sample and water. The aluminum rod is placed on the grooved part of top cap for imposing a vertical load, if needed. Figure 3.5 shows the rod assembled with the top cap. The rod serves two purposes: first, it is used to ensure uniform settlement of the soil sample, as it has a small buoyant weight of about 0.1 kPa; and second, it helps prevent side wash of the sample during testing (Znidarcic, 1994).

Figure 3.5. Top Cap, loading rod assembly

Figure 3.6 shows the sample setup in the Triaxial chamber with all of the different parts.

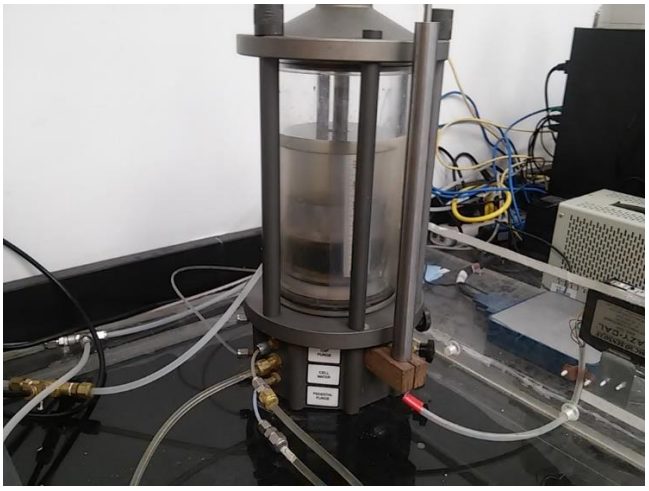

Figure 3.6. The sample setup

2.2. Syringe Pump

One of the most important parts of the seepage-induced consolidation device is the capability of the setup to provide constant discharge of water through sample. For this purpose, a pump is needed to withdraw and infuse water. The pump's ability to withdraw water provides the required suction from underneath of the sample to induce a very small gradient across the soil sample, ensuring minimal disturbance to the sample. All of the permeability measurements depend on the accuracy of the pump to withdraw water. In order to achieve this small gradient a syringe pump, typically used for medical applications, is used to withdraw and infuse water. The withdrawal setting is used for testing and the infusing setting is used to reset the pump when it reaches its capacity. The minimum withdrawal rate of the pump is 15 nL/min, which is equivalent to 5.5×10^{-11} m/s for a sample of 3 inches in diameter (45.6 cm^2 area). This value is simply the Darcian velocity, resulting from the division of discharge over the sample area. In low density soils like dredged materials or mine tailings, this low velocity is preferred because it causes very little disturbance across the sample. The Harvard apparatus PHD Ultra 4400 syringe pump is used in this research (Figure 3.7). This type of syringe pump is completely programmable with high accuracy and precision. It has the capability to change the flow with time and volume and accommodates a wide range of flow rates.

Figure 3.7. Harvard Apparatus Syringe Pump

2.3. Water Flow Tubing System

The water flow system consists of several tubes and valves. The first part is a water reservoir (Figure 3.8), which is connected to the Triaxial cell and the outside of inner cell.

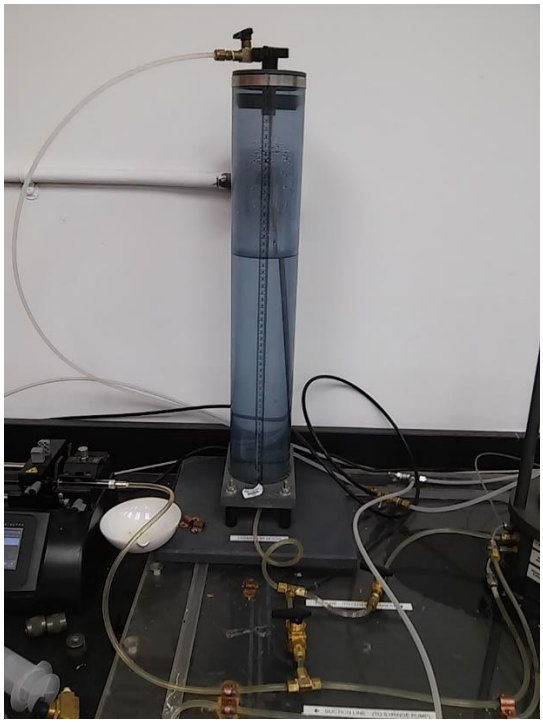

Figure 3.8. Water Reservoir

The reservoir provides the required water for filling up the surroundings of the sample and keeping it saturated throughout the test. There are two valves on the tube connecting the reservoir to the Triaxial cell. One is on the line that goes to the cell and the other is connected to the syringe pump. Upon starting the test, the valve going to the cell is open and the other should be closed. When the pump needs resetting, on the other hand, the valve from syringe pump is open and the valve providing water to the cell is closed.

When the test starts, the differential pressure between the two sides of the sample will change due to the withdrawal of water. Seepage through sample thus begins, causing the soil grains to move and slide through the void spaces and initiate consolidation. There are two connections for the differential pressure transducer to measure the difference of head between two sides of sample. It should be noted that the differential pressure is connected to the sample chamber and bottom of the sample to measure the difference between top and bottom of the sample. Figure 3.9 shows the differential pressure transducer, manufactured by Validyne engineering.

Figure 3.9. Differential pressure transducer

The positive port of the transducer is connected to the Triaxial cell and the negative port is connected to the bottom of the sample. This model of pressure transducer is

specifically designed for industrial pressure measurement applications. It has an on-board microprocessor, which provides high accuracy and stability. It is powered and connected to a data acquisition system via USB port, providing remote digital pressure readings. It is designed for wide range of low pressure measurements with acceptable resistance to vibration. The measurements are taken through a sensitive diaphragm inside of the stainless steel part, which is connected to positive and negative ports.

The final component of the water tubing system is the connection between the bottom of the sample and the syringe pump. A purge valve is also provided for the end of the test, when the water must be emptied and the sample must be removed from the chamber.

In summary, one line feeds the chamber, two lines are connected to the differential pressure transducer, one line is connected to the syringe pump, and one line is meant for emptying the system of water. The Figure 3.10 shows the connections of the different parts with tubes and valves.

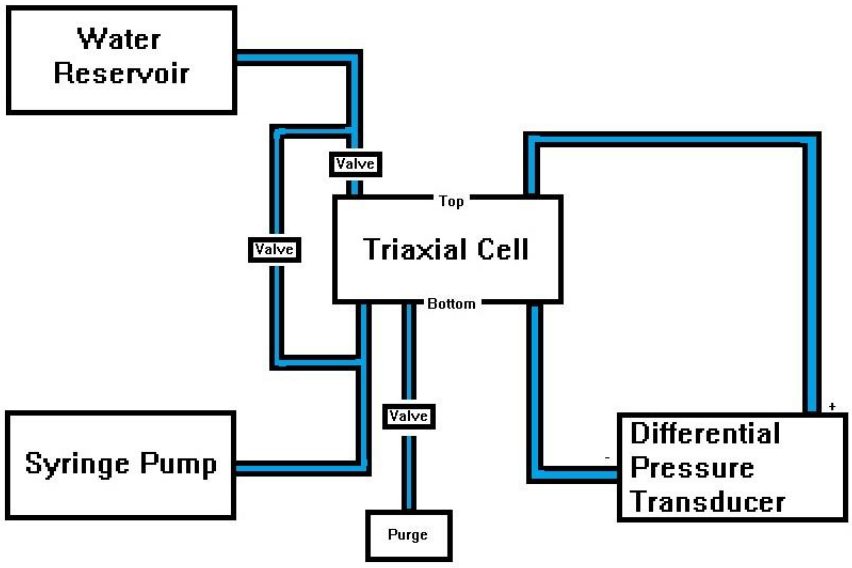

Figure 3.10. Schematic of Water Flow System

2.4. Loading System

The loading system is a dead-weight loading system, which can provide different loads on the sample. The use of a dead weight was selected due to its ease of maintenance and simplicity in trouble shooting. Figure 3.11 shows the loading of the weight. It consists of a connecting circular plate with a steel rod, which rests on the aluminum rod atop the sample, and can be loaded with weights.

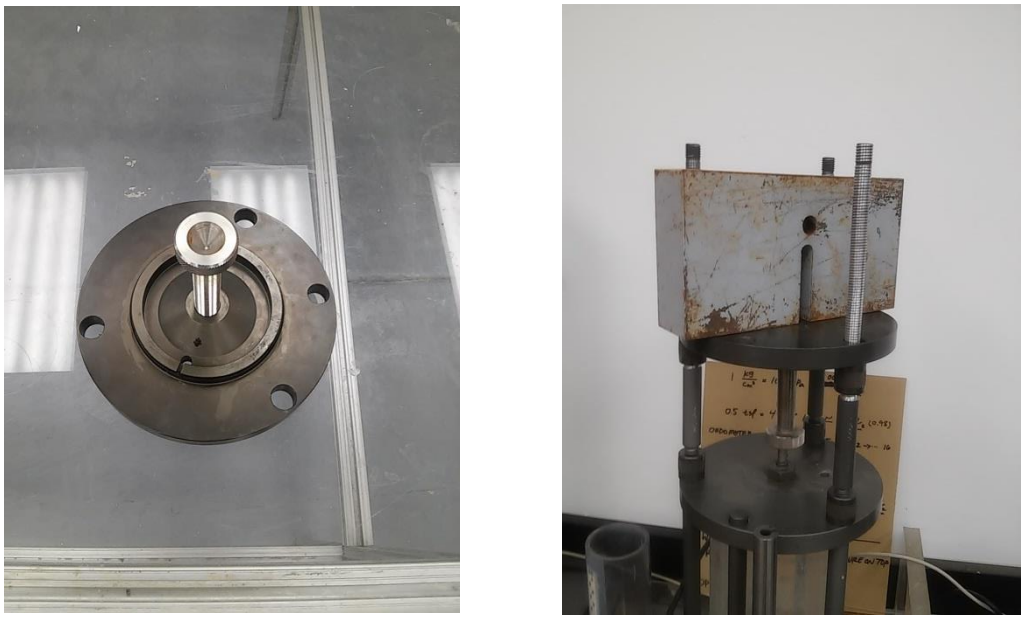

Figure 3.11. Loading System (Dead Weight)

The alternative loading system consists of a Bellofram air cylinder with a pressure sensor underneath, which rests on the loading rod and measures the magnitude of load. These load measurements are recorded via the data acquisition system. The Bellofram has nominal area of nine square inches and can be controlled via a computer (Figure 3.12).

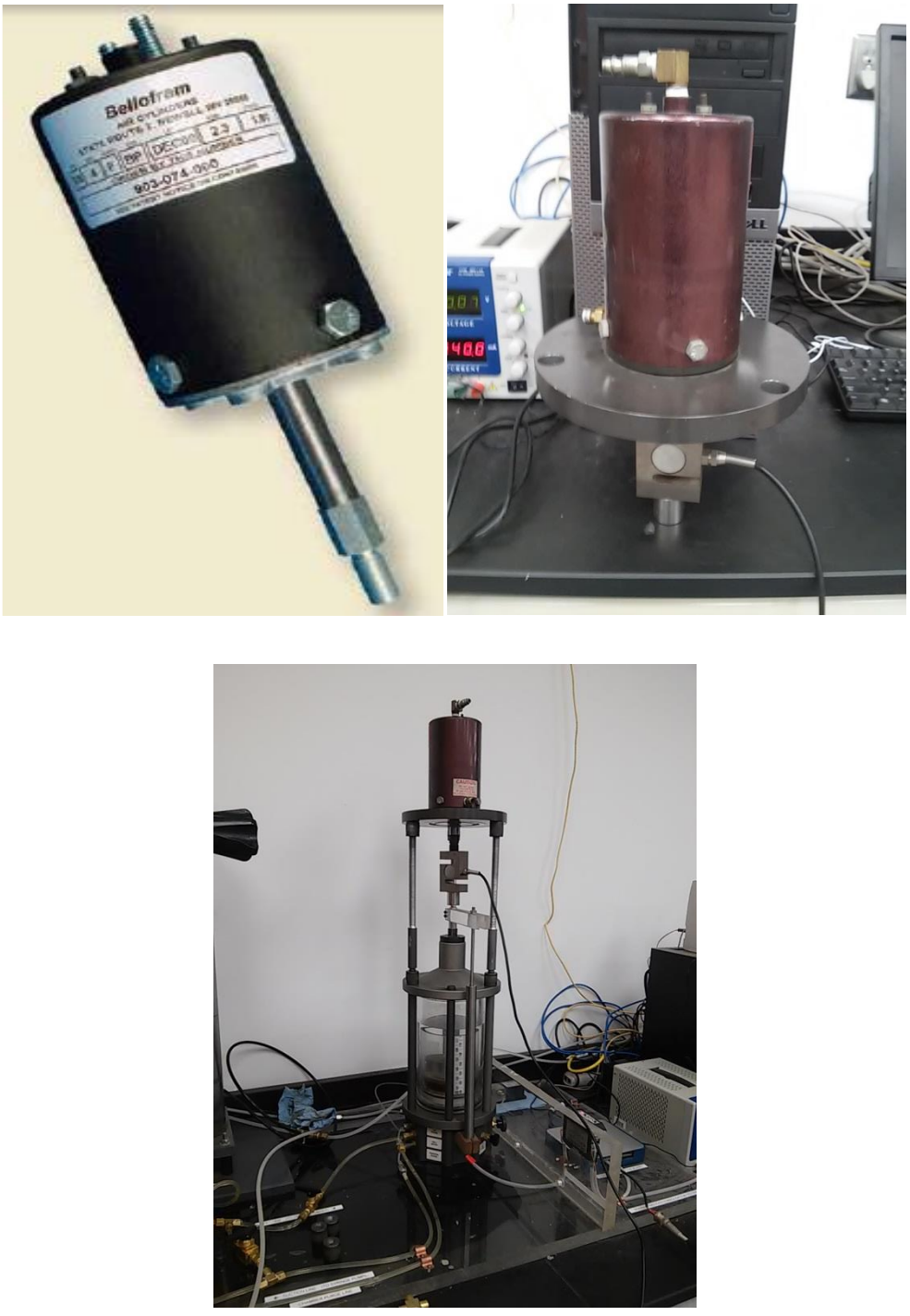

Figure 3.12. Loading System (Bellofram)

Based on the author's experience, the dead weight system is much more reliable and easier to use. Difficulty sealing the valves on the Bellofram can cause leaks in the air pressure system, resulting in loss of pressure on the Bellofram and sample. Since the

loading stage requires that the sample be constantly under uniform pressure, this can cause significant problems in testing.

2.5. Linear Variable Differential Transformer (LVDT)

The LVDT has wide range of applications, including satellites, aircrafts, and hydraulics. It converts the position of linear displacement from a mechanical zero position into two electrical signals. One is the phase showing the direction of the LVDT, and the other is the amplitude for the distance it travels. The LVDT consists of a rod, which is a moving part, and a core assembly, which converts the linear displacement into the electrical signal. LVDTs are inherently frictionless and can produce reliable and repeatable readings. Figure 3.13 shows the LVDT used for this application.

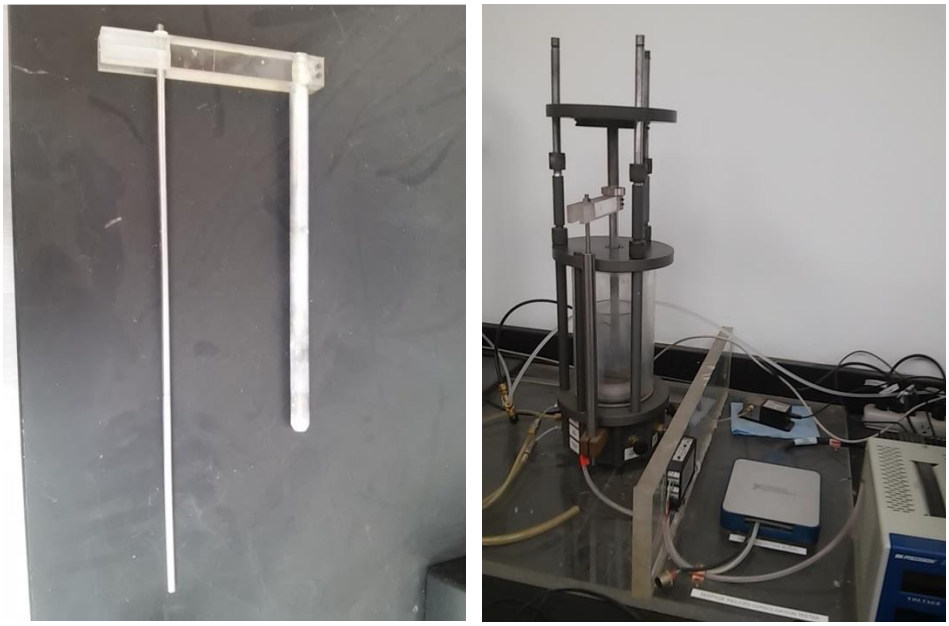

Figure 3.13. LVDT

As shown in the figure, the rod assembly is connected to the vertical load rod to monitor the top cap displacement throughout the test. The core assembly, which converts the linear movement to electrical signal, is connected to the data acquisition unit and records the vertical movement throughout the test.

2.6. Data Acquisition System

The Data Acquisition System (DAQ) is a signal processor that converts real-world physical signals into digital numeric values that can be manipulated by a computer. The DAQ for this apparatus continuously records data from the flow pump, LVDT, and differential pressure transducer. The LabView program is used with a National Instrument data acquisition system in order to record all of the abovementioned data within a Microsoft Excel file for further manipulation. LabView allows for the digital recording and visual presentation of real-time data for the duration of the test. It is very user-friendly and has a short learning time for first-time programmers due to its visual programming aspects. Figure 3.14 shows a view of the real-time data recording of the DAQ. The data shown include the LVDT position, settlement with time, differential pressure and amount of load.

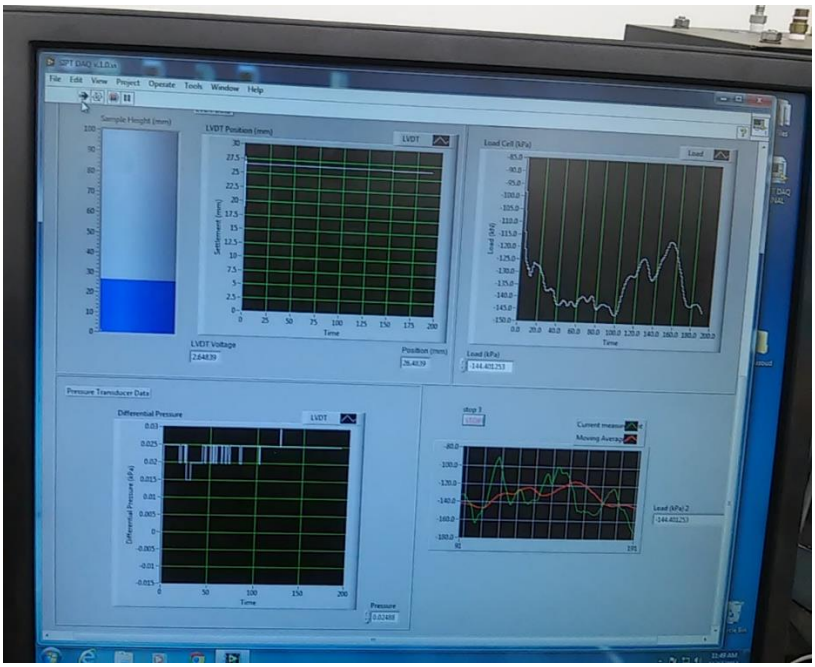

Figure 3.14. Real-time Data Acquisition System

3. General Testing Procedure

The seepage-induced consolidation test has three distinct phases. The first phase involves the sedimentation column. Slurry is left to settle under its own weight, resulting

in a zero stress void ratio i.e. e_0. Figure 3.15 shows a typical sedimentation jar for the first part of consolidation test. The jar has a scale on it to measure the length of supernatant water and solid parts.

Figure 3.15. Sedimentation column

The initial (not zero stress) void ratio is calculated based on the specific gravity of solids and the moisture content, since the sample is saturated. Then the dilute sample is left to settle under its own weight, a process that may take as long as two weeks. Self-weight consolidation happens when the effective stress is almost zero and there is no contact pressure between soil grains. After the sedimentation of the sample is finished, the soil grains come to impose force on each other and consolidation begins.

Following the first stage, the zero void ratio (e_0) is calculated based on the height of solids and total height on the sedimentation column.

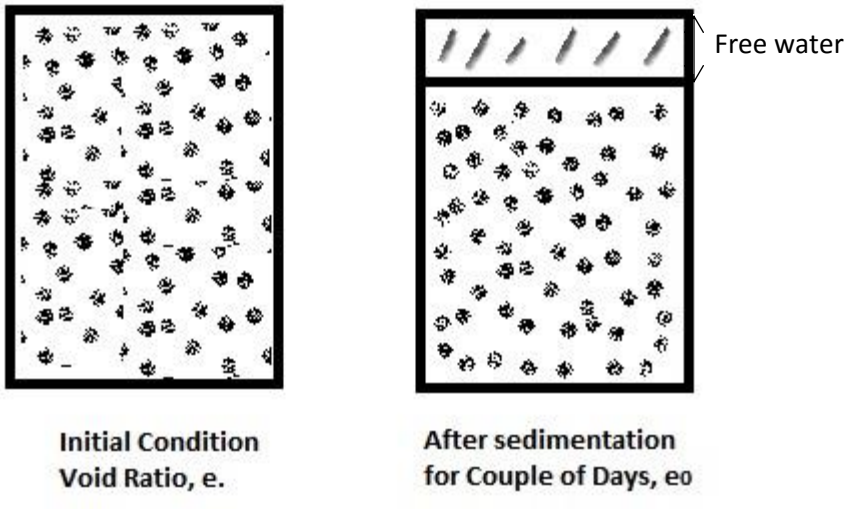

Figure 3.16. Sedimentation column for void ratio calculations

Upon the Initial poring of the slurry, the mixture has a void ratio that can be calculated by Equation 3.7, based on the specific gravity (G_s) and initial saturated ($S_r=1$) water content (w):

$$e \times S_r = w \times G_s \tag{3.7}$$

After sedimentation finishes, there is free water atop the sample (Figure 3.16). At this point, the zero void ratio based on almost zero effective stress can be calculated. Figure 3.17 shows the phase diagram for the calculation of e_0, based on e.

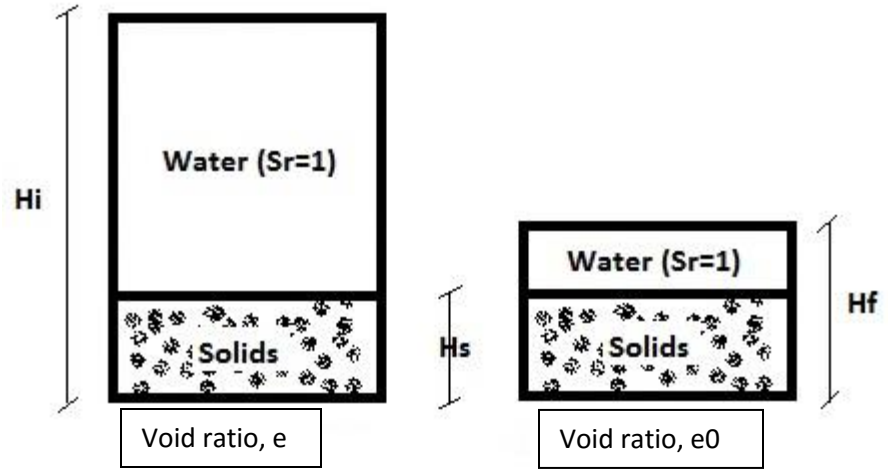

Figure 3.17. Phase diagram for Initial state (left Figure) and after sedimentation (right Figure)

The height of solids, H_s, is constant when the dilute is initially poured and when consolidation is about to start. The void ratio, which is the division of the volume of voids, V_v, by the volume of solids, V_s, can be calculated in Equation 3.8 as:

$$e = \frac{V_v}{V_s} = \frac{H_w \times A}{H_s \times A} = \frac{H_w}{H_s} \tag{3.8}$$

where H_w is height of voids filled with water. Since the sample is saturated at all time, Equation 3.8 can be rearranged and calculated as:

$$e = \frac{H_i - H_s}{H_s} = \frac{H_i}{H_s} - 1 \tag{3.9}$$

where:

$$H_s = \frac{H_i}{1 + e} \tag{3.10}$$

The void ratio at zero effective stress can then be calculated as:

$$e_0 = \frac{H_f}{H_s} - 1 \tag{3.11}$$

The second phase is the seepage phase, in which water is forced to percolate through the sample. This causes differential pressure between the top and bottom of the sample and consolidation begins in low effective stress ranges based on the seepage force. At this stage, the sample is poured into the inner cell of Triaxial chamber and let to settle for a while under its own weight and a small surcharge (about 0.3 kPa). The surcharge weight is made up of the filter paper, porous stone, Plexiglas top cap, and LVDT and loading rod assembly. Once the sample's top surface is finished settling, a small flow rate is applied by the syringe pump from underneath the sample to suck the water through the sample. This water percolation starts the consolidation process, under very small seepage stress between about 0.3 and 1.0 kPa. The settlement and differential pressure between the two sides of sample are monitored and recorded over time via the DAQ system.

The final phase of the test is the loading phase, in which a normal load based on the application (top cap on impoundment ponds) is imposed on the sample. Usually the load is applied in increments up to the desired load, typically about 100 kPa. Then, a flow rate lower than that used in the second phase is imposed on sample to measure the permeability at the lowest void ratio. At the end of the test (Figure 3.18), the sample is oven-dried for the measurement of solid contents. Three void ratios corresponding to the three distinct stages are calculated and used later for the estimation of model parameters.

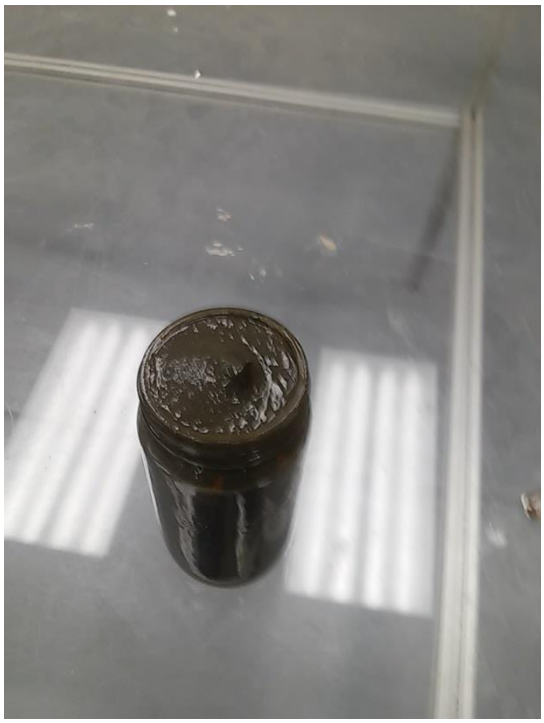

a) Initial condition

b) Sample extrusion after the test

c) Sample from the oven

d) Final result

Figure 3.18. Soil sample at different stages

4. Seepage-induced consolidation Methodology

The use of large strain consolidation theory requires the definition of the compressibility and permeability functions with the void ratio. The follow equations by Liu and Znidarcic (1991) for compressibility and Somogyi (1979) for permeability are used for the constitutive relationships for this research:

$$e = A(\sigma' + Z)^B \tag{3.5}$$

$$k = Ce^D \tag{3.6}$$

These equations are widely accepted because they have proven to be practical for soft soils. In the above equations, e is void ratio, σ' is effective stress, k is hydraulic conductivity and *A, B, Z, C*, and *D,* are consolidation model parameters. In previous formulations, as effective stress reached zero, the void ratio approached infinity; however, in this model, *Z* has the units of stress and *A* and *B* are unit less. Therefore, when the stress approaches zero the void ratio is actually $e_0 = AZ^B$.

The permeability function was proposed in 1979 by Somogyi for low density soils. *C* has the desired unit for hydraulic conductivity and *D* is unit less.

Bartholomeesusen et al. (2002) summarized the numerical models for predicting the constitutive relationships for low density sediments, and concluded that among the models available, Znidarcic's model gives the closest prediction to the experimental data. He used batches of sediment from a river in Belgium, gave the data to different scientists to calibrate their numerical models, and then asked them to predict the next experiment. The calibration data was based on a settling column (0.2-0.6 m in height) with density and pore pressure measurements at different points. The models he used in his studies are presented in Table 3.1.

Table 3.1. Numerical Models in Sidere Study (Bartholomeesun, et al., 2002)

Participants	Dependent variable	Parameter choice
Bartholomeeusen	Void ratio	$e = -1{\cdot}07\ \sigma'^{0.14} + 2{\cdot}52$ $e = 0{\cdot}27 \ln(k) + 5{\cdot}95$
Carrier (Carrier III *et al.*, 1983)	Void ratio	$e = 2{\cdot}933[\text{Pa}]\ (\sigma' + 5{\cdot}32)^{-0.10}$ $k = \dfrac{8{\cdot}96 \times 10^{-9} e^{8.08}}{1+e}$
Lin & Penumadu	Void ratio	$e = -0{\cdot}22 \ln(\sigma') + 1{\cdot}46$ $k = 0{\cdot}0072\, e^{6.75}$
Masala & Chan	Void ratio	$e = 2{\cdot}81[\text{Pa}^{-1}]\ \sigma'^{-0.102}$ $k = 1{\cdot}38 \times 10^{-3}$ m/day $e^{5.75}$
Merckelbach (Merckelbach, 2000)	Solids vol. fraction, Φ $\Phi = \dfrac{\phi_{\text{fines}}}{1-\phi_{\text{sand}}}$	$\sigma' = 3 \times 10^{13}\ \Phi^{-14.3}$ $k = 2 \times 10^{-19}\ \Phi^{14.3}$ (26% fines)
Pyke	Void ratio	Linear interpolation for k(e) and $\sigma'(e)$ from a table
Sills	Excess pore pressure	$\sigma' \leqslant 0{\cdot}2$ $e = -0{\cdot}21 \ln(\sigma') + 1{\cdot}26$ $\sigma' > 0{\cdot}2$ $e = -0{\cdot}11 \ln(\sigma') + 1{\cdot}42$ $c_v = 3 \times 10^{-7}$ m^2/s
Van Kesteren (Van Kessel & Van Kesteren, 2002)	Void ratio	$\sigma' = \exp(11{\cdot}27 - 8{\cdot}0\ e)$ $k = \exp(-21{\cdot}55 + 3{\cdot}6\ e)$
Winterwerp (Winterwerp, 1999)	Solids vol. fraction Φ	$\sigma' = 6 \times 10^{-6}\ \Phi^{-19}$ $k = 1{\cdot}6 \times 10^{-10}\ \Phi^{19}$
Znidarčić (Yao *et al.*, 2002)	Void ratio	$e = 1{\cdot}69\ (\sigma' + 0{\cdot}046)^{-0.12}$ $k = 4{\cdot}14 \times 10^{-9} e^{6.59}$

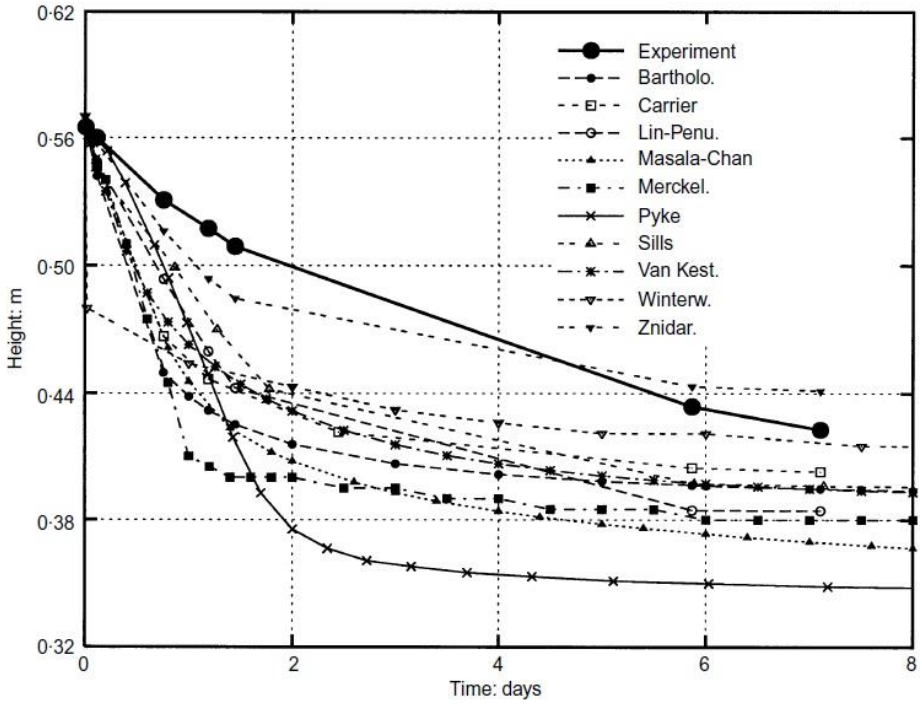

Figure 3.19. Comparative study between different settlement prediction models (Bartholomeeusen, et al., 2002)

Figure 3.19 shows the comparative study based on the models on Table 3.1. As shown in the figure, the first part of the settlement in the early stages of consolidation happens very quickly. In the first couple of days (1-3 days), the amount of surface settlement is significant. The Znidarcic model proved to be the best model in prediction of settlement between the models presented in Sidere's study. Therefore, it will be used for the purpose of this thesis.

The governing equation for finite strain consolidation is in the form:

$$\left(\frac{\gamma_s}{\gamma_w}-1\right)\frac{d}{de}\left[\frac{k(e)}{(1+e)}\right]\frac{\partial e}{\partial z}+\frac{\partial}{\partial z}\left[\frac{k(e)}{\gamma_w(1+e)}\frac{d\sigma'}{de}\frac{\partial e}{\partial z}\right]+\frac{\partial e}{\partial t}=0 \tag{2.34}$$

At the steady-state condition, the void ratio is constant with time since the soil does not undergo any consolidation and soil grains do not move. Therefore the term $\frac{\partial e}{\partial t}$ is equal to zero and the governing equation becomes:

$$\left(\frac{\gamma_s}{\gamma_w}-1\right)\frac{d}{de}\left[\frac{k(e)}{(1+e)}\right]\frac{\partial e}{\partial z}+\frac{\partial}{\partial z}\left[\frac{k(e)}{\gamma_w(1+e)}\frac{d\sigma'}{de}\frac{\partial e}{\partial z}\right]=0 \tag{3.12}$$

At this state, compressibility is highly non-linear (Abu-hejleh & Znidarcic, 1994). In addition, the steady-state condition is controlled by the compressibility and permeability functions of the soil. This is why measured data is necessary for the estimation of these functions.

Rewriting the effective stress equation in integral form, we have:

$$\int_0^z \frac{d\sigma'}{dz}dz=\int_0^z \frac{d\sigma}{dz}dz-\int_0^z \frac{dU_h}{dz}dz-\int_0^z \frac{dU_e}{dz}dz \tag{3.13}$$

where U_h, is hydrostatic water pressure, U_e is excess pore water pressure, σ' is effective stress, and σ is total stress. As stated earlier:

$$\frac{dU_e}{dz} = \frac{v_d \times \gamma_w}{k}(1+e) \tag{3.14}$$

$$\frac{dU_h}{dz} = (1+e)\gamma_w \tag{3.15}$$

$$\frac{d\sigma}{dz} = (e\gamma_S + \gamma_w) \tag{3.16}$$

$$\int_0^z \frac{d\sigma'}{dz}\,dz = \sigma'_Z - \sigma'_0 \tag{3.17}$$

In the above equations, v_d is the Darcian velocity of water. This is also known as the relative velocity between the water and soil particles, since they do not consolidate in steady-state phase. The governing equation is now:

$$\sigma'_Z - \sigma'_0 = \int_0^z (e\gamma_S + \gamma_w)\ dz - \int_0^z (1+e)\gamma_w\,dz - \int_0^z \frac{v_d \times \gamma_w}{k}(1+e)\,dz \tag{3.18}$$

which can be rewritten in the form of:

$$\sigma'_Z = \sigma'_0 + \int_0^z (\gamma_S - \gamma_w)\ dz - \int_0^z \frac{v_d \times \gamma_w}{k}(1+e)\,dz \tag{3.19}$$

Equation 3.19 is the governing equation of finite strain consolidation in steady-state phase. The first term is the applied load (σ'_0), the second term is the self-weight effect and the third term is the seepage force. In order to find the five model parameters, *A, B, Z, C* and *D*, an iterative procedure is used. In addition, the effective stress at the bottom of the sample and final height of the sample are calculated. Different data is collected

throughout the test. The zero effective stress void ratio, e_0, is collected from the sedimentation column. The steady state height, H_s, and effective stress, σ'_b, at the bottom of the sample is collected from the seepage phase. The final effective stress, σ'_f, permeability, k_f, and final void ratio, e_f, are collected from the step loading phase. All of these data are used to produce the constitutive relationships (e-k and e- σ'). Based on these relationships, the final height and bottom effective stress of the sample in steady state can be calculated using Equation 3.19 which then will be compared with the test final height and effective stress.

Therefore, for the calculation of model parameters:

$$A = \frac{e_0}{Z^B} \tag{3.20}$$

$$C = \frac{K_f}{{e_f}^D} \tag{3.21}$$

$$Z = \frac{\sigma'_f}{(\frac{e_f}{e_0})^{\frac{1}{B}-1}} \tag{3.22}$$

Initially, B and D are guessed and the other three, A, C and Z are calculated based on these above equations. Then, based on initial height of the sample, H_i, and the zero stress void ratio, e_0, the height of solids is calculated:

$$H_s = \frac{H_i}{1 + e_0} \tag{3.23}$$

The H_s is divided into 10 points, at each of which the effective stress and the void ratio and permeability are calculated, based on the governing equation at steady-state seepage and constitutive relationships, respectively. The first iteration does not include any seepage force, therefore there only exists effective stress due to self-weight and top

imposed stress. From this effective stress, the void ratio and permeability can be calculated for each point. Then the bottom effective stress is calculated based on the governing equation. From this new value for bottom effective stress, a new set of void ratios and permeability are calculated. The procedure continues until the difference between the two void ratios at each point is negligible.

Chapter 4 Numerical Modeling and Laboratory Results

1. SICT Data Analysis

As stated in the previous chapter, the model used to calculate the constitutive relationships of the sediments is based on the works by Liu and Znidarcic (1991) for the void ratio-stress relationship (Equation 3.5) and Somogyi (1979) for the permeability function (Equation 3.6):

$$e = A(\sigma' + Z)^B \tag{3.5}$$

$$k = Ce^D \tag{3.6}$$

The compressibility function is widely used because, at zero effective stress, it overcomes the other models' deficiencies and the zero stress void ratio, e_0, can be defined as, AZ^B.

Five parameters, *A, B, Z, C*, and *D,* must be determined through experimentation. The seepage-induced consolidation test and the inverse problem solution, which identify the final height and bottom effective stress at steady state, enable the determination of these five parameters.

The SICTA program by Abu-Hejleh and Znidarcic (1994) was developed in accordance with the seepage-induced consolidation test to determine the model parameters. It employs an iterative scheme to solve the governing equation of consolidation at steady state. The void ratio at zero effective stress is calculated Based on the seepage-induced consolidation test. In addition, the bottom effective stress and sample height at steady state are recorded (σ'_b, H_{ss}).

The final effective stress at the step loading phase, hydraulic conductivity, and final void ratio are calculated at the conclusion of the test, enabling the estimation of the five model parameters. Based on the iterative procedure, data from the beginning and end of

the test are used to back-calculate the steady state parameters (σ'_b and H_{ss}). This procedure continues in iterations until the difference between the calculations and actual measurements is minimal.

The iterations start with assumed values for *B* and *D*. Solutions are found for *A, Z* and *C*, then for each set of the five parameters, the void ratio distribution at steady state is determined. By assuming *B* and *D*, the other three parameters, based on the steady-state measurements, are:

$$A = \frac{e_0}{Z^B} \tag{3.20}$$

$$C = \frac{K_f}{{e_f}^D} \tag{3.21}$$

$$Z = \frac{\sigma'_f}{(\frac{e_f}{e_0})^{\frac{1}{B}-1}} \tag{3.22}$$

The initial guesses yield the first set of five parameters, then *B* and *D* are modified in the iterative scheme.

The iterative scheme consists of dividing the height of solids into nodes. The height of solids maintains a constant value throughout the test. It is calculated by:

$$H_s = \frac{H_i}{1 + e_0} \tag{3.23}$$

where H_i is the initial height of the sample. The height of the sample at steady state or at the final stage may alternatively be used, but the void ratio should be used accordingly. For example, the final height of the sample is used to measure the height of solids, and then e_f must be used in the denominator.

After the height of solids is divided to a certain number of nodes, *N*, the void ratio distribution is calculated for each node in a way that simultaneously satisfies the constitutive relationships and governing equation. The first iteration is based on the effective stress calculation regarding self-weight and top cap only; initially, there is no seepage stress imposed. The void ratio is then calculated for each node based on Equation 3.5. Based on the calculated void ratio, the permeability is calculated by Equation 3.6. The next step involves calculation of the new effective stress using Equation 3.19, based on the permeability and void ratio, and considering the seepage force effect.

$$\sigma'_Z = \sigma'_0 + \int_0^Z (\gamma_S - \gamma_w)\, dz - \int_0^Z \frac{v_d \times \gamma_w}{k}(1+e)\, dz \tag{3.19}$$

Using the new effective stress value, the new void ratio is calculated via Equation 3.5. This process continues until the difference between two consecutive iterations is satisfactory. Table 4.1 shows the iterative scheme.

Table 4.1. Iterative scheme for Void ratio calculations

Node #	Z	$(\sigma'z)_1$	e_1	K_1	$(\sigma'z)_2$	e_2	K_2	…	$(\sigma'z)_n$	e_n	K_n
1	(Hs/N)x1										
2	(Hs/N)x2										
…	…										
N-1	(H_s/N)x(N-1)										
N	Hs										

For each set of *B* and *D*, this iterative scheme is followed and the steady state height, H_n, and bottom effective stress, σ'_{Bn} are calculated:

$$H_n = \int_0^{Hs}(1+e)dz \tag{4.1}$$

$$\sigma'_{Bn} = \left(\frac{e_B}{A}\right)^{\frac{1}{B}} - Z \tag{4.2}$$

where, e_B is the estimated void ratio at the bottom of the sample based on the last step of iterations.

A Microsoft Excel spread sheet was created for the iteration scheme, and the Excel Solver function was used to find the best solution for the five parameter estimation. Three different values for the effective stress at zero, steady state and step loading are used with corresponding void ratios in Equation 3.5 to find the three unknown parameters*, A, B,* and *Z*.

Figure 4.1 shows an example of the Excel Solver program for solving three equations for three unknowns (A, B, and Z) with three sets of known values, (e_0, σ'_0; e_s, σ'_s; and e_f, σ'_f).

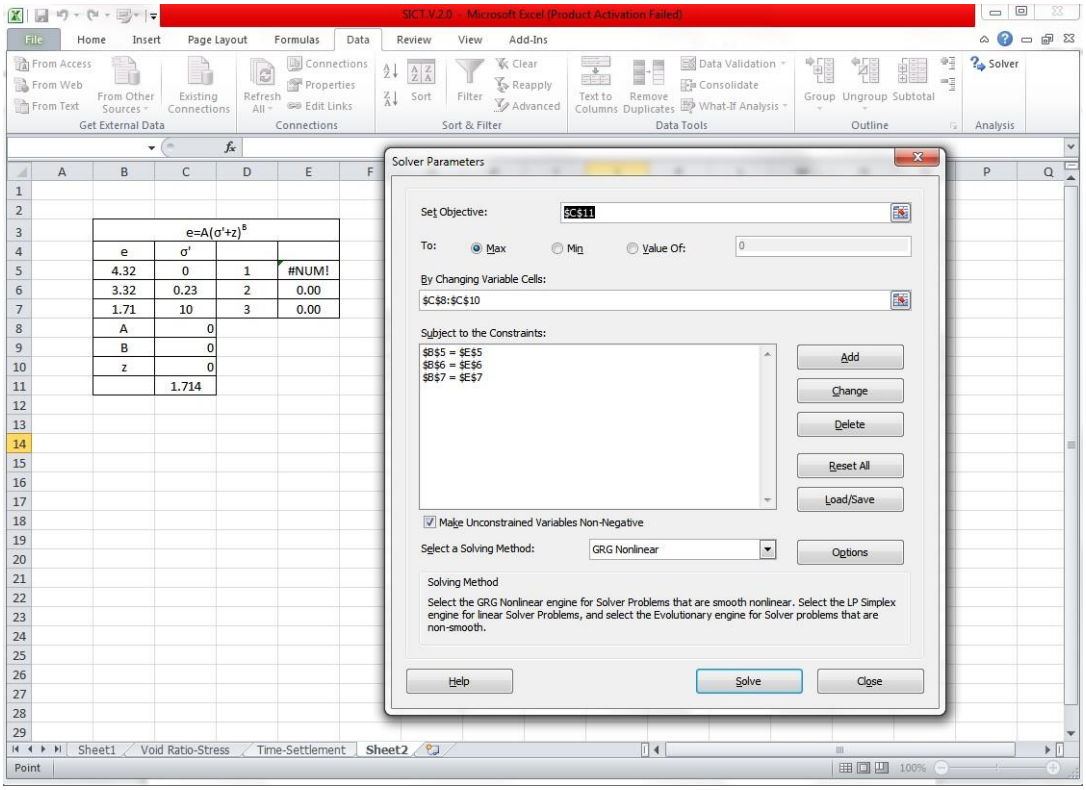

Figure 4.1. Excel Solver program for parameter estimation

In Figure 4.1, cells B5:B8 contain the void ratio values obtained from the seepage-induced consolidation test. The parameter values are found within cells C8:C10. The calculated effective stresses based on the estimated parameters are in cells E5:E7. The equation used for the calculated effective stresses is based on Equation 4.1. Cell C11 contains the difference between any of the calculated values in columns E and B. Any stage may be used for optimization. In this case, the final void ratio's difference is minimized by changing the model parameters *A, B*, and *Z*.

Excel Solver's purpose is to find a solution that satisfies all of the constraints and optimizes the objective cells' values. The required time for solution depends primarily on the complexity of the model, the number of parameters involved, and the type of mathematical relationship.

In this case, the objective cell is C11. The optimization constraint is the equality of cells C5:C7 to E5:E7. This equality is made possible by changing the values in cells C8:C10.

If an attempt is made to run Solver without an initial guess, an error message is displayed. Figure 4.2 shows one such error message.

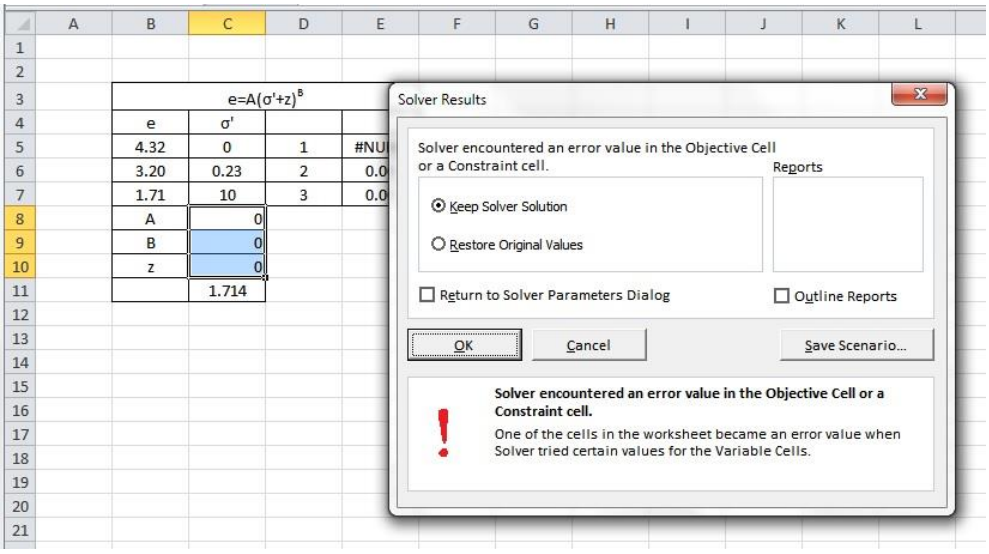

Figure 4.2. Error message for the first solution

However, if the initial guess for the cells C8:C11 is applied, as shown in Figure 4.3, a solution like the one shown in Figure 4.4 is achieved.

	A	B	C	D	E	F
1						
2						
3		$e=A(\sigma'+z)^B$				
4		e	σ'			
5		4.32	0	1	1.00	
6		3.20	0.23	2	1.23	
7		1.71	10	3	11.00	
8		A	1			
9		B	1			
10		z	1			
11			-9.286			
12						
13						

Figure 4.3. Initial guesses for model parameters

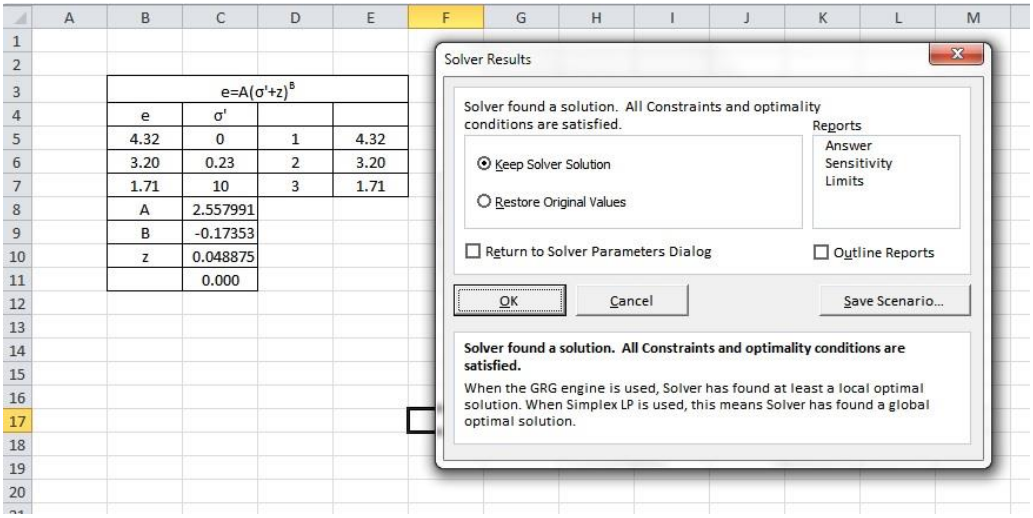

Figure 4.4. Solution message

Through this method, the three unknown model parameters can be easily determined. The other two parameters, *C* and *D*, are readily calculated by adding a power function trend line to the *e-k* graph for two values of the void ratio versus two permeability measurements, at steady state and step loading stage. This is shown in Figure 4.5. In this case, *C* is equal to 10^{-13}, and *D* is equal to 11.447.

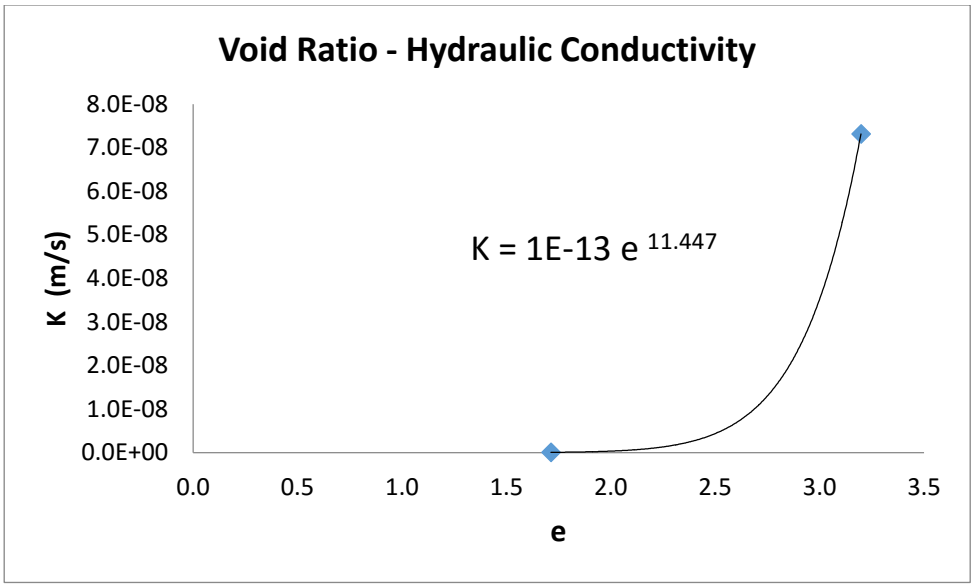

Figure 4.5. Void Ratio-Hydraulic Conductivity graph for model parameter estimation

2. SICT benchmark testing

Following the construction of the seepage induced consolidation tester in the Rutgers soil and sediment management laboratory, two check tests were performed on Kaolinite Clay and compared with test results from Znidarcic at the Boulder CU laboratory and Estepho at the UBC laboratory which is reported in Estepho (2014). The benchmark testing helped to build confidence in the repeatability and reliability of the manufactured device. The sample of Georgia Kaolinite Clay was prepared with an initial water content of 136%, resulting in an initial void ratio of 3.67. The initial sample data are presented in Table 4.2.

Table 4.2. Initial Sample Characteristics

	Initial Water content	Specific Gravity G_s	Initial Void ratio e	Solid Content
Kaolinite Clay	136%	2.7	3.67	42%

The results of the seepage-induced consolidation test and sedimentation column are presented in Table 4.3.

Table 4.3. Sedimentation Column and Seepage-induced consolidation test results

Test #	Void Ratio			Height			Effective Stress			Permeability	
	e_0	e_s	e_f	H_i (mm)	H_s (mm)	H_f (mm)	σ'_0 (kPa)	σ'_{ss} (kPa)	σ'_f (kPa)	K_{ss} (m/s)	K_f (m/s)
1	3.52	2.18	0.97	25.22	17.75	11	0.0	1.30	140.0	1.46E-08	4.22E-10
2	3.36	2.09	1.01	23.52	16.68	10.83	0.0	1.80	110.0	2.74E-08	5.42E-10

The resulting compressibility and permeability functions are given as follows:

Test 1,

$$e = 2.309(\sigma' + 0.0907)^{-0.175}$$

$$k = 5E - 10\ e^{4.28}$$

Test 2,

$$e = 2.339(\sigma' + 0.130)^{-0.178}$$

$$k = 5E - 10\ e^{5.37}$$

The average results of tests from University of Colorado at Boulder and the University of British Columbia are presented in Table 4.4.

Table 4.4. Comparison of Results, CU, UBC, and Rutgers

	Compressibility	Permeability
CU Boulder	$e = 2.332(\sigma' + 0.075)^{-0.181}$	$k = 5.9E - 10\ e^{4.22}$
UBC	$e = 2.559(\sigma' + 0.317)^{-0.175}$	$k = 6.73E - 10\ e^{4.03}$
Rutgers	$e = 2.324(\sigma' + 0.11)^{-0.176}$	$k = 5E - 10\ e^{4.82}$

A comparison of the three different test results is presented in Figure 4.6 and Figure 4.7.

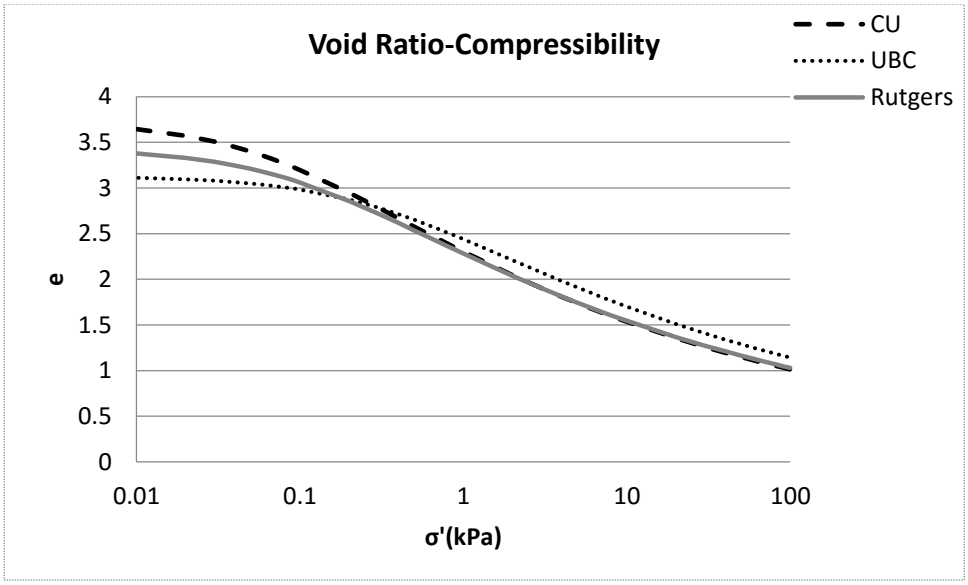

Figure 4.6. Comparison of Results (Compressibility Curve)

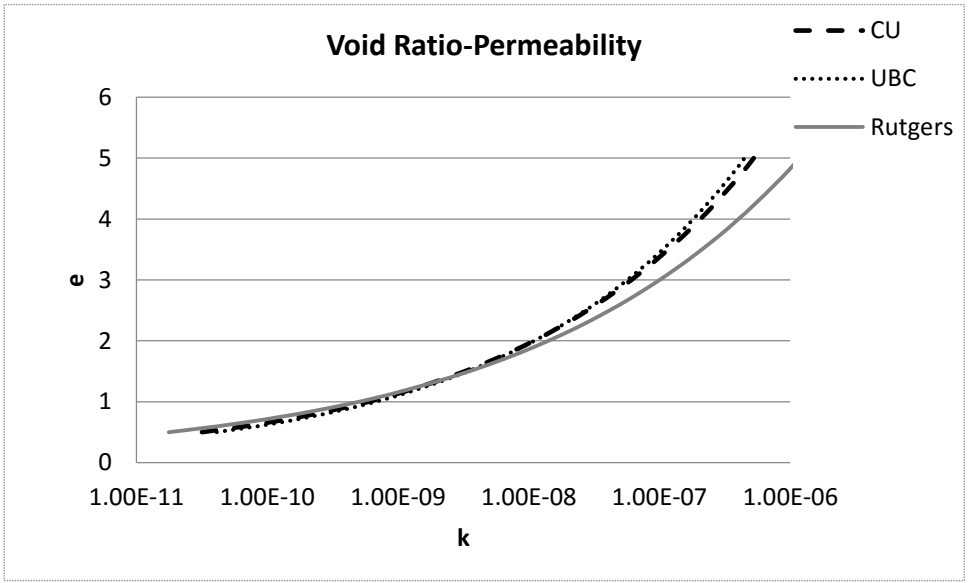

Figure 4.7. Comparison of Results (Permeability Curve)

The benchmark test results compare well with the results of UBC and CU laboratory tests. This assures that the testing procedures and data analysis at Rutgers are in good compatibility with previous seepage-induced consolidation test setups. The following sections of this thesis present the results of eleven seepage-induced consolidation tests on samples taken from Newark Bay area. Each sample is tested for index properties, and

then sedimentation tests and seepage-induced consolidation tests are performed on the samples.

2.1. Index property tests

The index property tests are designed to indicate each sample's natural moisture content, grain size distribution (by wet sieve analysis and hydrometer tests), Atterberg limits, and soil particle specific gravity.

Table 4.5 presents the natural moisture content of the samples, specific gravity of solids, and Atterberg limits (Liquid limit and Plastic Limit).

Table 4.5. Natural Moisture Content

Test #	1	2	3	4	5	6	7	8	9	10	11
w%	193.61	183.53	189.6	207.02	193.61	195.7	193.7	189.78	181.36	182.53	195.6
Gs	2.61	2.55	2.58	2.42	2.68	2.95	2.52	2.38	2.34	2.31	2.81
LL%	128	118	120	125	119	124	116	121	110	120	130
PL%	98	85	87	94	82	74	88	95	91	99	71

The grain size distribution curves for the eleven samples are presented in Figure 4.8.

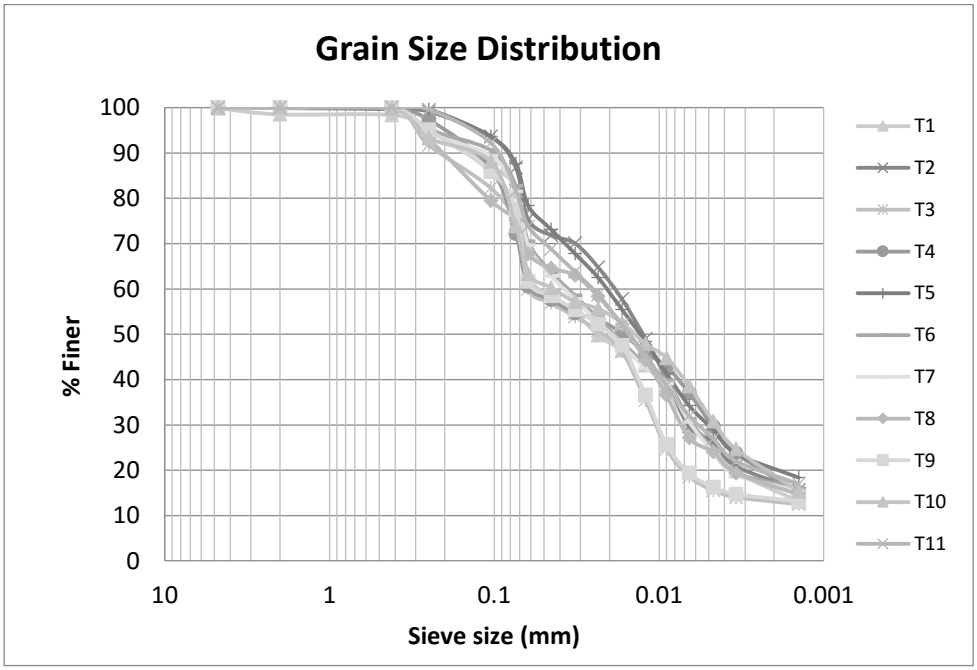

Figure 4.8. Grain Size distribution

The wet sieve analyses are performed based on the ASTM C117 procedures and the hydrometer tests are based on the ASTM D422 procedures. As is shown in Figure 4.8, the samples are between 55 to 75 percent finer than sieve 200. The detailed test results are presented in Appendix A.

2.2. Numerical Simulation

The constitutive relationship obtained by Microsoft Excel's Solver function is used as an input for the numerical solution of the governing equation. Yao and Znidarcic (1997) developed a one-dimensional large strain consolidation and desiccation computer model that uses the finite difference implicit method to solve the nonlinear equation of large strain consolidation. The numerical simulation of the settlement-time curve for the samples is computed via this program. In other words, the program uses the constitutive relationships developed by the seepage test at steady state to simulate the observed settlement with time. If the constitutive relationships are well-defined, the program's predictions should suitably fit the observations.

3. Results

The results of the seepage-induced consolidation tests for eleven sediment samples and five soft clay samples are presented in the following sections. The index properties of the samples are also correlated with the seepage-induced consolidation model parameters.

3.1. Sediment Sample Results

The detailed results of the eleven seepage-induced consolidation tests on samples obtained from Newark Bay are presented in Appendix A. Table 4.6 shows the result of numerical estimation of constitutive relationships.

Table 4.6. Constitutive relationship

Test	Compressibility	Permeability
1	$e = 2.557(\sigma' + 0.0485)^{-0.173}$	K (m/s) = 1E-13 $e^{11.447}$
2	$e = 2.803(\sigma' + 0.0449)^{-0.154}$	K (m/s) = 9E-12 $e^{5.367}$
3	$e = 2.859(\sigma' + 0.1354)^{-0.209}$	K (m/s) = 2E-11 e^{6}
4	$e = 3.164(\sigma' + 0.0208)^{-0.117}$	K (m/s) = 2E-16 $e^{14.461}$
5	$e = 2.807(\sigma' + 0.0964)^{-0.196}$	K (m/s) = 5E-11 $e^{5.038}$
6	$e = 2.18(\sigma' + 0.2317)^{-0.401}$	K (m/s) = 2E-10 $e^{5.188}$
7	$e = 2.669(\sigma' + 0.0341)^{-0.136}$	K (m/s) = 3E-14 $e^{11.422}$
8	$e = 3.266(\sigma' + 0.1501)^{-0.176}$	K (m/s) = 3E-13 $e^{9.561}$
9	$e = 3.142(\sigma' + 0.1387)^{-0.123}$	K (m/s) = 3E-16 $e^{15.35}$
10	$e = 2.959(\sigma' + 0.0435)^{-0.114}$	K (m/s) = 5E-17 $e^{16.053}$
11	$e = 2.757(\sigma' + 0.485)^{-0.773}$	K (m/s) = 4E-12 $e^{4.882}$

Figure 4.9 and Figure 4.10 present the compressibility and permeability results of the samples.

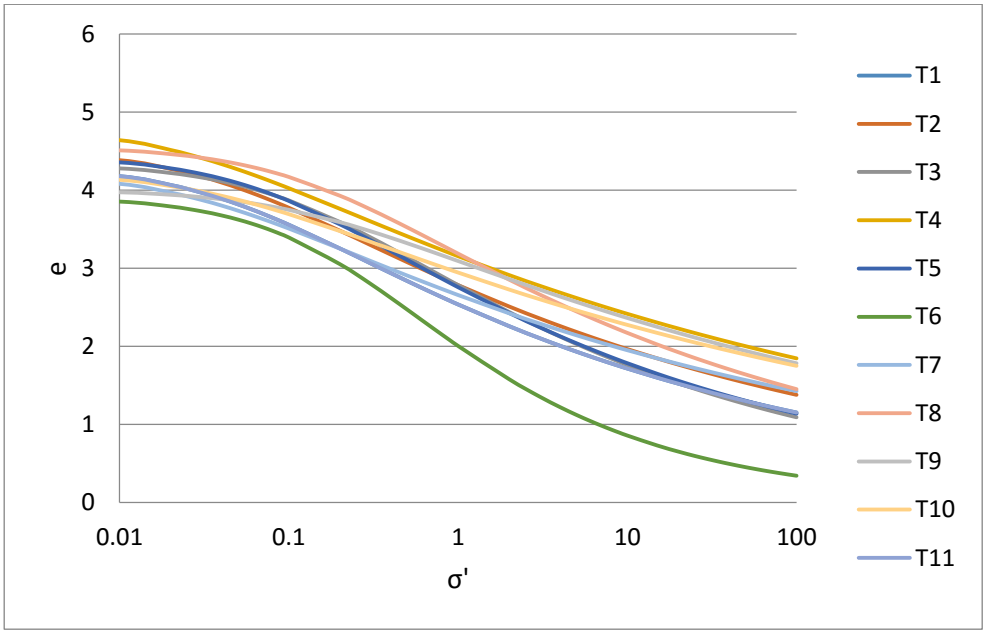

Figure 4.9. Compressibility Comparison

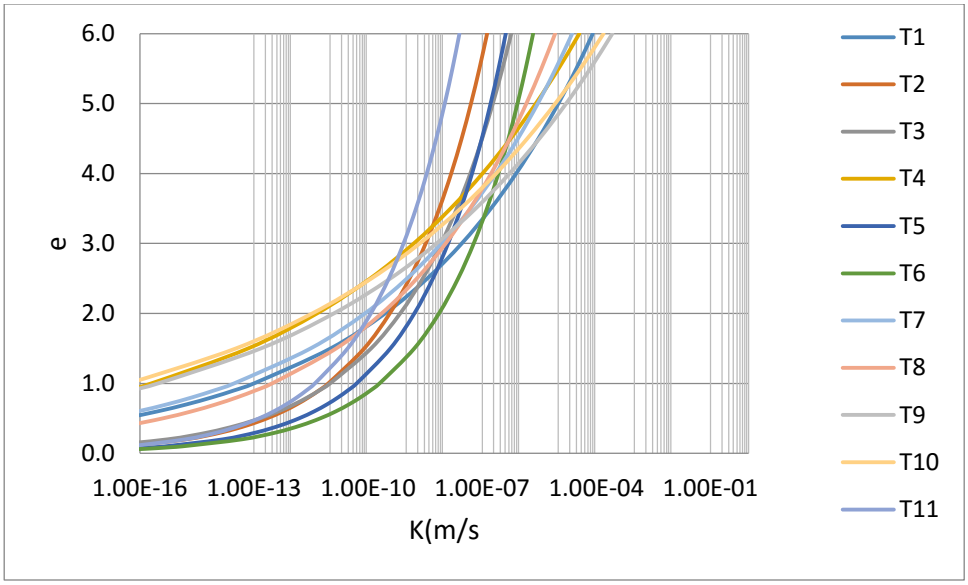

Figure 4.10. Permeability Comparison

The full result for one of the tests is presented below. The remaining details are included in Appendix A. A summary of the seepage test is provided in Table 4.7.

Table 4.7. Seepage test summary

G_s	e_i	e_{00}	e_s	e_f	k_s (m/s)	k_f (m/s)	σ'_s (kPa)	σ'_f (kPa)	Q_s (nl/s)	Q_f (nL/min)
2.61	5.05	4.319	3.2	1.71	7.31E-08	5.8E-11	0.22	10	100	15

The estimation of parameter based on Microsoft Excel's Solver program is presented in Table 4.8.

Table 4.8. Model Parameters

A	B	Z	C	D
2.557	-0.173	0.048	1.00E-13	11.447

Figure 4.11 shows the observed time settlement curve for the seepage-induced consolidation test.

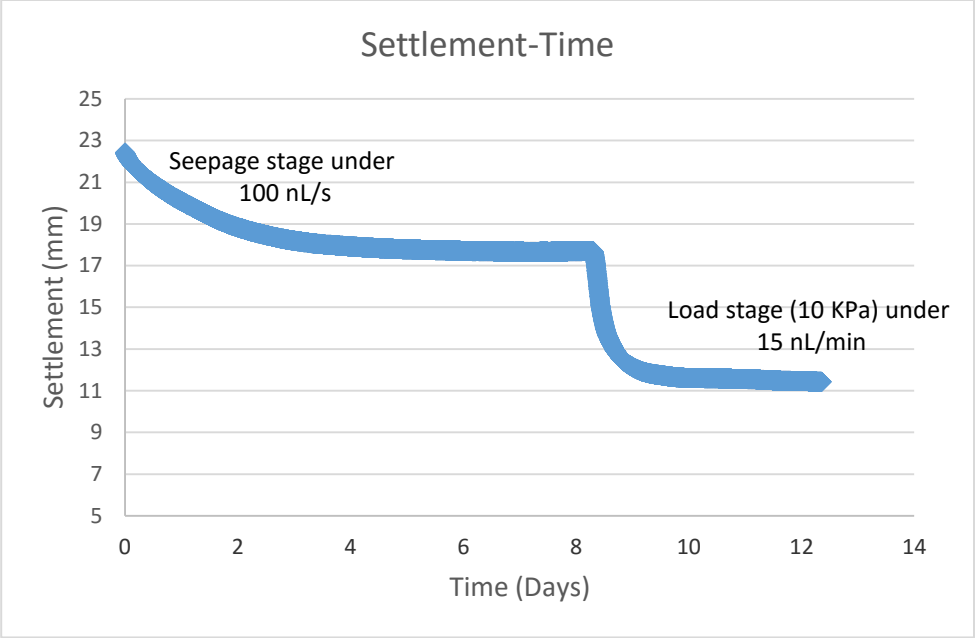

Figure 4.11. Observed Time-Settlement curve (Test 1)

The compressibility curve, based on the model's estimation parameters, is presented in Figure 4.12.

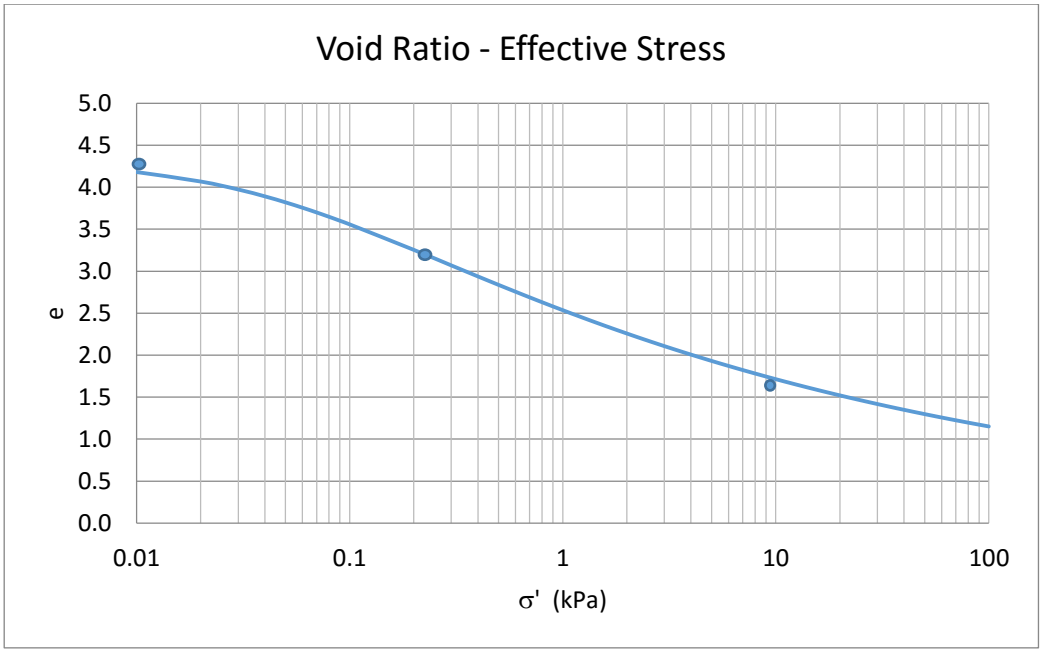

Figure 4.12. Compressibility Curve (Test 1)

The following compressibility equation is used to find the numerical solution:

$$e = 2.557(\sigma' + 0.0485)^{-0.173}$$

The permeability curve is presented in Figure 4.13.

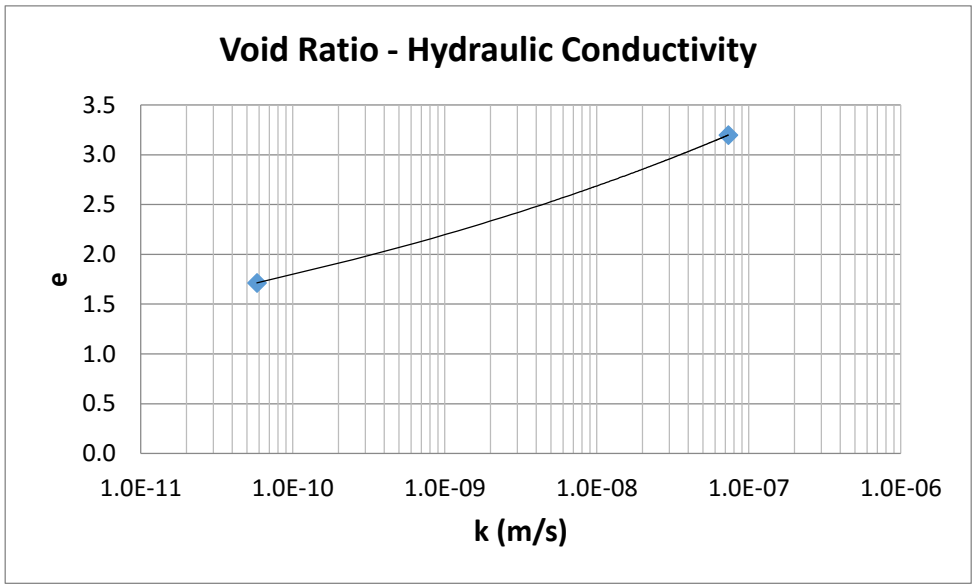

Figure 4.13. Permeability Curve (Test 1)

The corresponding permeability equation, in terms of the void ratio, is:

$$k(\text{m/s}) = 1\text{E-}13\ e^{11.447}$$

The model parameters are input to the CONDES.0 program to simulate the time settlement curve and make comparisons with the observed test data. Figure 4.14 presents a comparison between the numerical simulation and the observed test data.

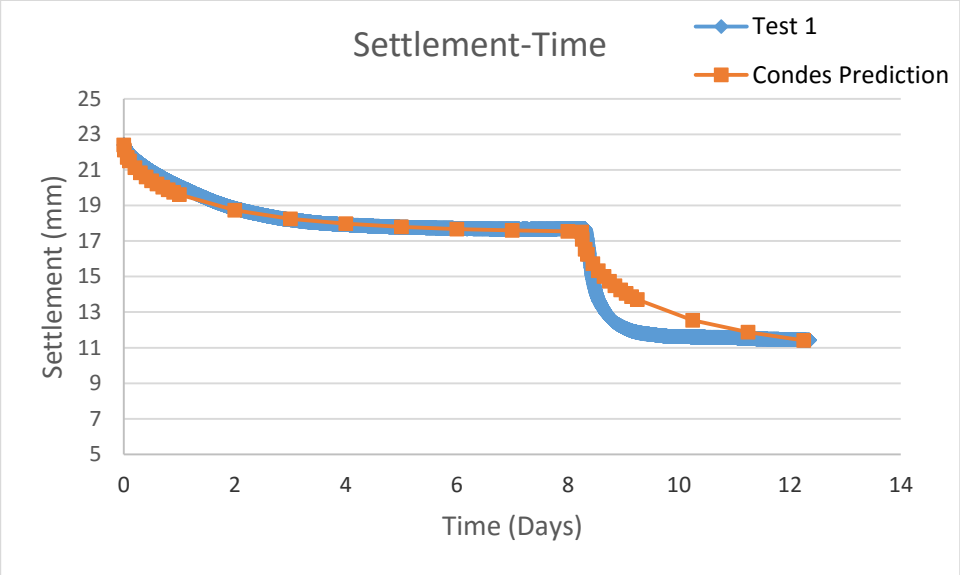

Figure 4.14. Numerical Simulation (Test 1)

The numerical simulation shows good compatibility between the observed and modeled settlements, confirming the capability of the model and model parameter estimator. From Figure 4.15 it can be concluded that there is a slight divergence from the observed data as the time settlement curve goes into the step loading phase.

3.2. Soft Clay Results

Five different soft clays were used to provide different plasticities and investigate the correlation of index properties and consolidation model parameters (*A, B, Z, C*, and *D*). A total of five samples were prepared for consolidation tests. To prepare the samples, water was added to dry soil until moisture content reached 133%. Clays with 133% moisture content (0.43 solids content) are believed to be moist enough to display soft sediment behavior. A summary of the soil and sediment sample tests is presented in Table 4.9.

Table 4.9. Summary of samples and tests

Type	Designation	Test Type
Kaolin Red Clay	KR	Gs (ASTM D854), Atterberg Limits (ASTM D4318), Natural water content (ASTM D2216), Hydrometer test (ASTM D422) Seepage-induced consolidation (SICT)
Kaolin White Clay	KW	
Sea Clay	SC	
Moroccan Clay	MC	
Rhassoul Clay	RC	

Index Properties

The natural water content (Wn), specific gravity of solids (Gs), Atterberg limits (LL, PL) and a hydrometer test were used to obtain the index properties of the materials for this research. The grain size distributions of the sediments are presented in Figure 4.15.

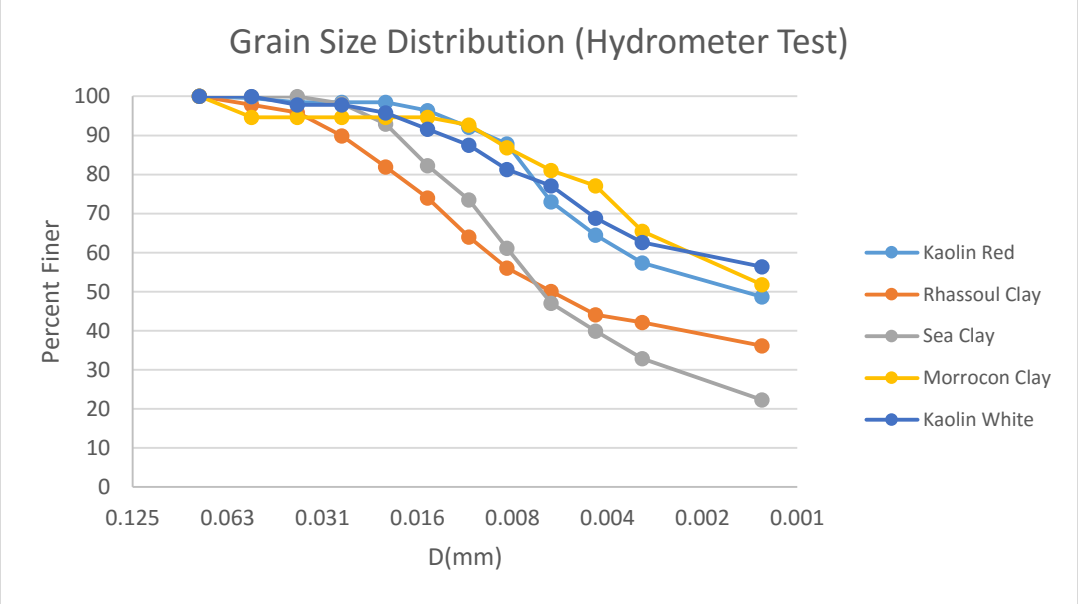

Figure 4.15. Grain Size Distribution

A summary of the index property test results is presented in Table 4.10.

Table 4.10. Index Properties of Soft Clays

	Kaolin Red	Rhassoul Clay	Sea Clay	Moroccan Clay	Kaolin White
LL%	50	44	36	53	55
PL%	36	27	27	23	30
PI	14	17	9	30	25
USCS Classification	OH	CL	CL	CH	CH
w%	133	133	133	133	133
LI	6.9	6.2	11.8	3.7	4.1
G_s	2.42	2.6	2.8	2.85	2.7
e_0	3.21	3.45	3.72	3.79	3.59

In the above table, LL is the liquid limit, PL is the plastic limit, PI is the plasticity index, W_n is the natural water content, LI is the liquidity index, G_s is the specific gravity of solids, and e_0 is the saturated void ratio. According to the index properties, the range of plasticity limits is between 9 and 30, covering a good range of plasticity indexes. The USCS classification includes low- to high-plasticity clays and organic clays.

4. Prediction of Model parameters with Index properties

It is very practical to be able to determine the model parameters (*A, B, Z, C* and *D*) and their empirical relationships with index properties. Obtaining index properties are simple and less time consuming compared to running a full scale consolidation test.

The results of sixteen seepage-induced consolidation tests, five on soft clays and eleven on Newark Bay mud, are statistically correlated with their index properties. The following equations are presented for the consolidation model parameters:

$$A = \frac{2}{G_s}\log_{G_s} PI \tag{4.3}$$

$$B = -\frac{PI}{20 \times e_0} \tag{4.4}$$

$$Z = \frac{1}{\log_{G_s} PI \times \log_{e_0} LI} \tag{4.5}$$

$$C = e^{(-F \times Ln(PI))} \tag{4.6}$$

$$D = LI \times (1 + \frac{PL}{100}) \tag{4.7}$$

The details of each test's resulting compressibility and permeability relationships are presented in Appendix B. Table 4.11 summarizes the coefficients of determination, R^2, for the compressibility equation.

Table 4.11. Summary of Coefficient of Determination for Compressibility

Sample ID	KR	RC	SC	MC	KW	1	2	3
R^2	0.98	0.98	0.99	0.99	0.99	0.63	0.86	0.64
Sample ID	4	5	6	7	8	9	10	11
R^2	0.84	0.31	0.69	0.94	0.77	0.45	0.64	0.90

Table 4.11 indicates that the proposed compressibility equations provide significant estimations for the consolidation model parameters.

The coefficient of determination for the permeability equation is presented in Table 4.12.

Table 4.12. Summary of Coefficient of Determination for Permeability

Sample ID	KR	RC	SC	MC	KW	1	2	3
R^2	0.79	0.92	0.97	0.94	0.95	0.93	1.00	0.98
Sample ID	4	5	6	7	8	9	10	11
R^2	0.87	0.93	0.97	0.77	0.96	0.83	0.92	0.86

It should be noted that the variable *F,* in Equation 4.13, changes based on the Plasticity Index. Figure 4.16 presents the *F* values for different PI values.

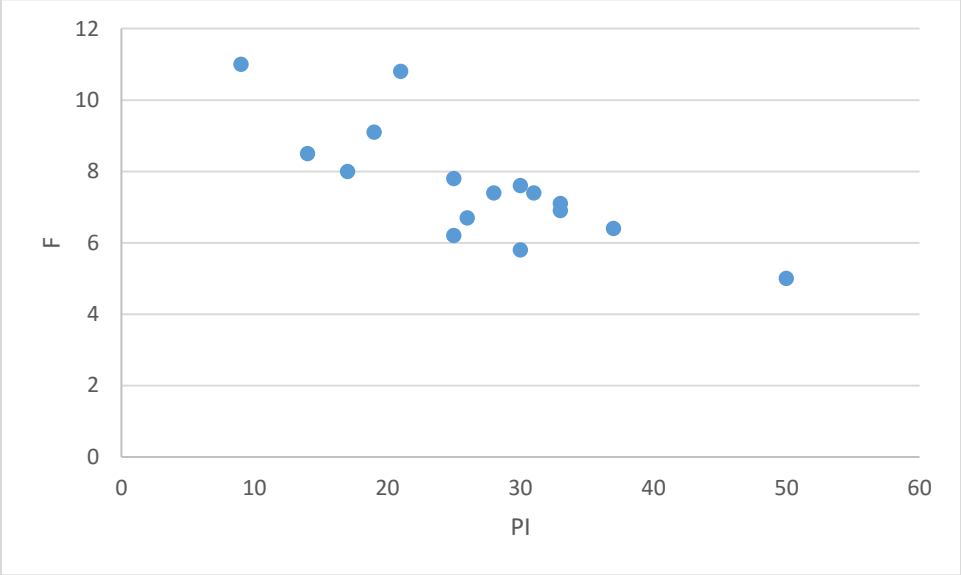

Figure 4.16. Variation of F with Plasticity Index

The compressibility and permeability relationships for different soft clays are presented in Figure 4.17 and Figure 4.18, respectively.

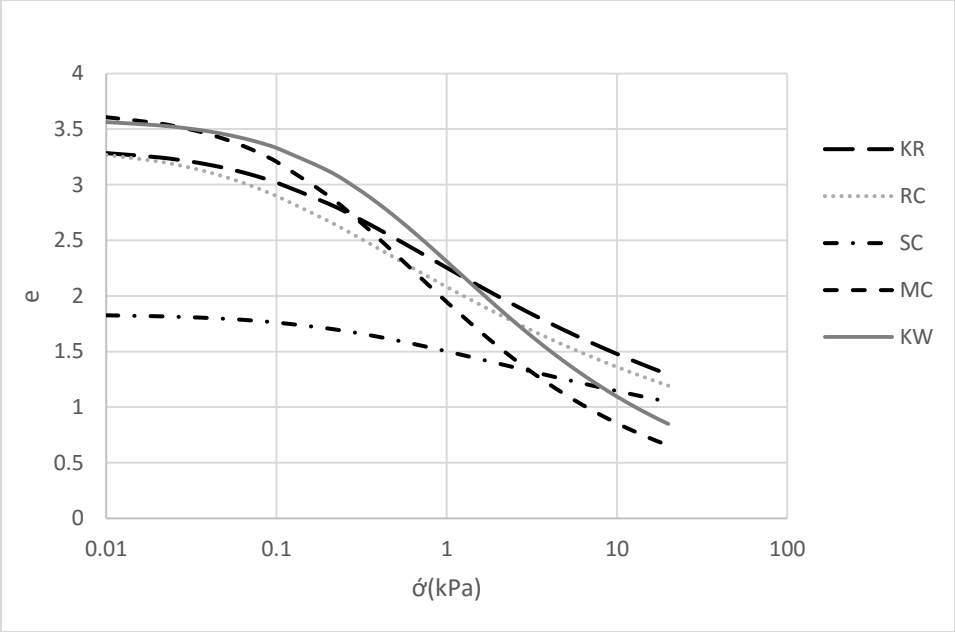

Figure 4.17. Compressibility of Soft Clays

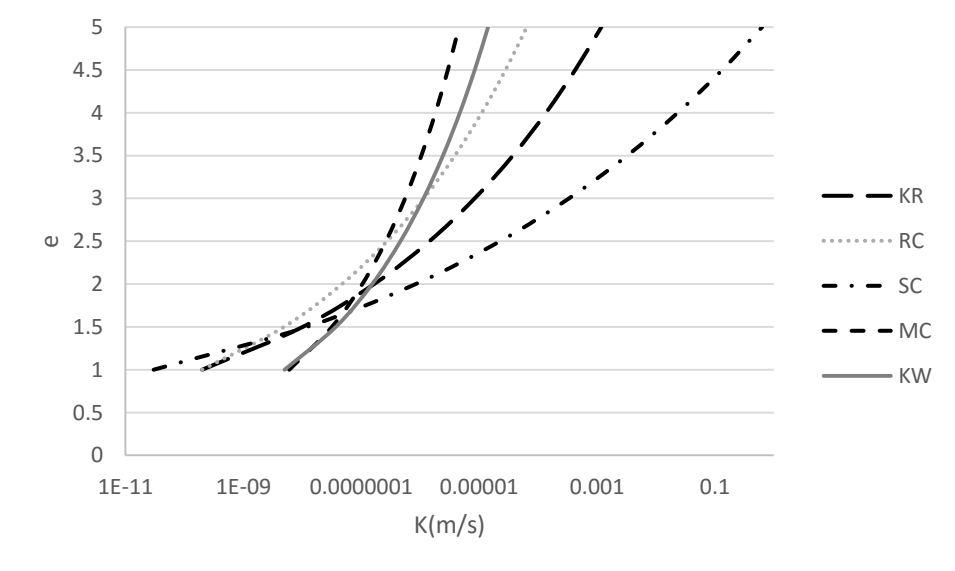

Figure 4.18. Permeability of Soft Clays

Summary of Major Outcomes

This research was designed and carried out to investigate the consolidation behavior of soft to very soft sediment to give engineers better understanding about the settlement issues related to confined disposal facility design. The major outcome is summarized as:

- The seepage induced consolidation tester were designed and constructed

- The consolidation characteristics of Newark bay sediments were evaluated with seepage induced consolidation tester
- The index properties of sediments were determined.
- Benchmark testing has been conducted on kaolinite clay and shown comparable results with similar testing at the SICT at Colorado University (CU) in Boulder and University of British Columbia (UBC).
- A series of relationships between void ratio- effective stress and void ratio-permeability were obtained to accurately determine the consolidation characteristics of sediments.
- Eleven test were conducted on soft sediments dredged from Newark bay and the result of consolidation test were simulated with CONDES program to predict the time settlement of samples
- Five seepage test were conducted on artificially made soft soils in the laboratory to investigate the effect of plasticity index along with eleven test results on soft dredged sediments on consolidation model parameters
- The new model parameter estimation equations based on index properties shows good agreement with the test data and can be used for material with similar characteristics
- The results are in good agreement with the published data which demonstrates seepage induced consolidation test as a reliable tool for consolidation characterization of low density soft sediments.

Recommendations for Future Work:

For future versions of the seepage induced consolidation tester, it is recommended that air pressure step loading system be replaced with a dead weight loading system for simpler troubleshooting or an electrical powered actuator for fine tuning of the applied load as well as more accurately measuring the load especially at low effective stresses. This is because as opposed to conventional step loading systems no air pressure is required to expand a rubber diaphragm, which then applies a force to a loading rod. On the other hand the author experienced pressure loss during testing for days which resulted in using the dead weight system instead. The conventional setup intrinsically brings up many possible errors in measuring the actual load applied especially since a pressure gauge is required to measure the pressure and there is a need for steady supply of air pressure which is never completely steady. Using a mechanical actuator to apply the load only requires an electrical signal to turn the actuator slightly to apply any given load which will be kept constant.

Appendix A

Test 1

A summary of the seepage test is provided in Table 6.

Table A.1. Seepage test summary (Test 1)

G_s	e_i	e_{00}	e_s	e_f	k_s (m/s)	k_f (m/s)	σ'_s (kPa)	σ'_f (kPa)	Q_s (nl/s)	Q_f (nL/min)
2.61	5.05	4.319	3.2	1.71	7.31E-08	5.8E-11	0.22	10	100	15

The parameters estimated by Microsoft Excel's Solver program are presented in Table 7.

Table A.2. Model Parameters (Test 1)

A	B	Z	C	D
2.557	-0.173	0.048	1.00E-13	11.447

Figure A.1 shows the observed time settlement curve for the seepage-induced consolidation test.

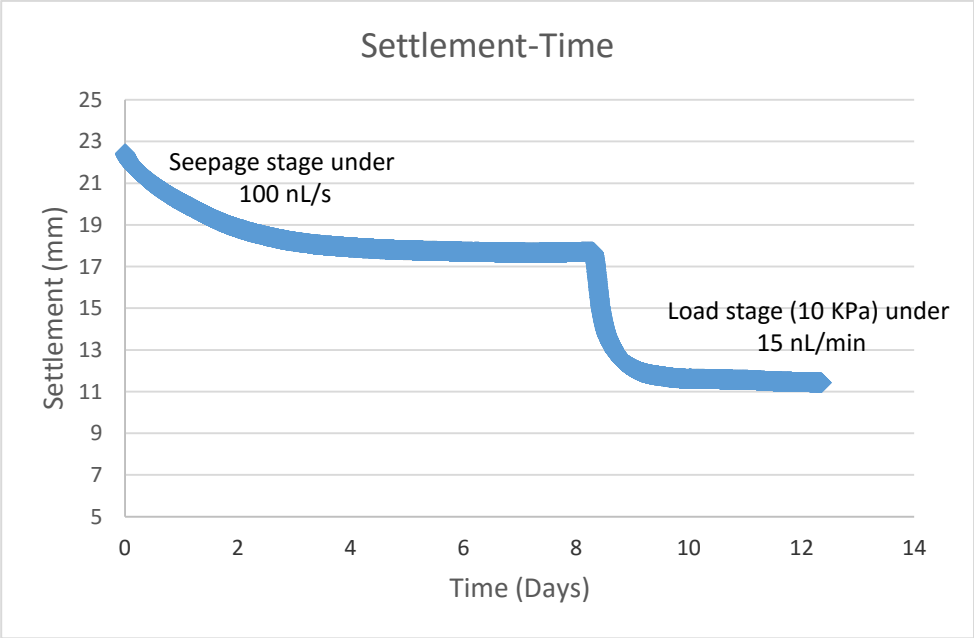

Figure A.1. Observed Time-Settlement curve (Test 1)

The compressibility curve is presented in Figure A.2.

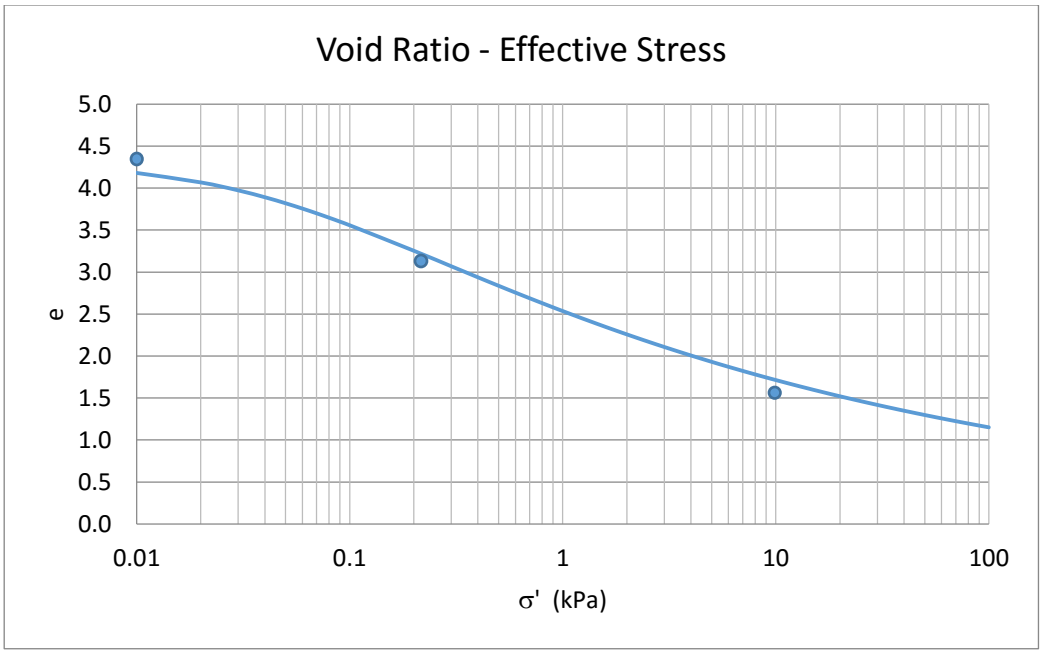

Figure A.2. Compressibility Curve (Test 1)

The compressibility equation used for finding the numerical solution is:

$$e = 2.557(\sigma' + 0.0485)^{-0.173}$$

The permeability curve is presented in Figure A.3.

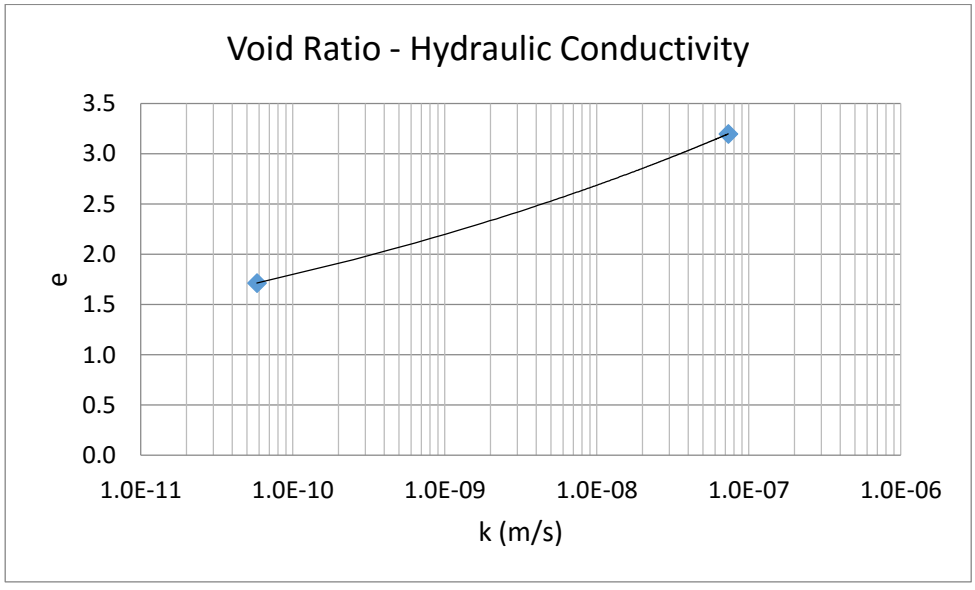

Figure A.3. Permeability Curve (Test 1)

The permeability equation, with respect to the void ratio, is:

$$K\ (\text{m/s}) = 1\text{E-}13\ e^{11.447}$$

Running CONDES0 to simulate the obtained model parameters with the observed testing data produces the results in Figure A.4.

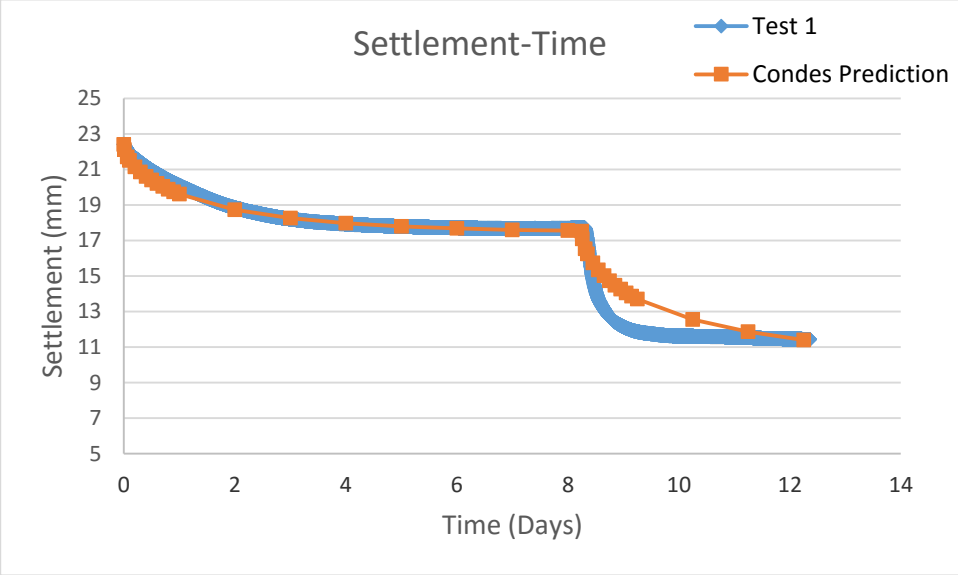

Figure A.4. Numerical Simulation (Test 1)

The numerical simulation shows good compatibility with the observed settlements and modeled settlements, confirming the capability of the model and the model parameter estimator. From Figure A.4 it can be concluded that there is a slight divergence from the observed data as the time settlement curve goes into step loading phase.

Test 2.

A summary of the seepage test is provided in Table A.3.

Table A.3. Seepage test summary (Test 2)

G_s	e_i	e_{00}	e_s	e_f	k_s (m/s)	k_f (m/s)	σ'_s (kPa)	σ'_f (kPa)	Q_s (nl/s)	Q_f (nL/min)
2.55	4.68	4.52	3.27	1.38	5.19E-09	5E-11	0.323	100	100	15

The parameters estimated by Microsoft Excel's Solver program are presented in Table A.4.

Table A.4. Model Parameters (Test 2)

A	B	Z	C	D
2.803	-0.154	0.045	9.00E-12	5.365

Figure A.5 shows the observed time settlement curve for the seepage-induced consolidation test.

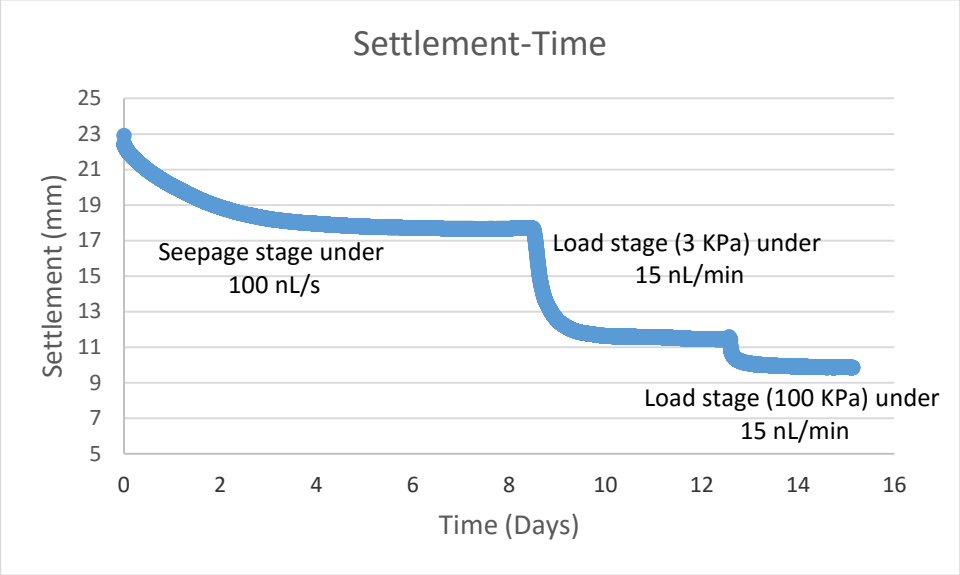

Figure A.5. Observed Time-Settlement curve (Test 2)

The compressibility curve is presented in Figure A.6.

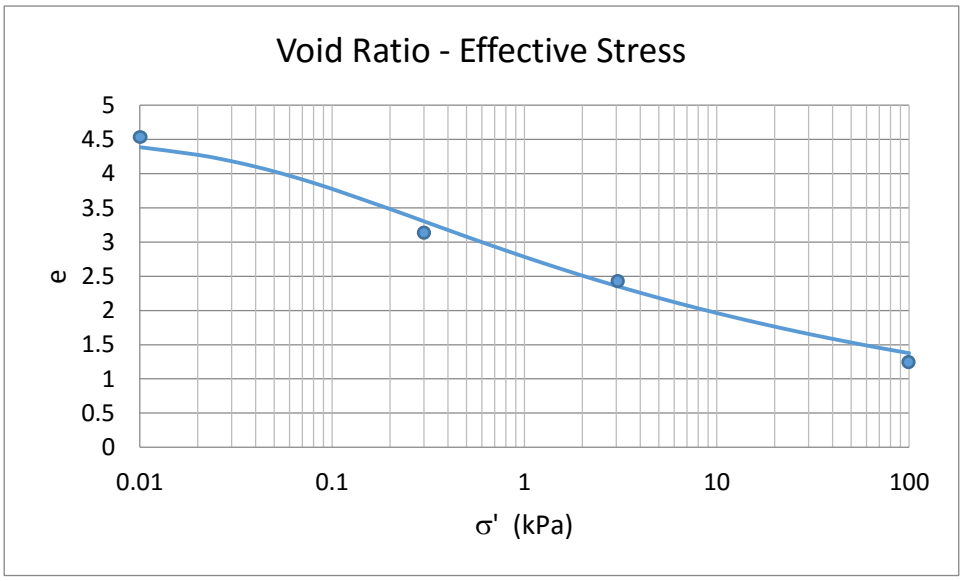

Figure A.6. Compressibility Curve (Test 2)

The compressibility equation used to find the numerical solution is:

$$e = 2.803(\sigma' + 0.0449)^{-0.154}$$

The permeability curve is presented in Figure A.7.

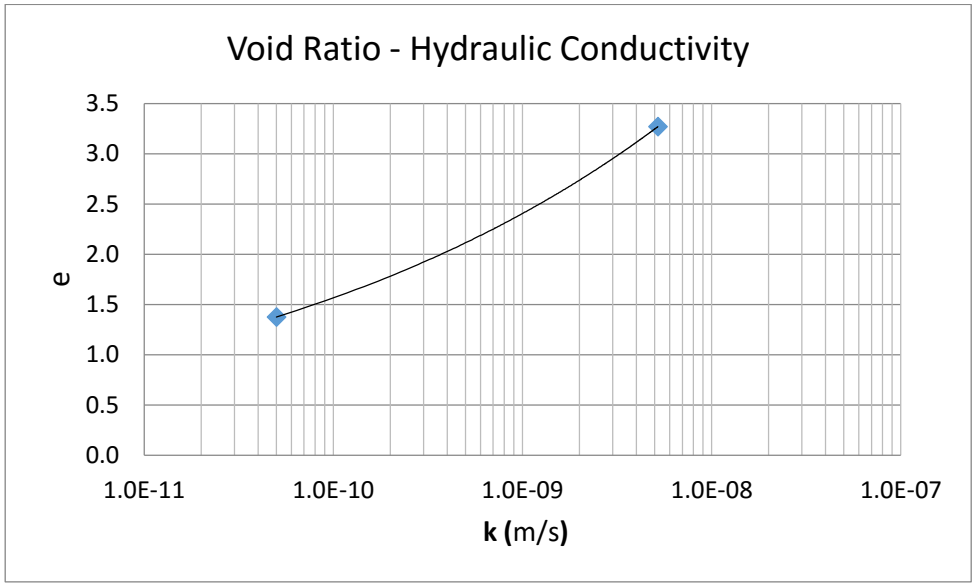

Figure A.7. Permeability Curve (Test 2)

The permeability equation, with respect to the void ratio, is:

$$K \text{ (m/s)} = 9\text{E-}12\ e^{5.367}$$

Running CONDES0 to simulate the obtained model parameters with the observed testing data produces the results in Figure A.8.

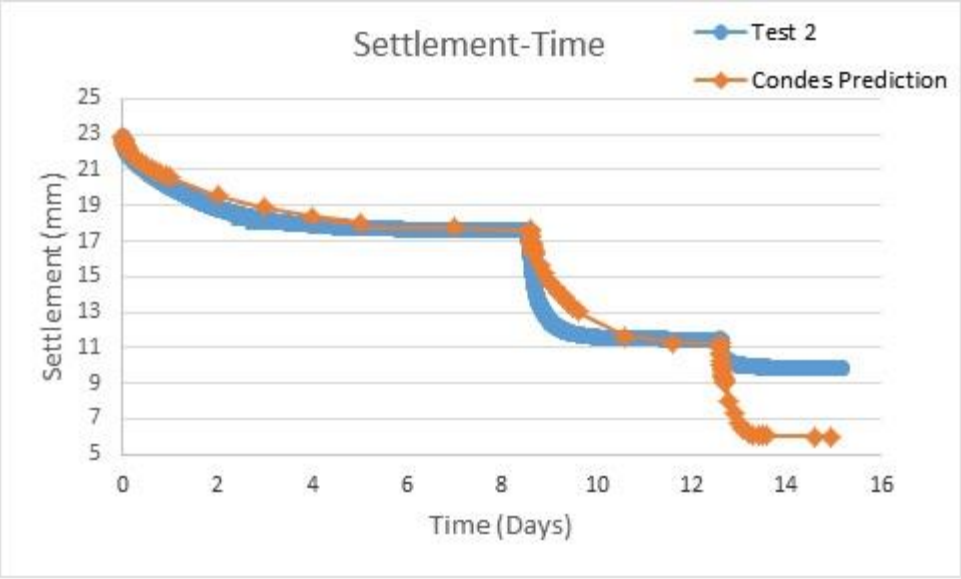

Figure A.8. Numerical Simulation (Test 2)

Figure A.8 shows that there also exists deviation from the observed data points under high stresses for Test 2. However, it seems as though CONDES0 is able to propose good estimates for the seepage-only stage of the test, as well as for the low range of stresses.

Test 3.

A summary of the seepage test is provided in Table A.5.

Table A.5. Seepage test summary (Test 3)

G_s	e_i	e_{00}	e_s	e_f	k_s (m/s)	k_f (m/s)	σ'_s (kPa)	σ'_f (kPa)	Q_s (nl/s)	Q_f (nL/min)
2.58	4.891	4.332	3.45	1.15	3.95E-08	5.24E-11	0.27	80	90	15

The parameters estimated by Microsoft Excel's Solver program are presented in Table A.6.

Table A.6. Model Parameters (Test 3)

A	B	Z	C	D
2.859	-0.209	0.1354	1.00E-11	6.122

Figure A.9 shows the observed time settlement curve for the seepage-induced consolidation test.

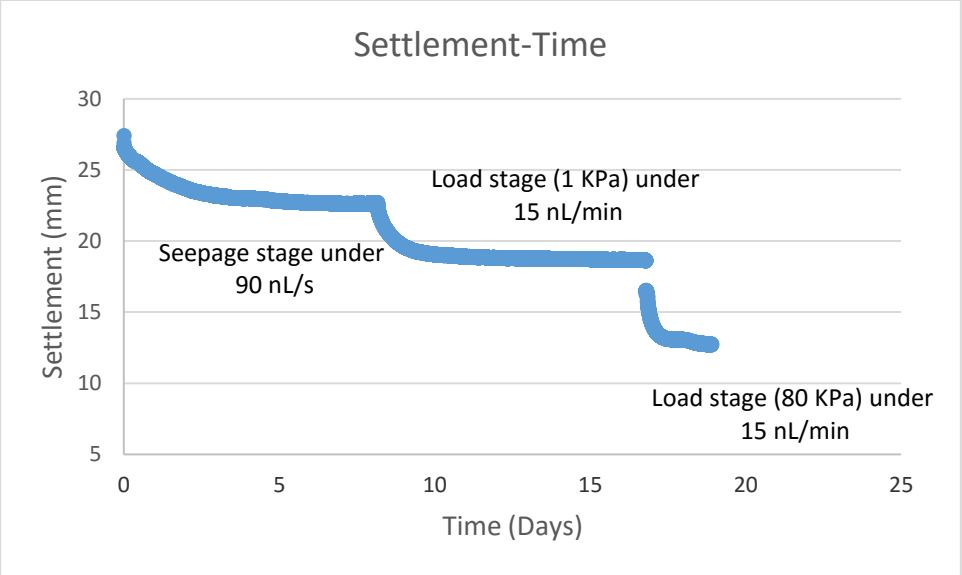

Figure A.9. Observed Time-Settlement curve (Test 3)

The compressibility curve is presented in Figure A.10.

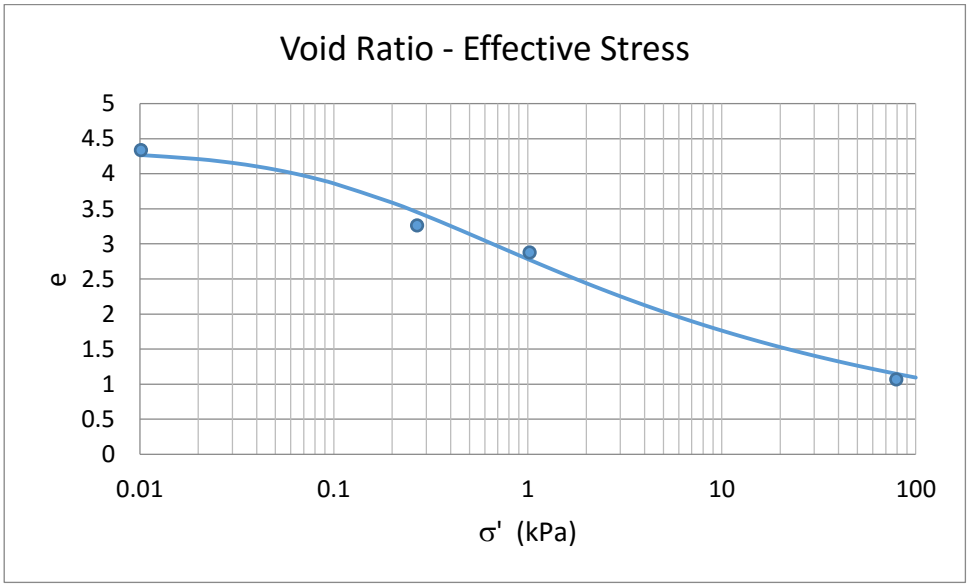

Figure A.10. Compressibility Curve (Test 3)

The compressibility equation used to find the numerical solution is:

$$e = 2.859(\sigma' + 0.1354)^{-0.209}$$

The permeability curve is presented in Figure A.11.

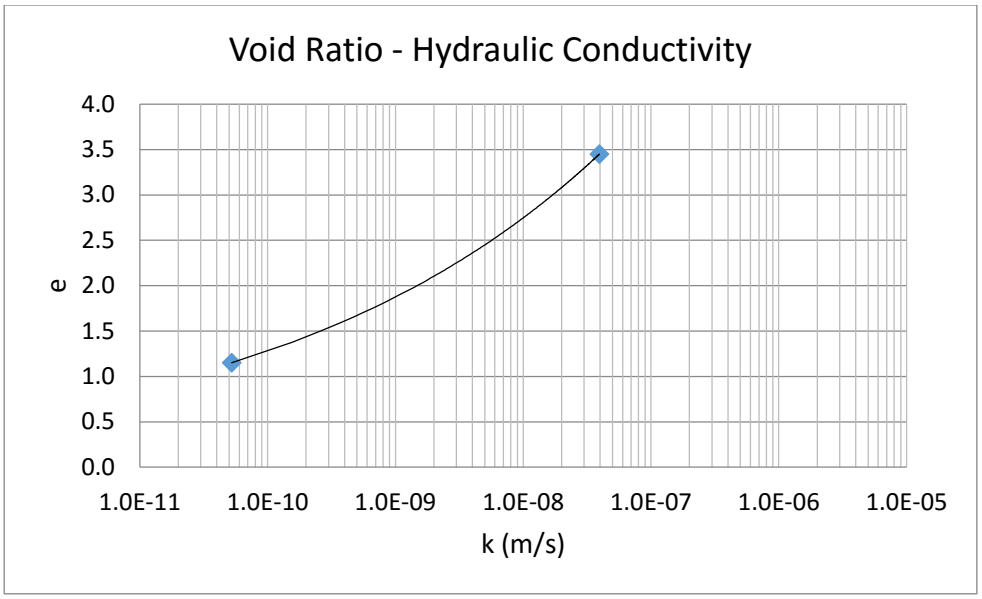

Figure A.11. Permeability Curve (Test 3)

The permeability equation, with respect to the void ratio, is:

$$K \text{ (m/s)} = 2\text{E-}11\ e^{6}$$

Running CONDES0 to simulate the obtained model parameters with the observed testing data produces the results in Figure A.12. Numerical Simulation (Test 3)

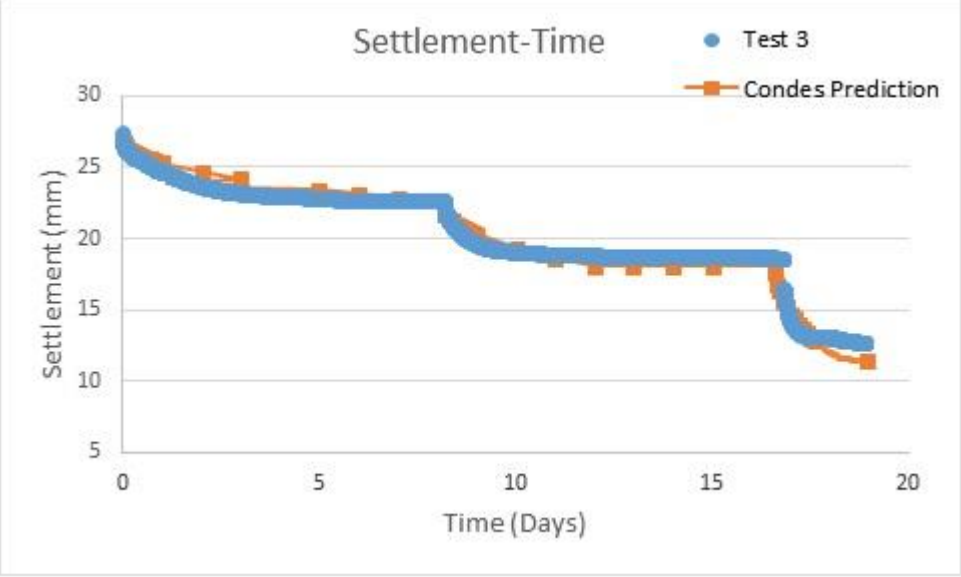

Figure A.12. Numerical Simulation (Test 3)

From Figure A.12, it can be concluded that CONDES0 is best for smaller ranges of stresses, and that as stress increases, the predictions deviate from the observations.

Test 4.

A summary of the seepage test is provided in Table A.7.

Table A.7. Seepage test summary (Test 4)

G_s	e_i	e_{00}	e_s	e_f	k_s (m/s)	k_f (m/s)	σ'_s (kPa)	σ'_f (kPa)	Q_s (nl/s)	Q_f (nL/min)
2.42	5.00	4.871	3.81	2.45	3.38E-08	5.57E-11	0.203	10	50	60

The parameters estimated by Microsoft Excel's Solver program are presented in Table A.8.

Table A.8. Model Parameters (Test 4)

A	B	Z	C	D
3.164	-0.117	0.028	2.00E-16	14.461

Figure A.13 shows the observed time settlement curve for the seepage-induced consolidation test.

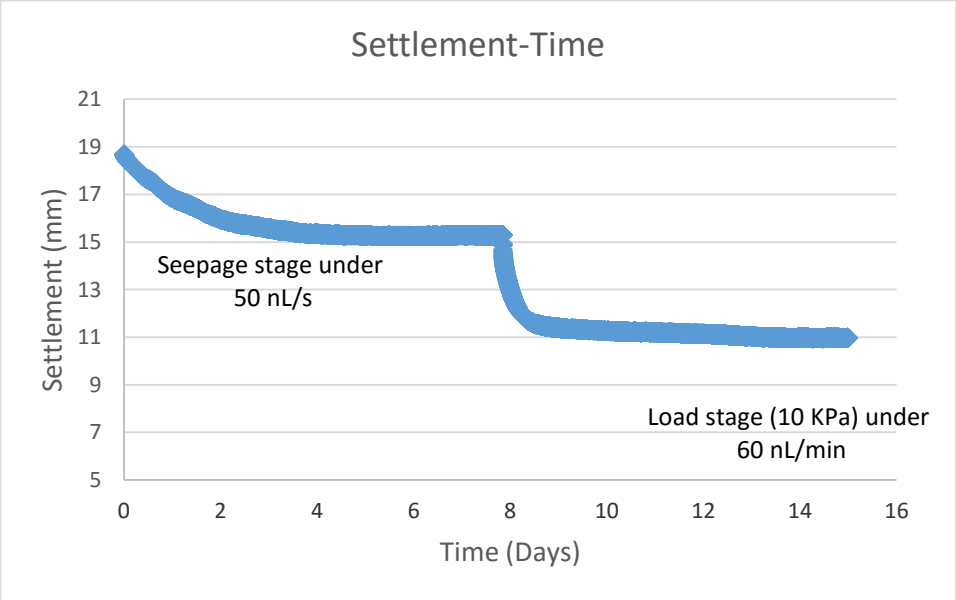

Figure A.13. Observed Time-Settlement curve (Test 4)

The compressibility curve is presented in Figure A.14.

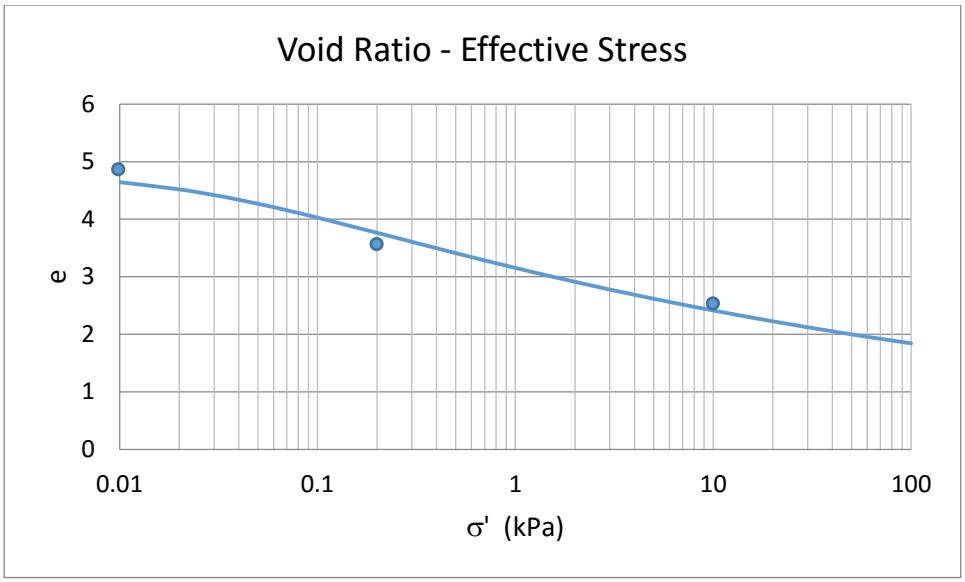

Figure A.14. Compressibility Curve (Test 4)

The compressibility equation used to find the numerical solution is:

$$e = 3.164(\sigma' + 0.0208)^{-0.117}$$

The permeability curve is presented in Figure A.15.

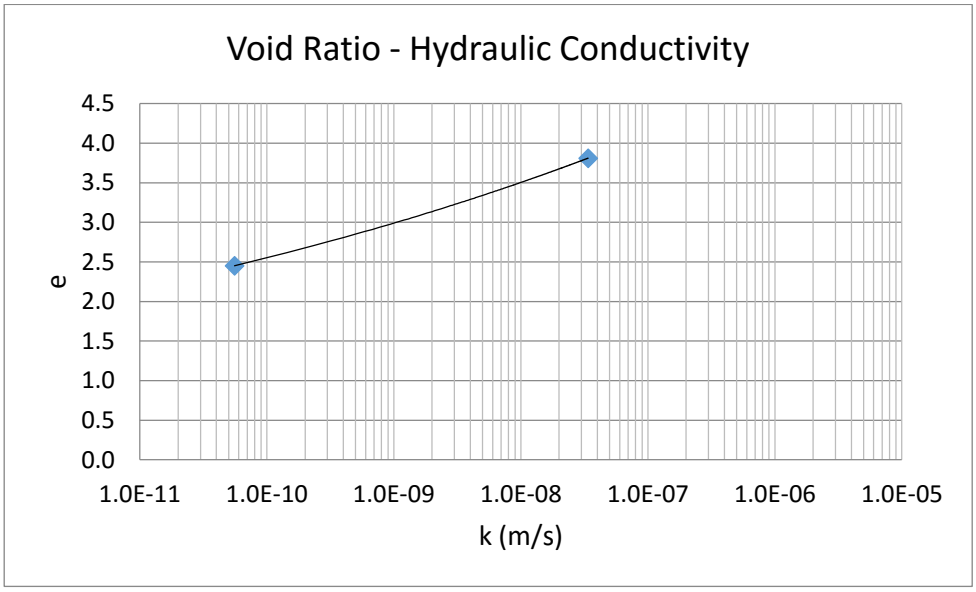

Figure A.15. Permeability Curve (Test 4)

The permeability equation, with respect to the void ratio, is:

$$K\ (\text{m/s}) = 2\text{E-}16\ e^{14.461}$$

Running CONDES0 to simulate the obtained model parameters with the observed testing data produces the results in Figure A.16.

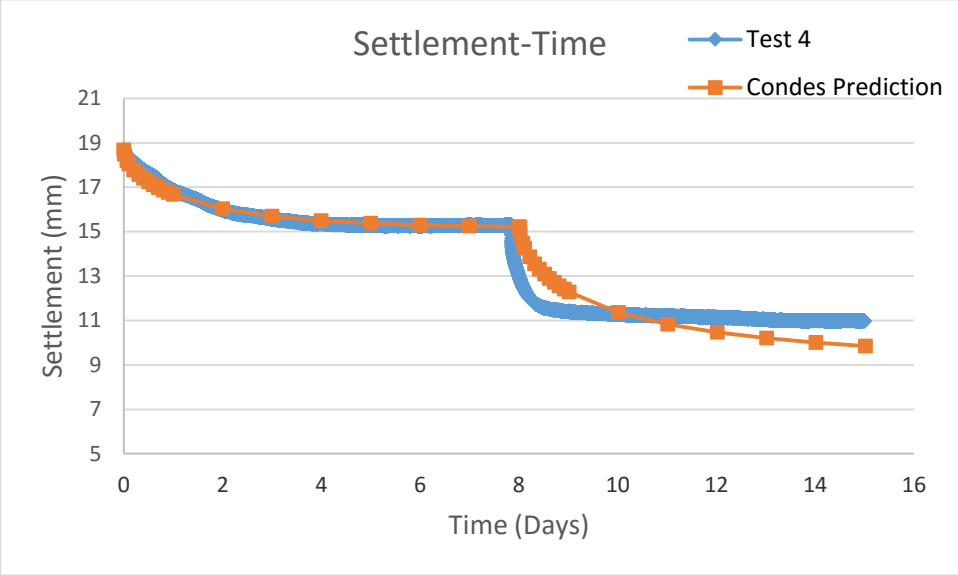

Figure A.16. Numerical Simulation (Test 4)

Test 5.

A summary of the seepage test is provided in Table A.9. Seepage test summary

Table A.9. Seepage test summary (Test 5)

G_s	e_i	e_{00}	e_s	e_f	k_s (m/s)	k_f (m/s)	σ'_s (kPa)	σ'_f (kPa)	Q_s (nl/s)	Q_f (nL/min)
2.68	5.188	4.405	3.31	0.98	2.24E-08	4.99E-11	0.317	100	50	15

The parameters estimated by Microsoft Excel's Solver program are presented in Table A.10.

Table A.10. Model Parameters (Test 5)

A	B	Z	C	D
2.807	-0.196	0.0964	5.00E-11	5.038

Figure A.17 shows the observed time settlement curve for the seepage-induced consolidation test.

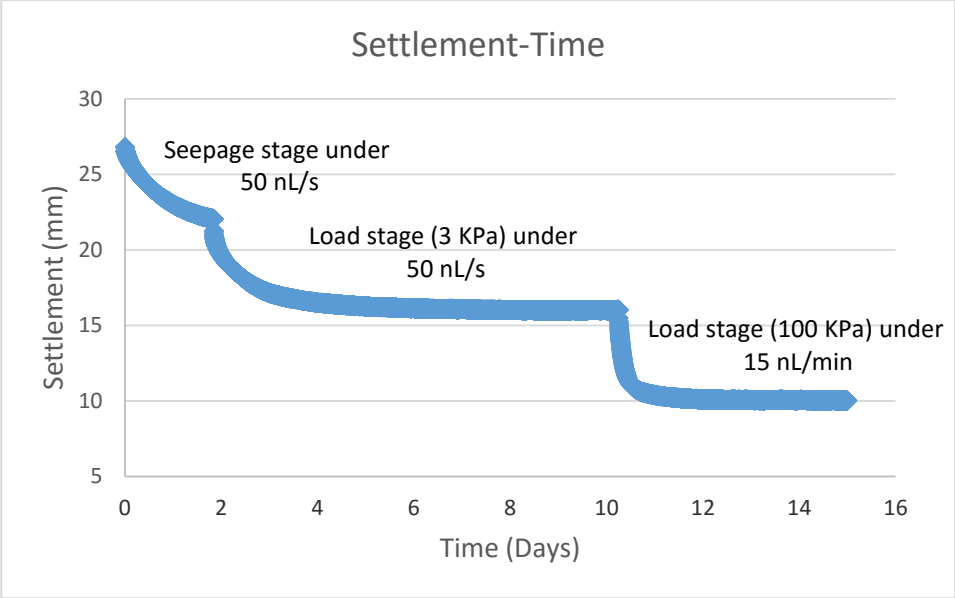

Figure A.17. Observed Time-Settlement curve (Test 5)

The compressibility curve is presented in Figure A.18.

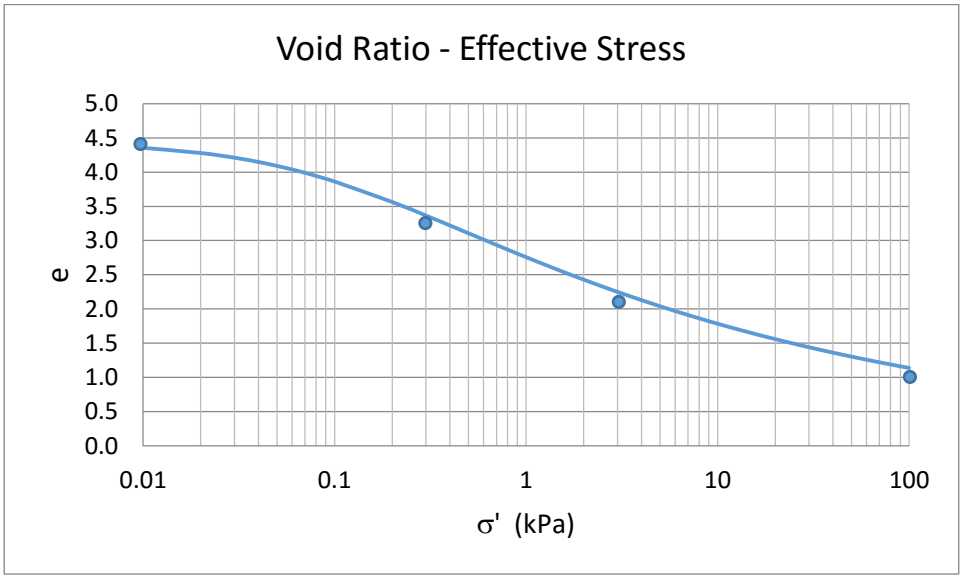

Figure A.18. Compressibility Curve (Test 5)

The compressibility equation used to find the numerical solution is:

$$e = 2.807(\sigma' + 0.0964)^{-0.196}$$

The permeability curve is presented in Figure A.19.

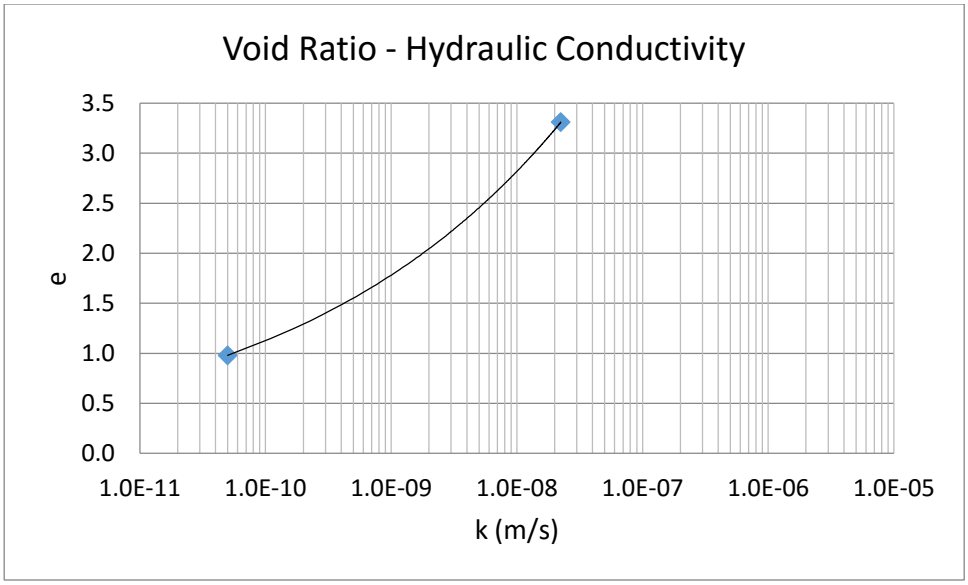

Figure A.19. Permeability Curve (Test 5)

The permeability equation, with respect to the void ratio, is:

$$K\ (\text{m/s}) = 5\text{E-}11\ e^{5.038}$$

Running CONDES0 to simulate the obtained model parameters with the observed testing data produces the results in Figure A.20.

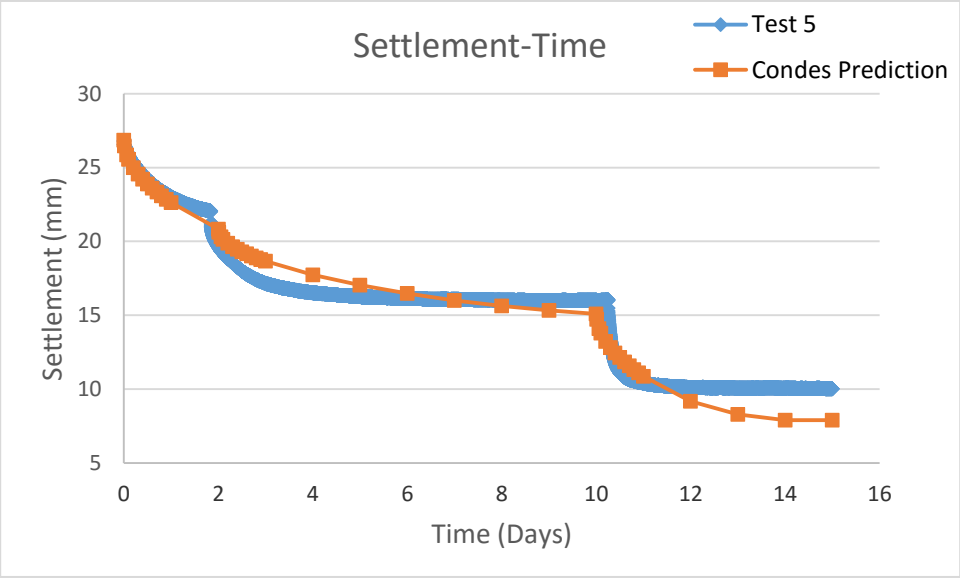

Figure A.20. Numerical Simulation (Test 5)

Test 6.

A summary of the seepage test is provided in Table A.11.

Table A.11. Seepage test summary (Test 6)

G_s	e_i	e_{00}	e_s	e_f	k_s (m/s)	k_f (m/s)	σ'_s (kPa)	σ'_f (kPa)	Q_s (nl/s)	Q_f (nL/min)
2.95	5.773	4.029	3.11	0.9	6.53E-08	9.65E-11	0.214	10	50	15

The parameters estimated by Microsoft Excel's Solver program are presented in Table A.12.

Table A.12. Model Parameters (Test 6)

A	B	Z	C	D
2.18	-0.401	0.2317	2.00E-10	5.1888

Figure A.21 shows the observed time settlement curve for the seepage-induced consolidation test.

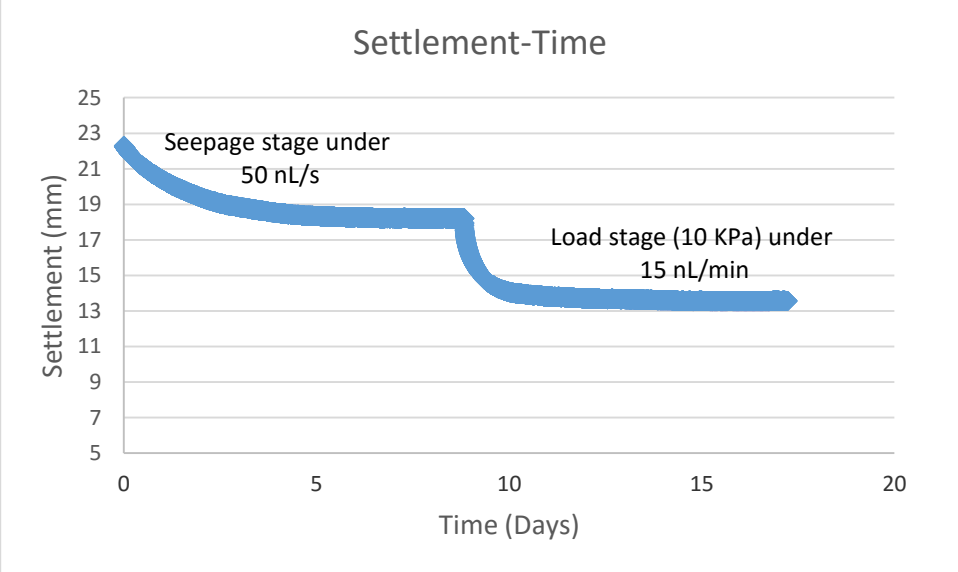

Figure A.21. Observed Time-Settlement curve (Test 6)

The compressibility curve is presented in Figure A.22.

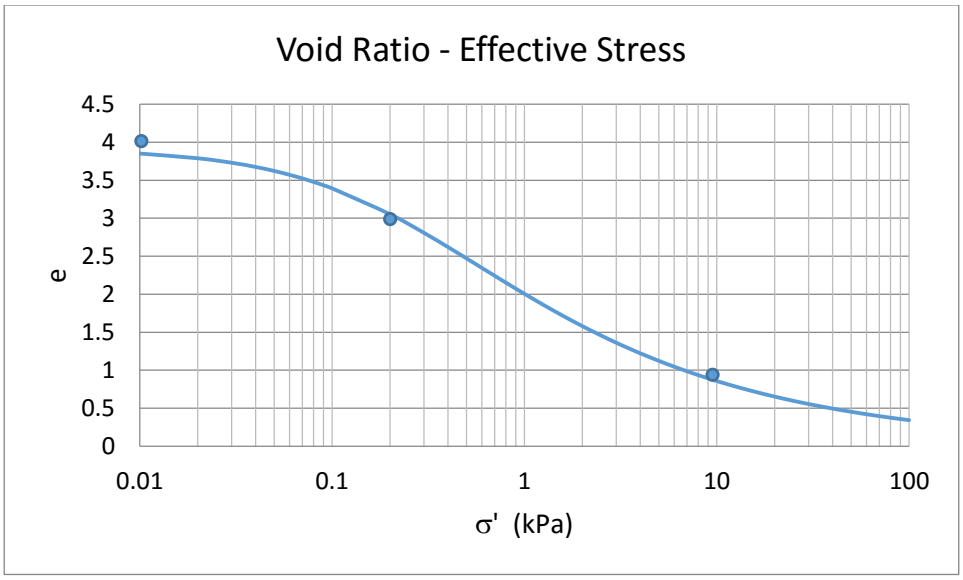

Figure A.22. Compressibility Curve (Test 6)

The compressibility equation used to find the numerical solution is:

$$e = 2.18(\sigma' + 0.2317)^{-0.401}$$

The permeability curve is presented in Figure A.23.

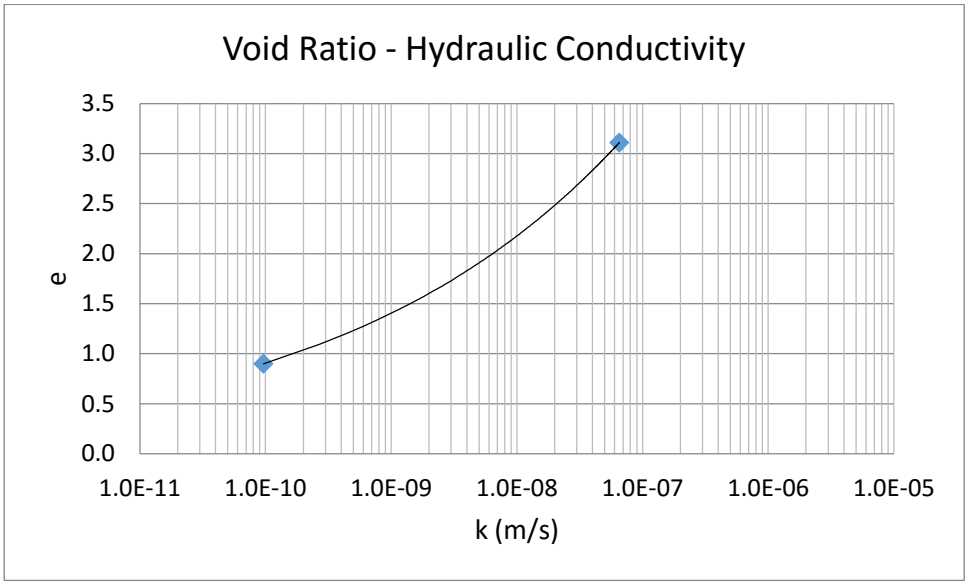

Figure A.23. Permeability Curve (Test 6)

The permeability equation, with respect to the void ratio, is:

$$K \text{ (m/s)} = 2\text{E-}10\ e^{5.188}$$

Running CONDES0 to simulate the obtained model parameters with the observed testing data produces the results in Figure A.24.

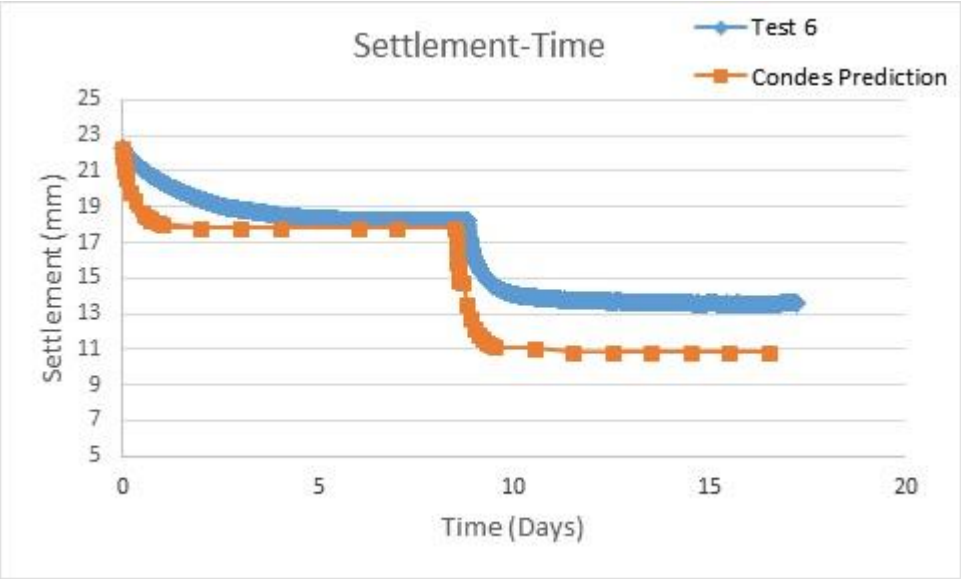

Figure A.24. Numerical Simulation (Test 6)

Test 7.

A summary of the seepage test is provided in Table A.13.

Table A.13. Seepage test summary (Test 7)

G_s	e_i	e_{00}	e_s	e_f	k_s (m/s)	k_f (m/s)	σ'_s (kPa)	σ'_f (kPa)	Q_s (nl/s)	Q_f (nL/min)
2.52	4.881	4.319	3.24	1.94	1.97E-08	6.72E-11	0.235	10	50	15

The parameters estimated by Microsoft Excel's Solver program are presented in Table 19.

Table A.14. Model Parameters (Test 7)

A	B	Z	C	D
2.669	-0.136	0.03413	3.00E-14	11.422

Figure A.25 shows the observed time settlement curve for the seepage-induced consolidation test.

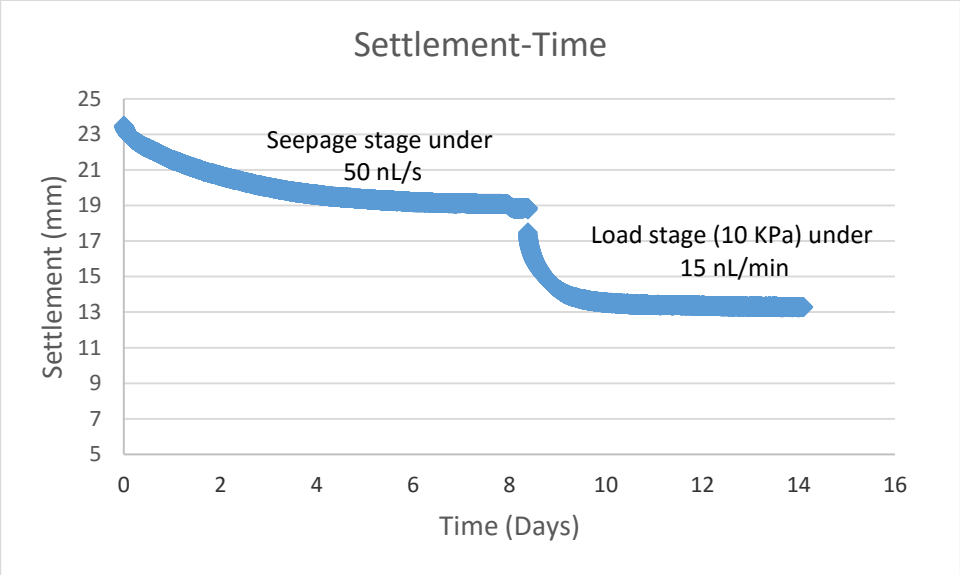

Figure A.25. Observed Time-Settlement curve (Test 7)

The compressibility curve is presented in Figure A.26.

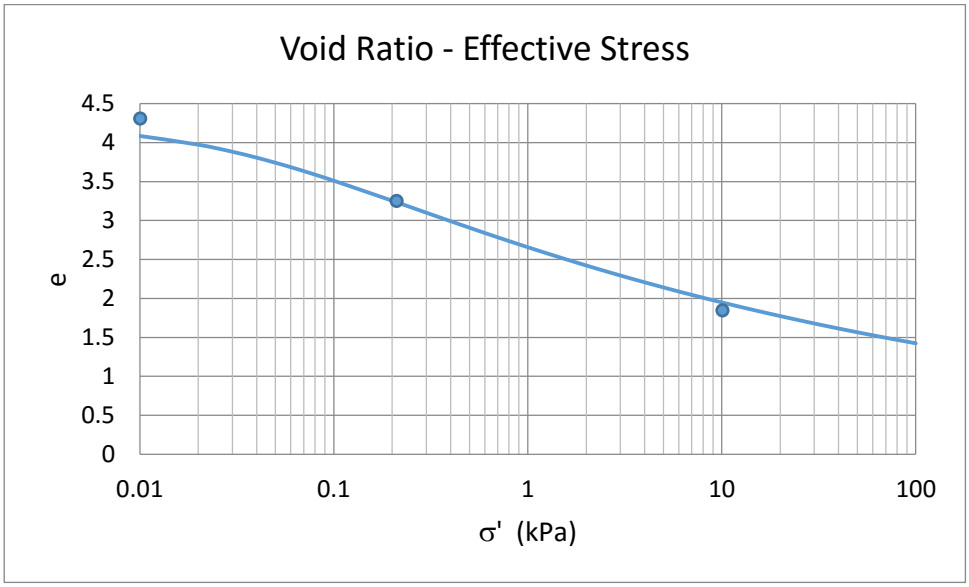

Figure A.26. Compressibility Curve (Test 7)

The compressibility equation used to find the numerical solution is:

$$e = 2.669(\sigma' + 0.0341)^{-0.136}$$

The permeability curve is presented in Figure A.27.

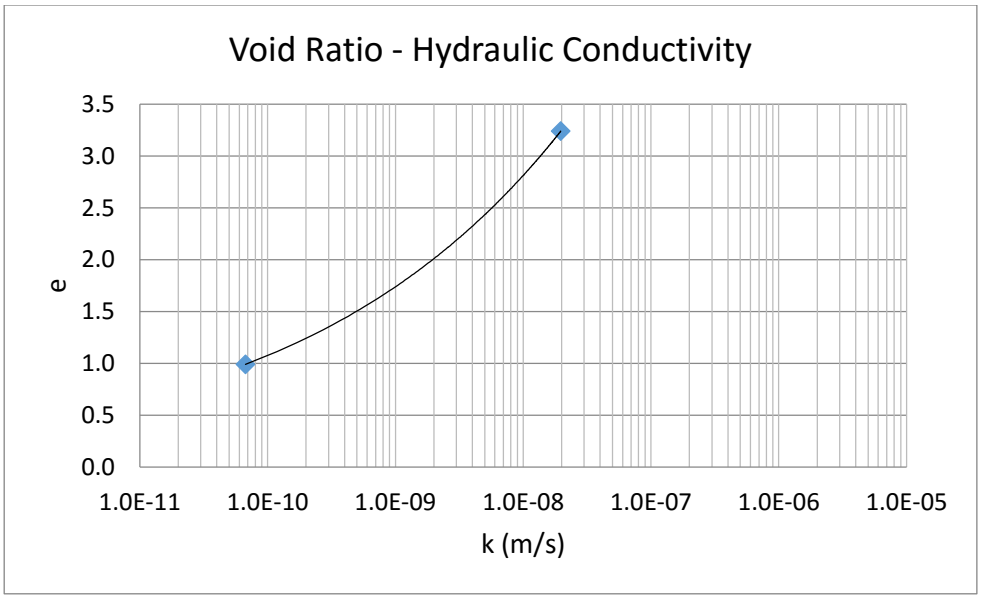

Figure A.27. Permeability Curve (Test 7)

The permeability equation, with respect to the void ratio, is:

$$K \text{ (m/s)} = 3E\text{-}14\ e^{11.422}$$

Running CONDES0 to simulate the obtained model parameters with the observed testing data produces the results in Figure A.28.

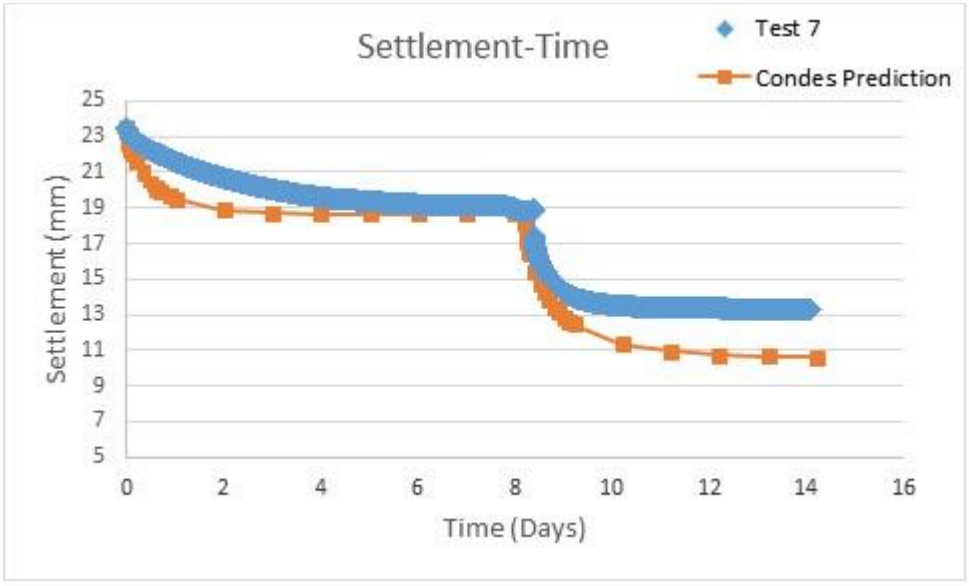

Figure A.28. Numerical Simulation (Test 7)

Test 8.

A summary of the seepage test is provided in Table A.15.

Table A.15. Seepage test summary (Test 8)

G_s	e_i	e_{00}	e_s	e_f	k_s (m/s)	k_f (m/s)	σ'_s (kPa)	σ'_f (kPa)	Q_s (nl/s)	Q_f (nL/min)
2.38	4.516	4.261	3.71	1.85	8.12E-08	1.04E-10	0.732	25	500	1500

The parameters estimated by Microsoft Excel's Solver program are presented in Table A.16.

Table A.16. Model Parameters (Test 8)

A	B	Z	C	D
3.266	-0.176	0.1501	3.00E-13	9.561

Figure A.29 shows the observed time settlement curve for the seepage-induced consolidation test.

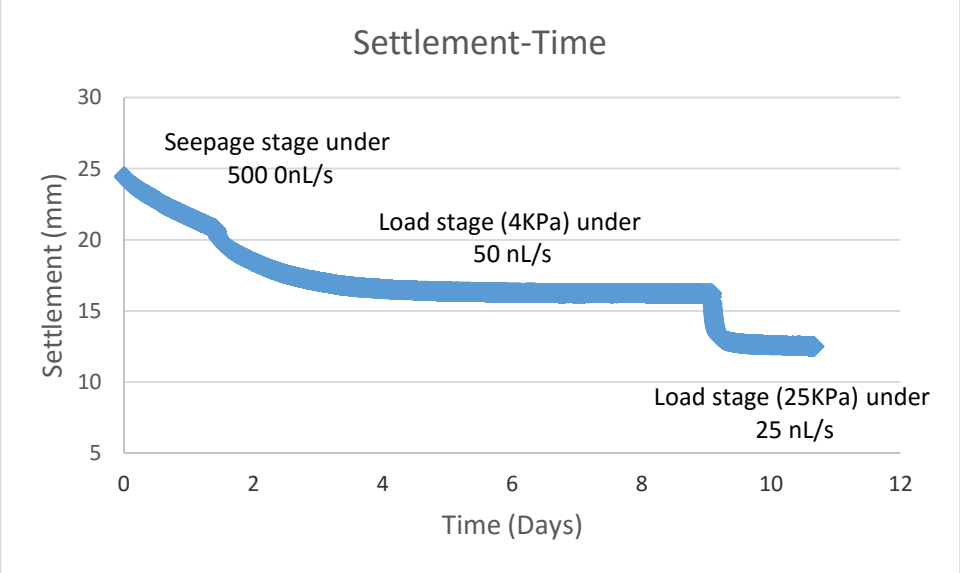

Figure A.29. Observed Time-Settlement curve (Test 8)

The compressibility curve is presented in Figure A.30.

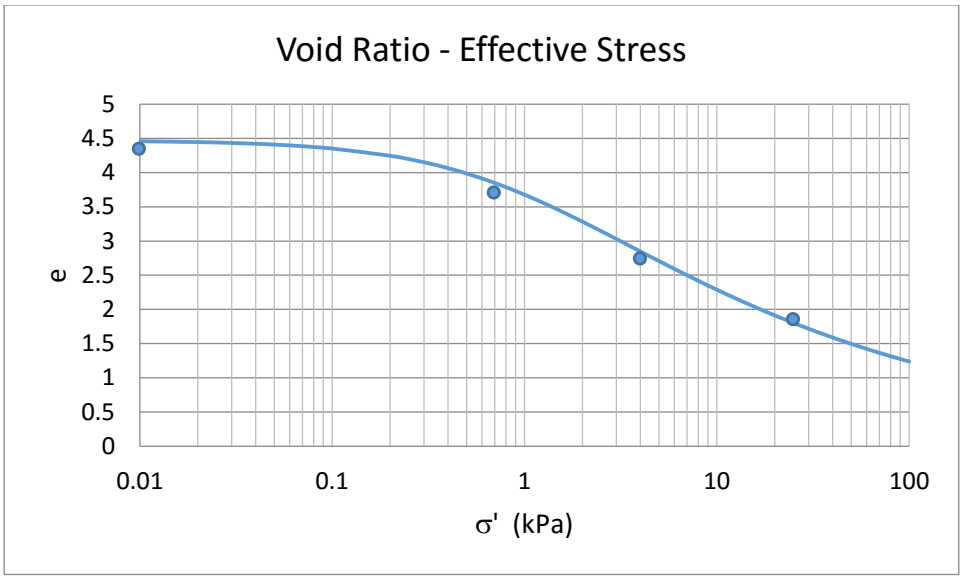

Figure A.30. Compressibility Curve (Test 8)

The compressibility equation used to find the numerical solution is:

$$e = 3.266(\sigma' + 0.1501)^{-0.176}$$

The permeability curve is presented in Figure A.31.

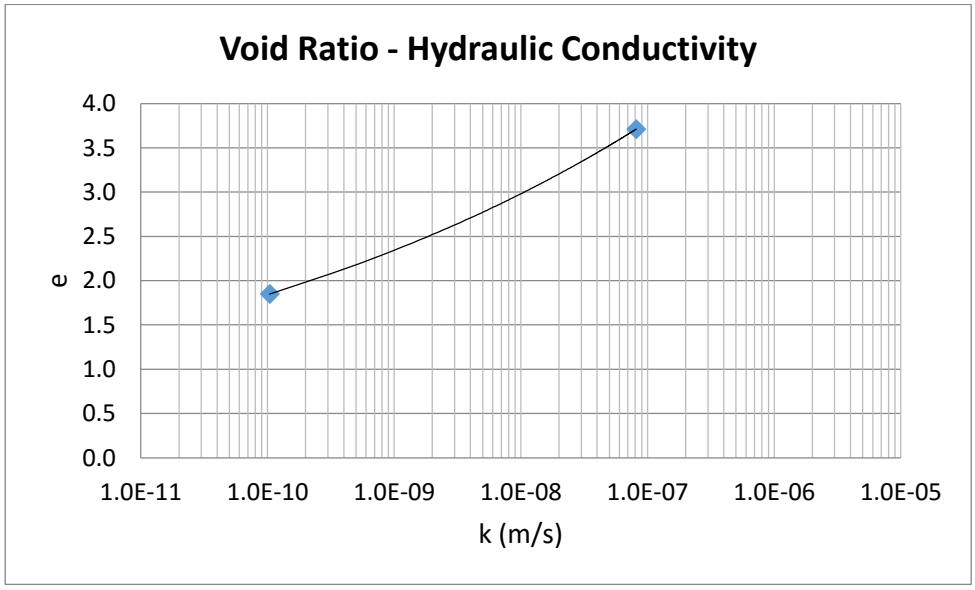

Figure A.31. Permeability Curve (Test 8)

The permeability equation, with respect to the void ratio, is:

$$K \text{ (m/s)} = 3\text{E-}13\ e^{9.561}$$

Running CONDES0 to simulate the obtained model parameters with the observed testing data produces the results in Figure A.32.

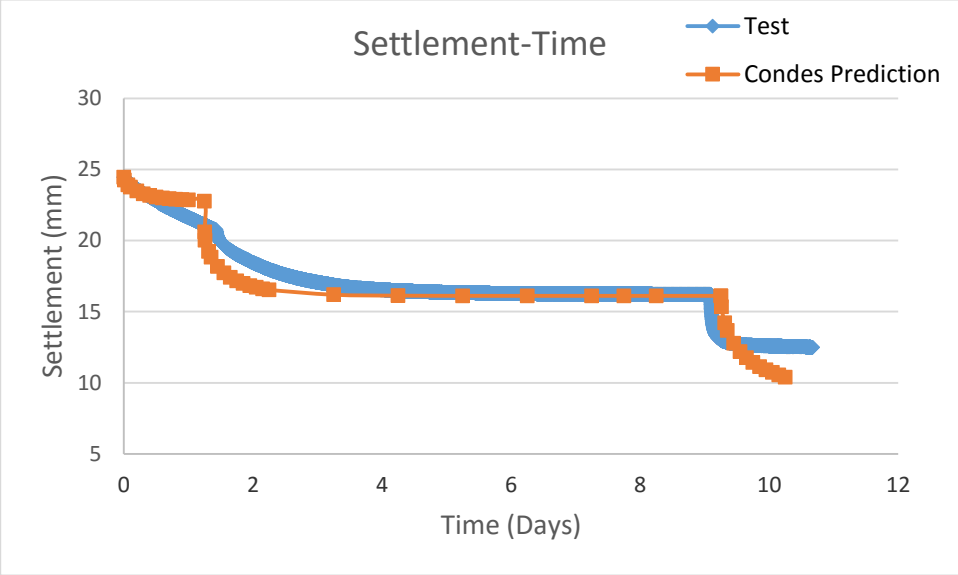

Figure A.32. Numerical Simulation (Test 8)

Test 9.

A summary of the seepage test is provided in Table A.17.

Table A.17. Seepage test summary (Test 9)

G_s	e_i	e_{00}	e_s	e_f	k_s (m/s)	k_f (m/s)	σ'_s (kPa)	σ'_f (kPa)	Q_s (nl/s)	Q_f (nL/min)
2.34	4.243	4.008	3.17	1.59	7.23E-09	1.07E-12	1	100	50	15

The parameters estimated by Microsoft Excel's Solver program are presented in Table A.18.

Table A.18. Model Parameters (Test 9)

A	B	Z	C	D
3.142	-0.123	0.138	3.00E-16	15.35

Figure A.33 shows the observed time settlement curve for the seepage-induced consolidation test.

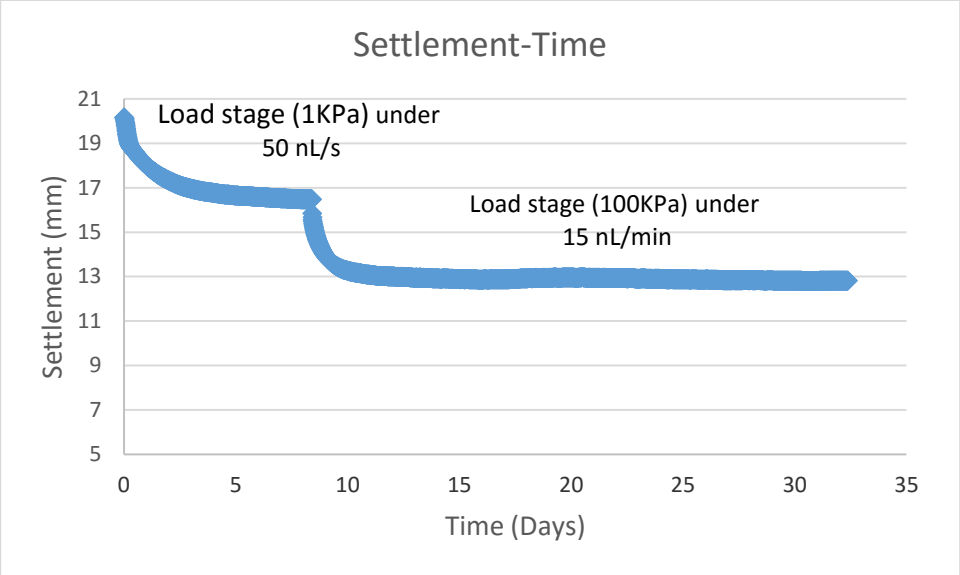

Figure A.33. Observed Time-Settlement curve (Test 9)

The compressibility curve is presented in Figure A.34.

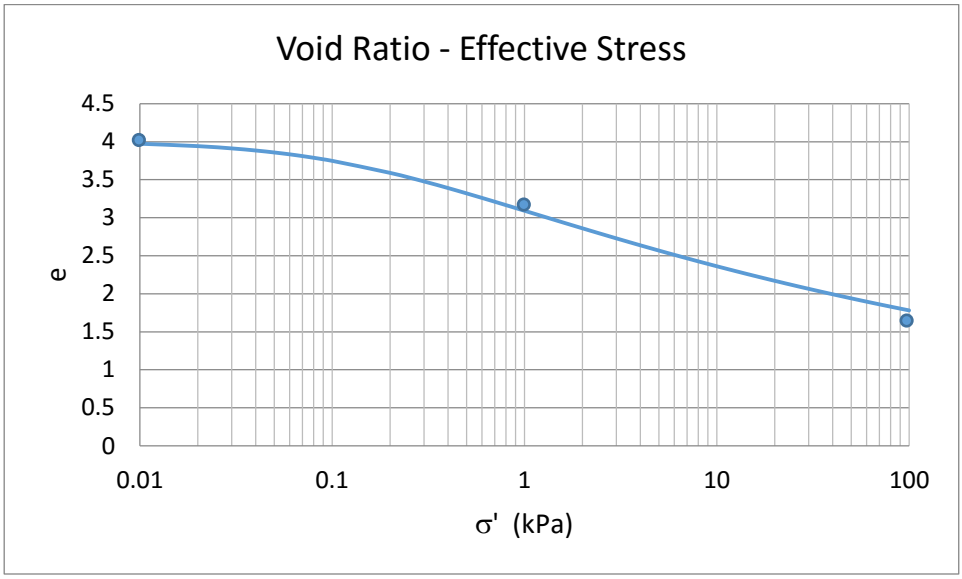

Figure A.34. Compressibility Curve (Test 9)

The compressibility equation used to find the numerical solution is:

$$e = 3.142(\sigma' + 0.1387)^{-0.123}$$

The permeability curve is presented in Figure A.35.

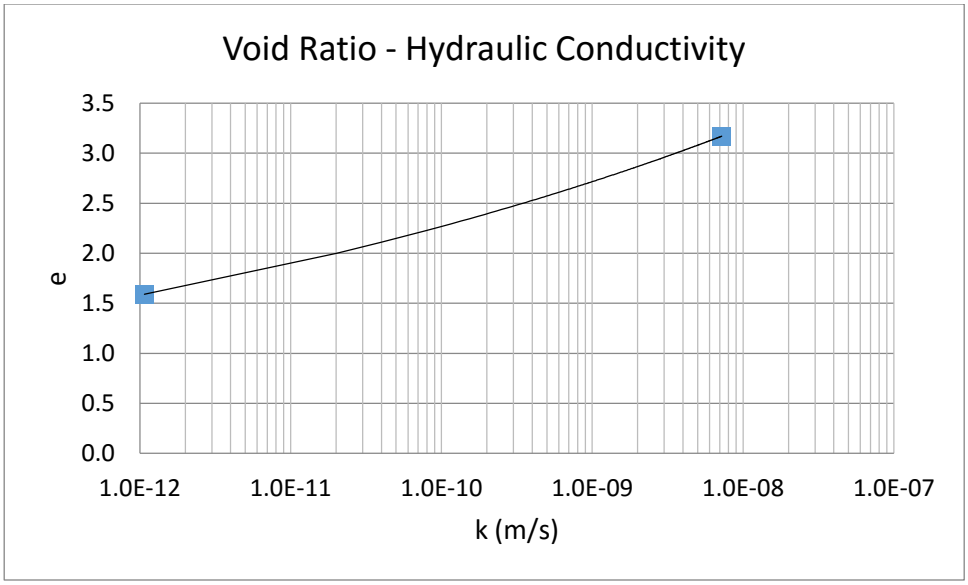

Figure A.35. Permeability Curve (Test 9)

The permeability equation, with respect to the void ratio, is:

$$K\ (\text{m/s}) = 3\text{E-}16\ e^{15.35}$$

Running CONDES0 to simulate the obtained model parameters with the observed testing data produces the results in Figure A.36.

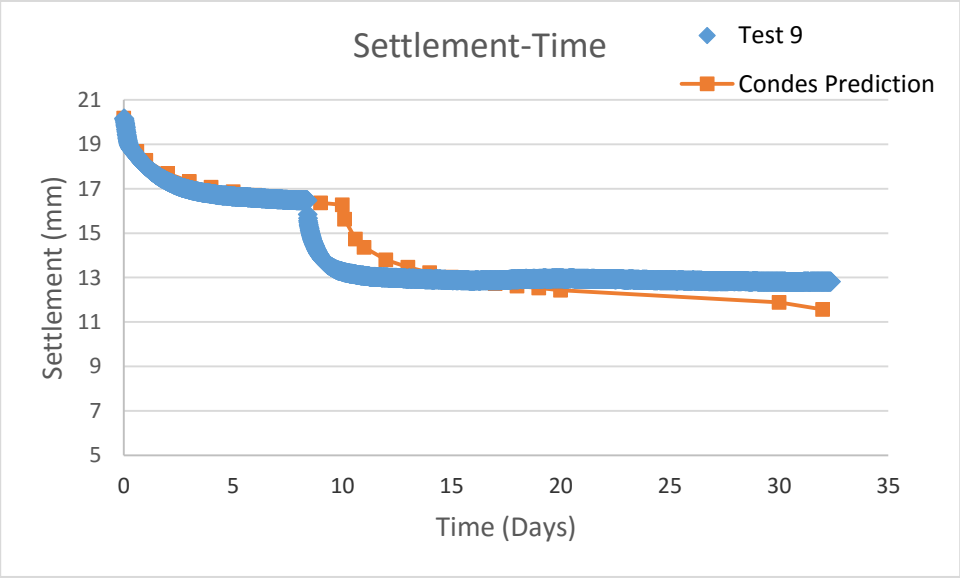

Figure A.36. Numerical Simulation (Test 9)

Test 10.

A summary of the seepage test is provided in Table A.19.

Table A.19. Seepage test summary (Test 10)

G_s	e_i	e_{00}	e_s	e_f	k_s (m/s)	k_f (m/s)	σ'_s (kPa)	σ'_f (kPa)	Q_s (nl/s)	Q_f (nL/min)
2.31	4.213	4.134	3.32	2.05	1.01E-08	4.54E-12	0.232	30	50	3000

The parameters estimated by Microsoft Excel's Solver program are presented in Table A.20.

Table A.20. Model Parameters (Test 10)

A	B	Z	C	D
2.959	-0.114	0.0435	5.00E-17	16.053

Figure A.37 shows the observed time settlement curve for the seepage-induced consolidation test.

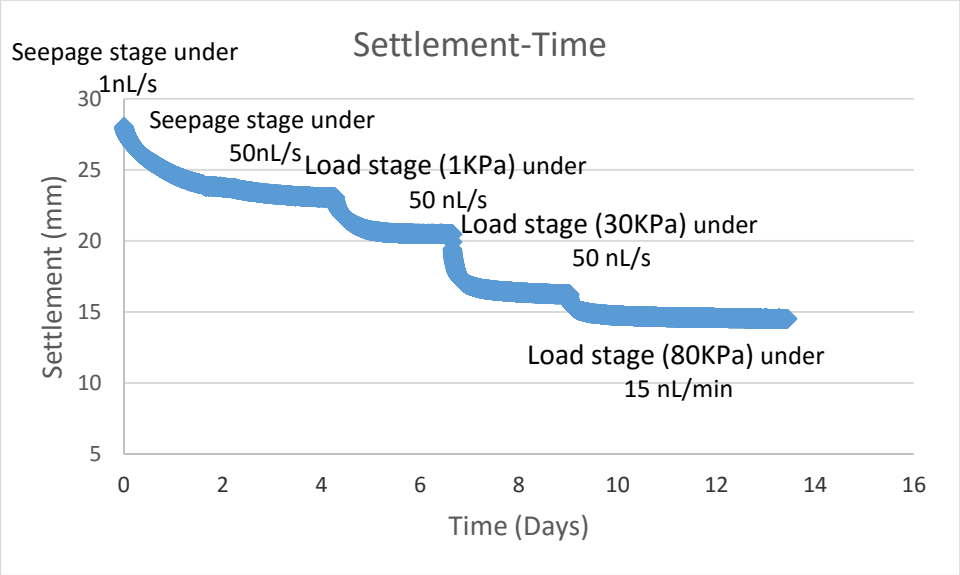

Figure A.37. Observed Time-Settlement curve (Test 10)

The compressibility curve is presented in Figure A.38.

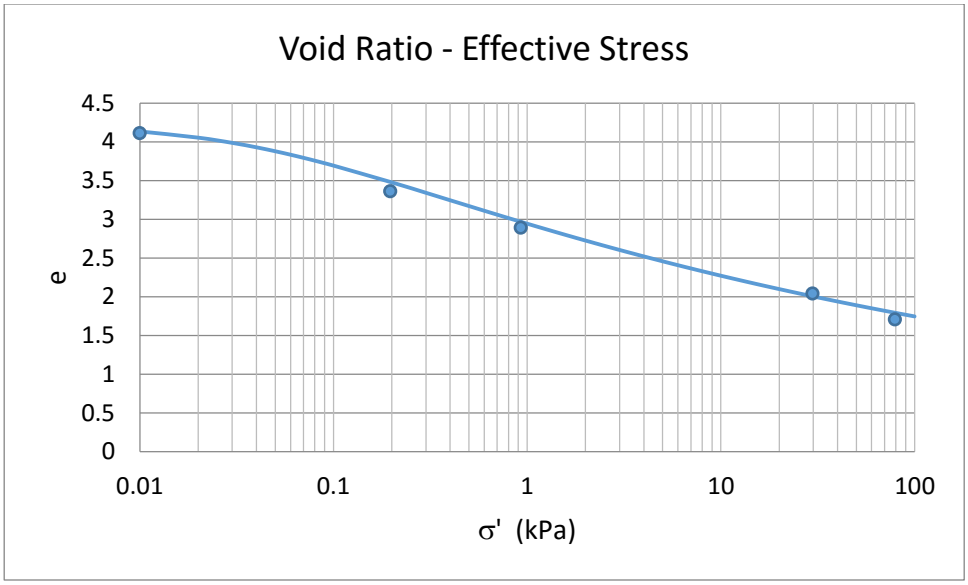

Figure A.38. Compressibility Curve (Test 10)

The compressibility equation used to find the numerical solution is:

$$e = 2.959(\sigma' + 0.0435)^{-0.114}$$

The permeability curve is presented in Figure A.39.

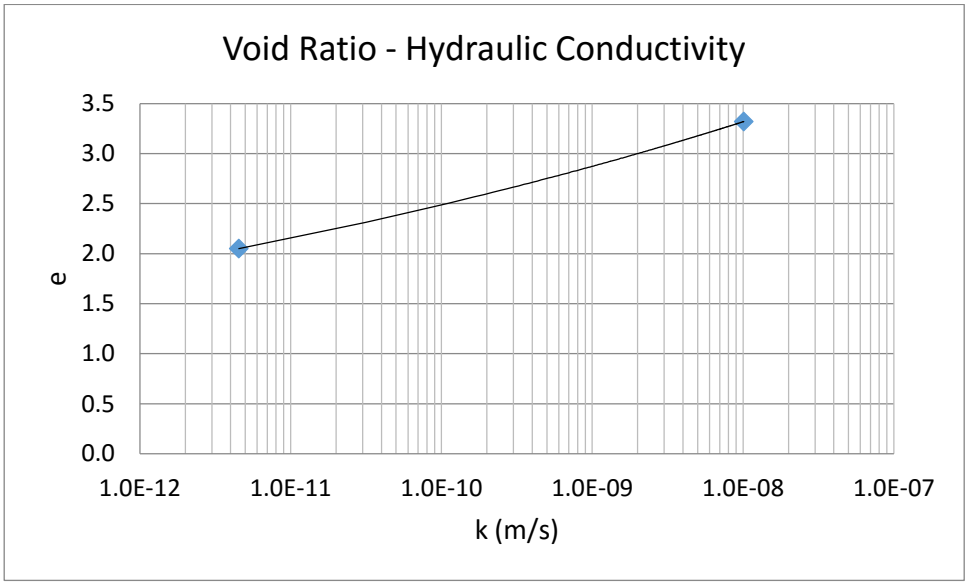

Figure A.39. Permeability Curve (Test 10)

The permeability equation, with respect to the void ratio, is:

$$K\ (\text{m/s}) = 5\text{E-}17\ e^{16.053}$$

Running CONDES0 to simulate the obtained model parameters with the observed testing data produces the results in Figure A.40.

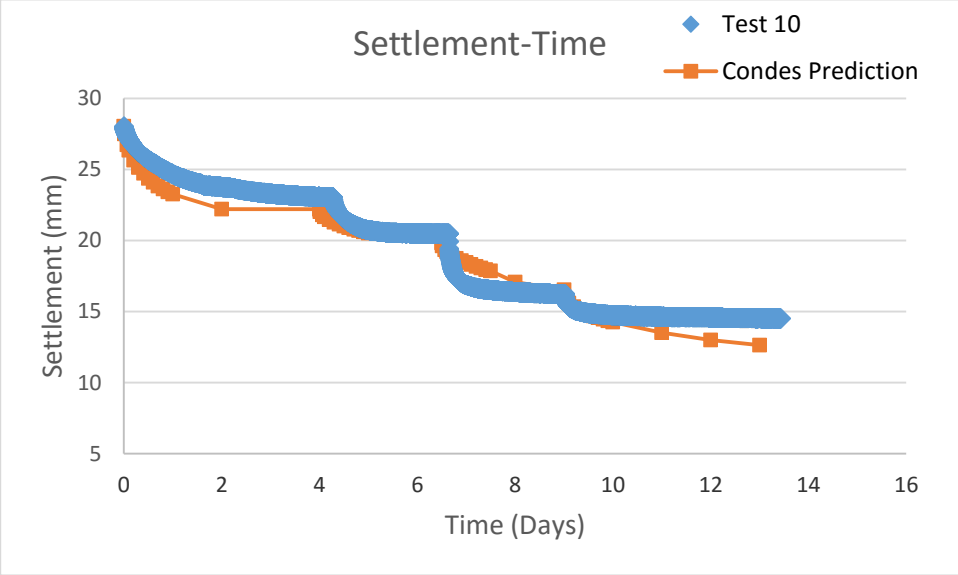

Figure A.40. Numerical Simulation (Test 10)

Test 11.

A summary of the seepage test is provided in Table A.21.

Table A.21. Seepage test summary (Test 11)

G_s	e_i	e_{00}	e_s	e_f	k_s (m/s)	k_f (m/s)	σ'_s (kPa)	σ'_f (kPa)	Q_s (nl/s)	Q_f (nL/min)
2.81	5.496	4.319	3.2	1.71	6.21E-11	5.91E-12	0.23	10	50	15

The parameters estimated by Microsoft Excel's Solver program are presented in Table A.22.

Table A.22. Model Parameters (Test 11)

A	B	Z	C	D
2.757	-0.773	0.485	4.00E-12	4.8829

Figure A.41 shows the observed time settlement curve for the seepage-induced consolidation test.

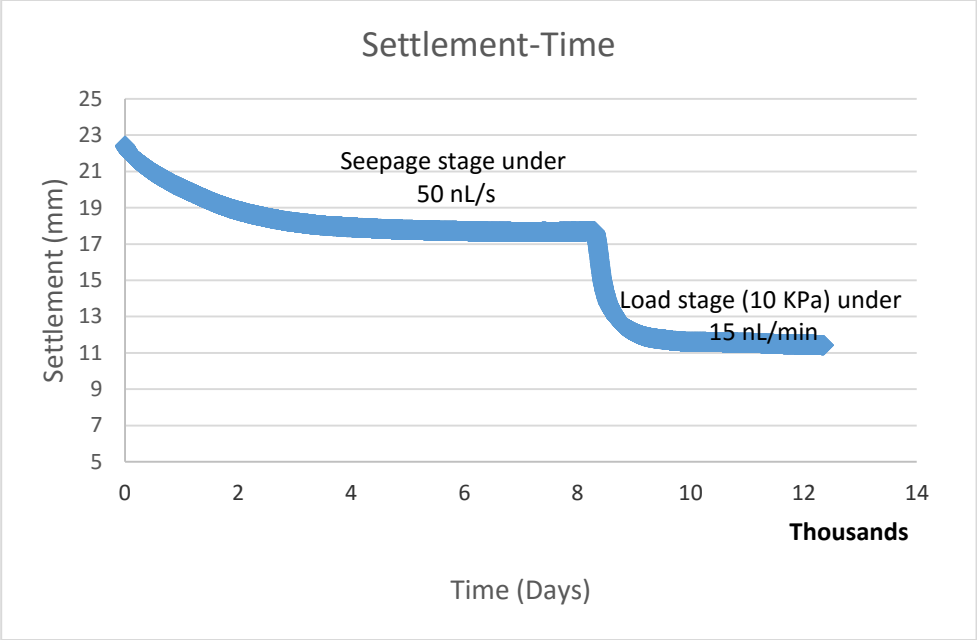

Figure A.41. Observed Time-Settlement curve (Test 11)

The compressibility curve is presented in Figure A.42.

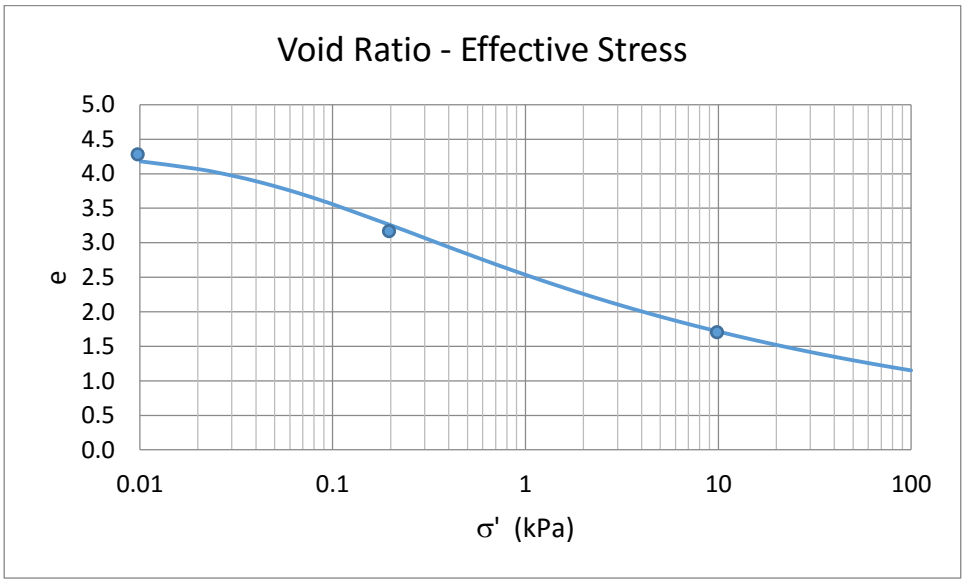

Figure A.42. Compressibility Curve (Test 11)

The compressibility equation used to find the numerical solution is:

$$e = 2.557(\sigma' + 0.0485)^{-0.173}$$

The permeability curve is presented in Figure A.43.

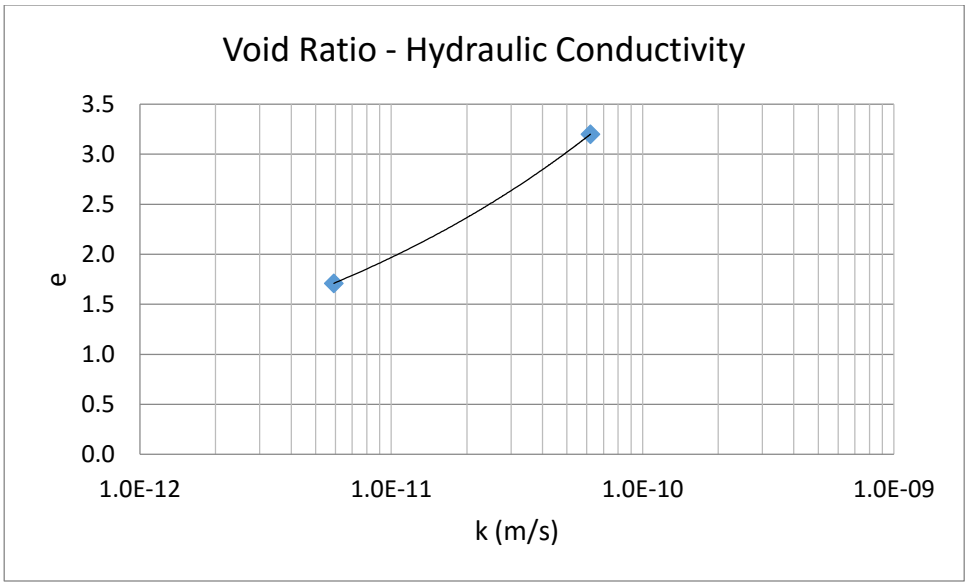

Figure A.43. Permeability Curve (Test 11)

The permeability equation, with respect to the void ratio, is:

$$K\ (\text{m/s}) = 4\text{E-}12\ e^{4.882}$$

Running CONDES0 to simulate the obtained model parameters with the observed testing data produces the results in Figure A.44.

Figure A.44. Numerical Simulation (Test 11)

Appendix B

The results of a statistical analysis of the proposed equations for consolidation model parameter estimation based on index properties are presented herein. The first section is devoted to the compressibility relationship, and the second part is devoted to the permeability relationship. Each graph is supported by statistical data for the R^2 value calculation.

If the test data set has n values marked $y_1,\ldots, y_n$, and the modeled data for each of the y values are $f_1,\ldots, f_n$, then:

The average of the test data is:

$$\bar{y} = \frac{1}{n}\sum_{1}^{n} y_i$$

The total sum of squares or SS_{TOT}, which is proportonal to the variance of the data, is:

$$SS_{TOT} = \sum_{1}^{n} (y_i - \bar{y})^2$$

The residual sum of squares is:

$$SS_{res} = \sum_{1}^{n} (y_i - f_i)^2$$

And R^2 is:

$$R^2 = 1 - \frac{SS_{res}}{SS_{TOT}}$$

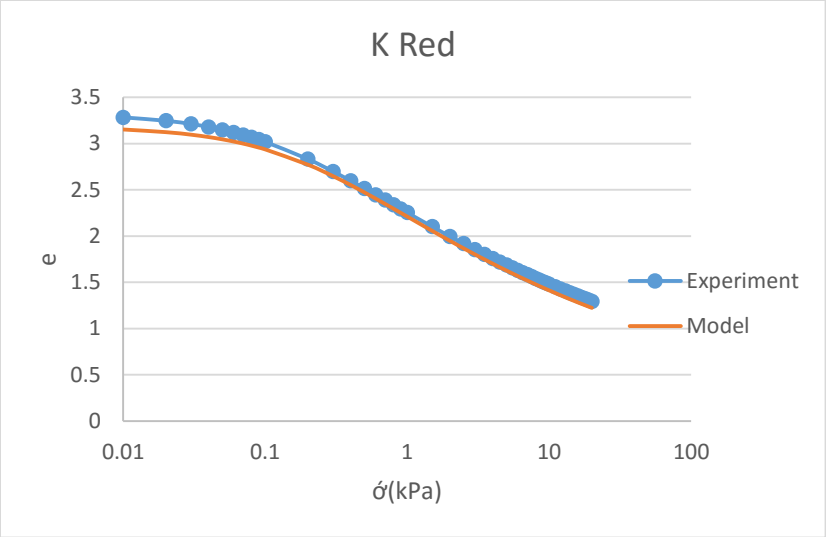

Figure B.1. Comparison between model-estimated and test results for proposed compressibility equation (Red Kaolinite Clay)

Table B.1. Statistical Analysis of proposed equations for Red Kaolinite Clay

Test Data Average	SS res	SS $_{TOT}$	R^2
2.082	0.2378	21.564	0.989

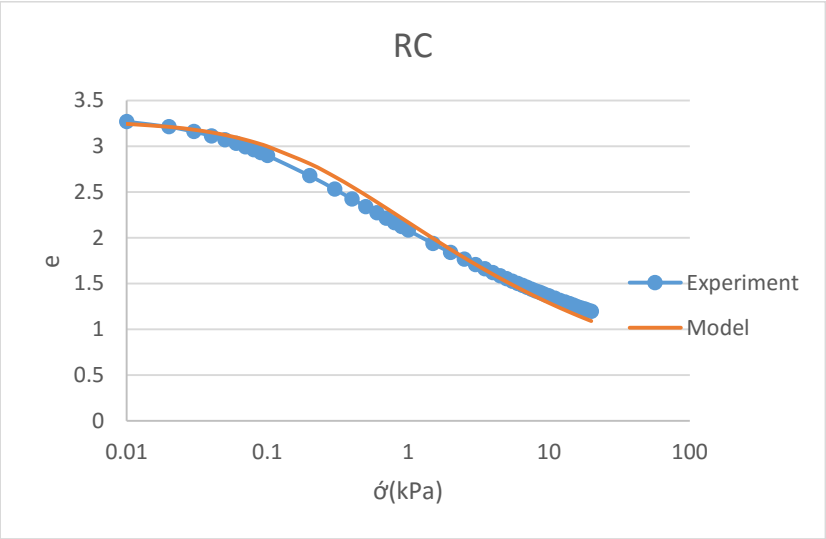

Figure B.2. Comparison between model-estimated and test results for proposed compressibility equation (Rhassoul Clay

Table B.2. Statistical Analysis of proposed equations for Rhassoul Clay

Test Data Average	SS res	SS $_{TOT}$	R^2
1.9579	0.2934	22.12	0.9867

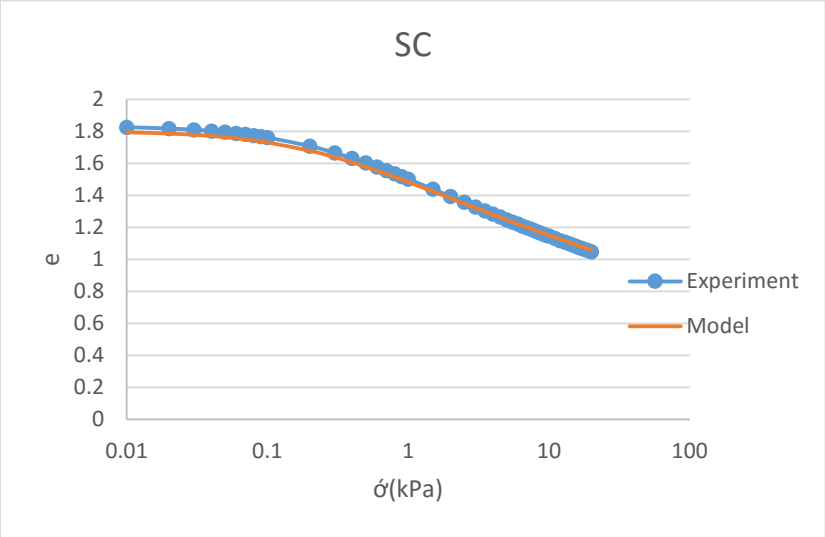

Figure B.3. Comparison between model-estimated and test results for proposed compressibility equation (Sea Clay)

Table B.3. Statistical Analysis of proposed equations for Sea Clay

Test Data Average	SS res	SS $_{TOT}$	R^2
1.3946	0.0163	3.4347	0.9953

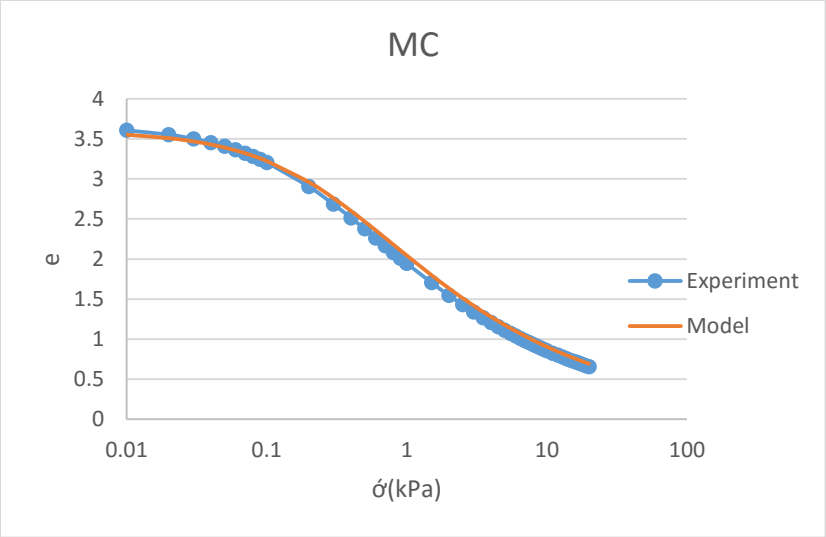

Figure B.4. Comparison between model-estimated and test results for proposed compressibility equation (Moroccan Clay)

Table B.4. Statistical Analysis of proposed equations for Moroccan Clay

Test Data Average	SS res	SS $_{TOT}$	R^2
1.7546	0.1792	49.507	0.9964

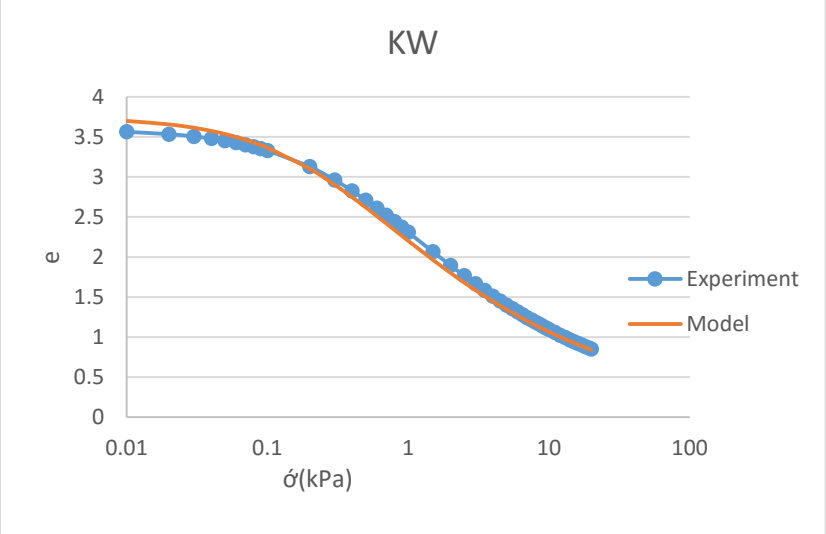

Figure B.5. Comparison between model-estimated and test results for proposed compressibility equation (White Kaolinite Clay)

Table B.5. Statistical Analysis of proposed equations for White Kaolinite Clay

Test Data Average	SS res	SS $_{TOT}$	R^2
1.9823	0.2142	44.123	0.9951

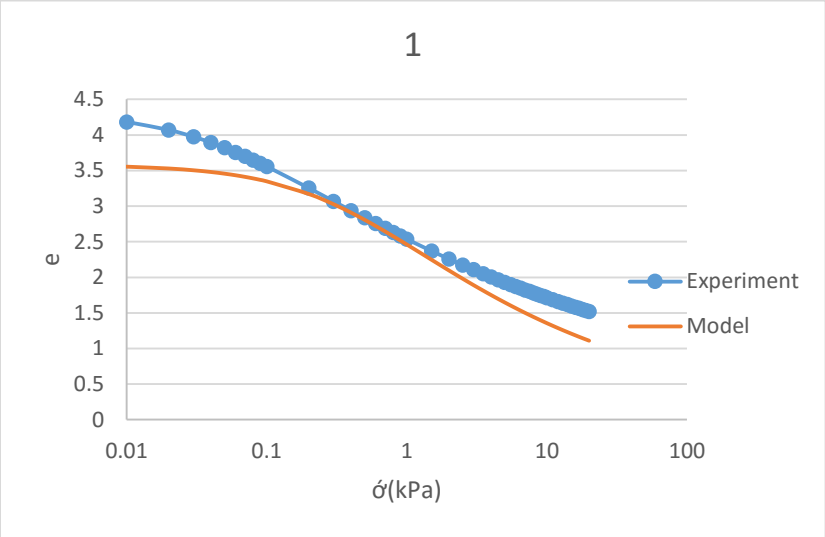

Figure B.6.. Comparison between model-estimated and test results for proposed compressibility equation (Test 1)

Table B.6. Statistical Analysis of proposed equations for Test 1

Test Data Average	SS res	SS_{TOT}	R^2
2.4326	4.6566	33.49	0.861

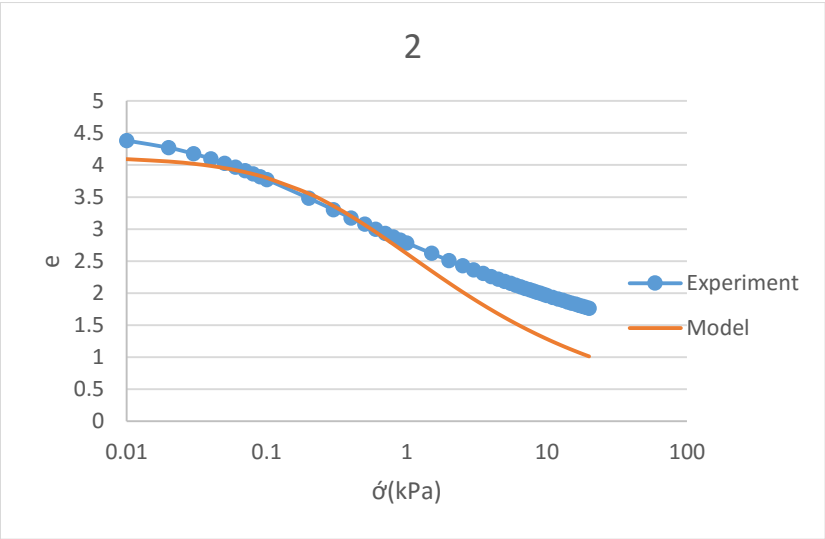

Figure B.7. Comparison between model-estimated and test results for proposed compressibility equation (Test 2)

Table B.7. Statistical Analysis of proposed equations for Test 2

Test Data Average	SS res	SS $_{TOT}$	R^2
2.6713	11.361	32.223	0.6474

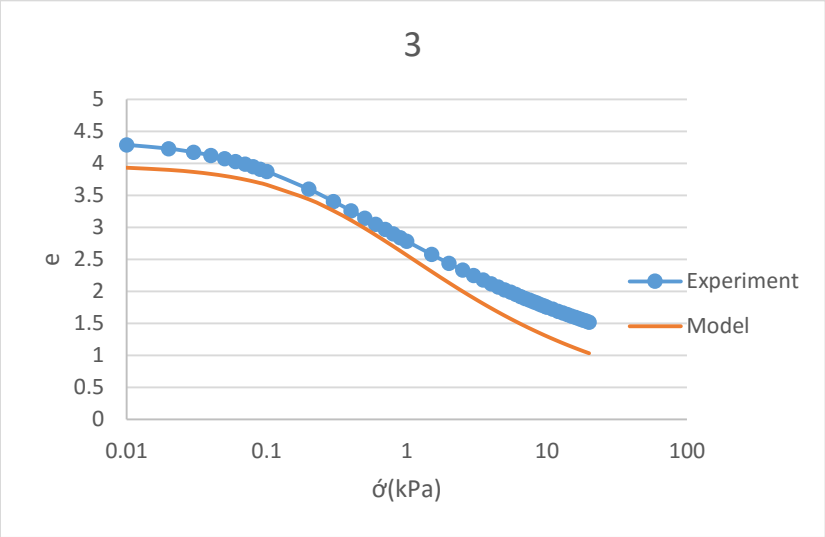

Figure B.8. Comparison between model-estimated and test results for proposed compressibility equation (Test 3)

Table B.8. Statistical Analysis of proposed equations for Test 3

Test Data Average	SS res	SS $_{TOT}$	R^2
2.5813	6.2762	41.034	0.847

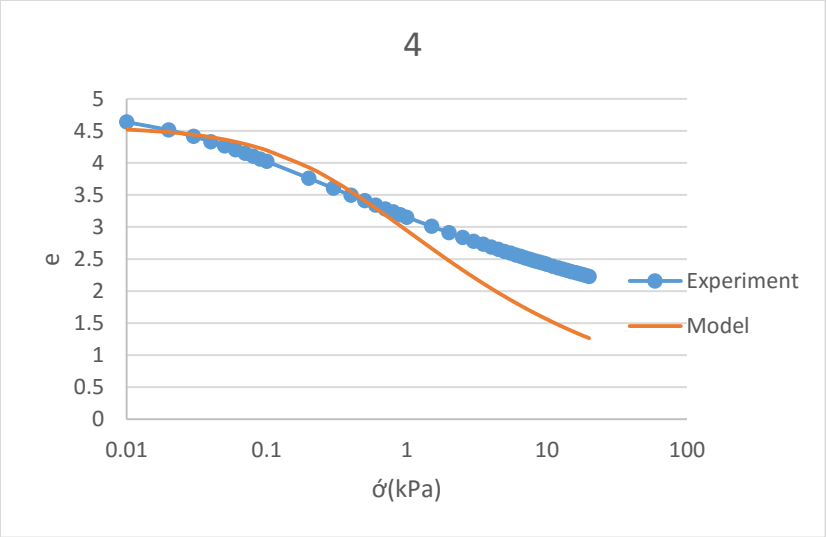

Figure B.9. Comparison between model-estimated and test results for proposed compressibility equation (Test 4)

Table B.9. Statistical Analysis of proposed equations for Test 4

Test Data Average	SS res	SS $_{TOT}$	R^2
3.0505	17.908	26.103	0.3139

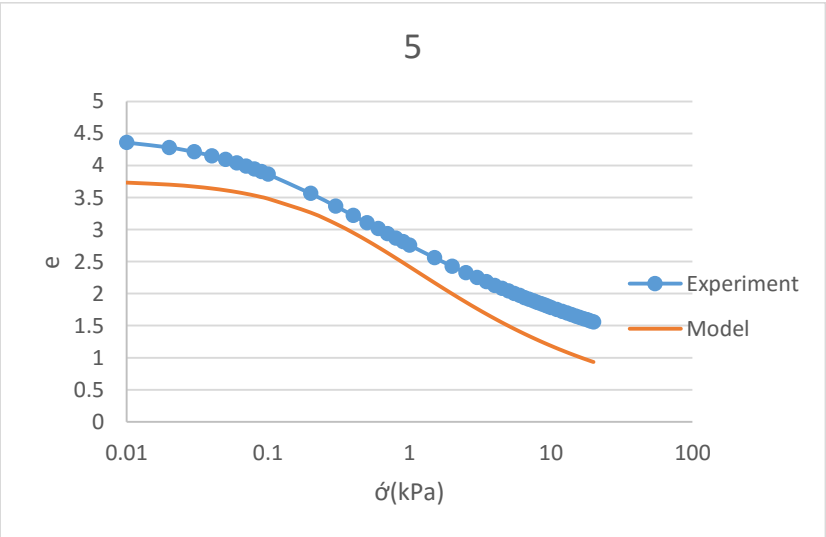

Figure B.10. Comparison between model-estimated and test results for proposed compressibility equation (Test 5)

Table B.10. Statistical Analysis of proposed equations for Test 5

Test Data Average	SS res	SS $_{TOT}$	R^2
2.5905	12.219	40.403	0.6976

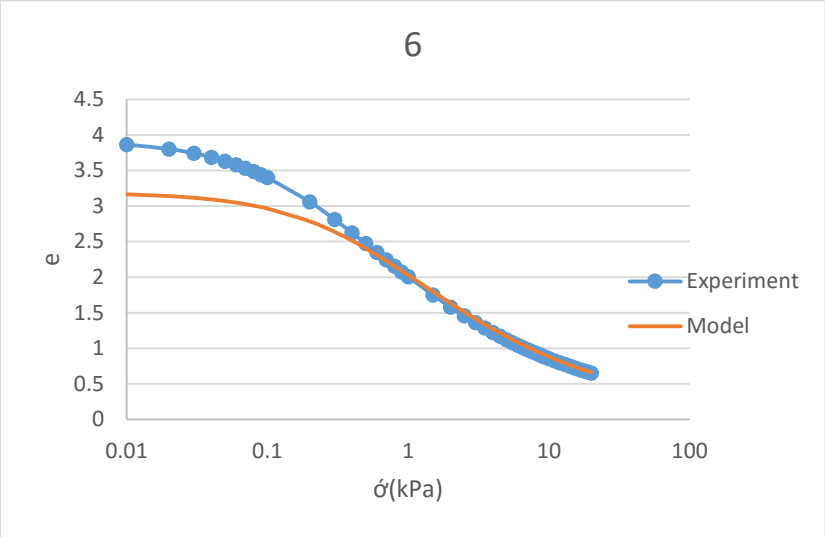

Figure B.11. Comparison between model-estimated and test results for proposed compressibility equation (Test 6)

Table B.11. Statistical Analysis of proposed equations for Test 6

Test Data Average	SS res	SS $_{TOT}$	R^2
1.825	3.3214	58.147	0.9429

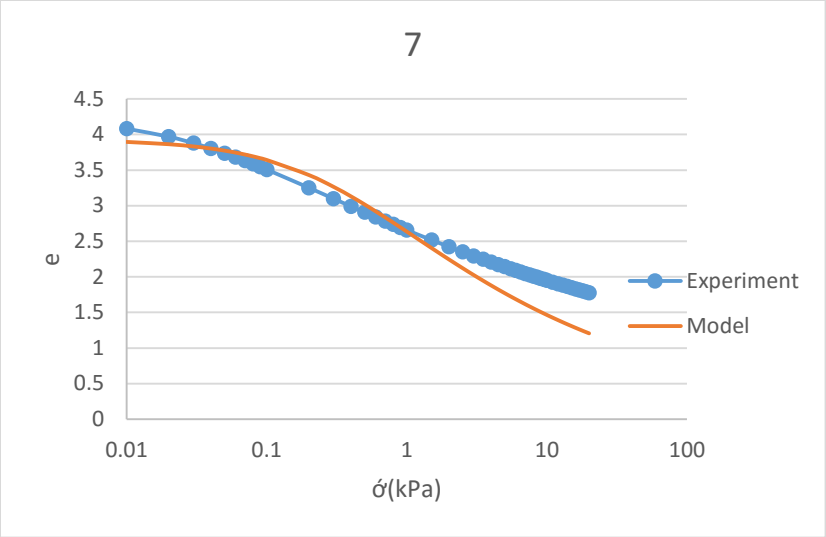

Figure B.12. Comparison between model-estimated and test results for proposed compressibility equation (Test 7)

Table B.12. Statistical Analysis of proposed equations for Test 7

Test Data Average	SS res	SS $_{TOT}$	R^2
2.562	5.7255	24.299	0.7644

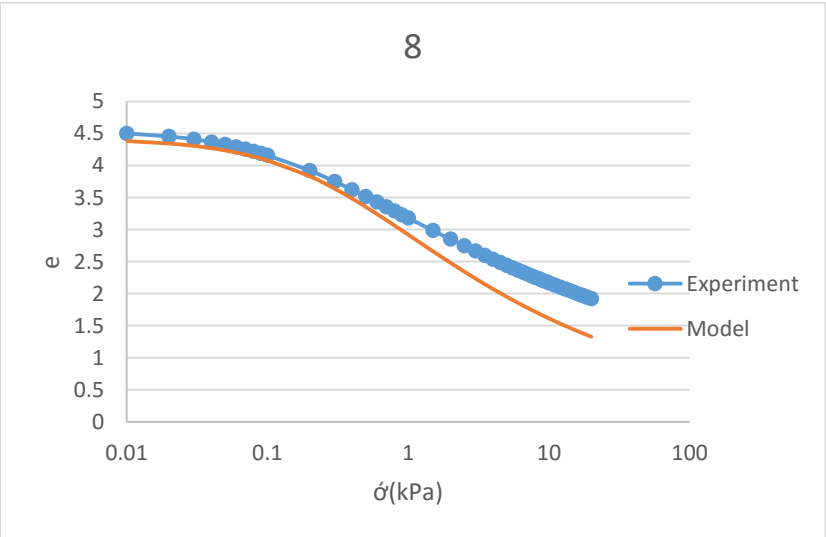

Figure B.13. Comparison between model-estimated and test results for proposed compressibility equation (Test 8)

Table B.13. Statistical Analysis of proposed equations for Test 8

Test Data Average	SS res	SS $_{TOT}$	R^2
2.9507	8.0777	36.115	0.7763

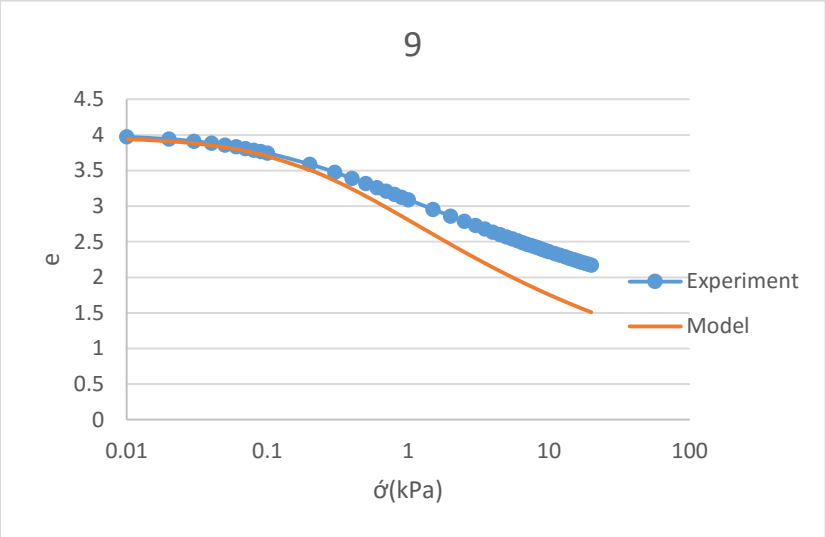

Figure B.14. Comparison between model-estimated and test results for proposed compressibility equation (Test 9)

Table B.14. Statistical Analysis of proposed equations for Test 9

Test Data Average	SS res	SS $_{TOT}$	R^2
2.9123	9.5529	17.525	0.4549

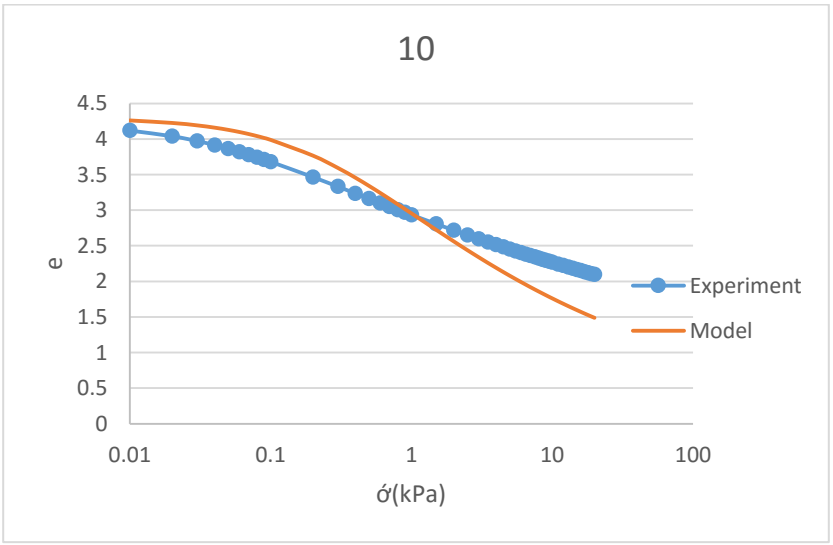

Figure B.15.Comparison between model-estimated and test results for proposed compressibility equation (Test 10)

Table B.15. Statistical Analysis of proposed equations for Test 10

Test Data Average	SS res	SS $_{TOT}$	R^2
2.8237	6.9036	19.458	0.6452

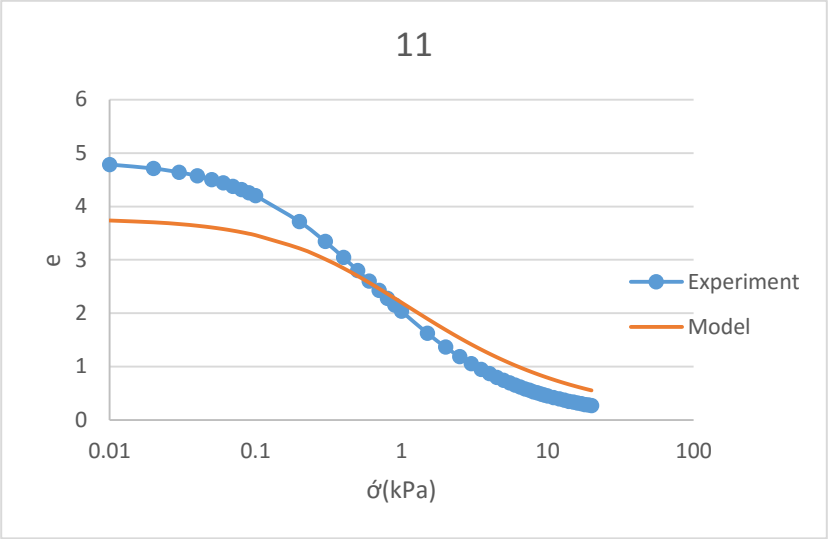

Figure B.16. Comparison between model-estimated and test results for proposed compressibility equation (Test 11)

Table B.16. Statistical Analysis of proposed equations for Test 11

Test Data Average	SS res	SS $_{TOT}$	R^2
1.842	11.656	124.22	0.9062

References

Abu-Hejleh, A. N., & Znidarcic, D. (1992). Consolidation Characteristics Determination for Phosphatic Clays. *Publication No. 02-084-104*. Boulder, University of Colorado.

Abu-Hejleh, A. N., & Znidarcic, D. (1994). Estimation of the Consolidation Constitutive Relations. *Computer Mehtods and Advances in Geomehcanics*, 499-504.

Abu-Hejleh, A. N., & Znidarcic, D. (1995). Desiccation Theory for Soft Cohesive Soils. *Journal of Geotechnical Engineering*, 493-502.

Aydilek, A. H., Edil, T. B., & Fox, P. J. (1999). Consolidation Characteristics of Wastewater Sludge. *Geotechnicas of High Water Content Materials, ASTM*, 309-323.

Berilgen, S. A., Berilgen, M. M., & Ozaydin, I. K. (2006). Compression and Permeability Relationships in High Water Content Clays. *Applied Clay Science*, Vol 31, 249-261.

Berry, P. L., & Poskitt, T. J. (1972). The Consolidation of Peat. *Geotechnique*, Vol 22, 27-52.

Bonin, M., Nuth, M., Dagenais, A., & Cabral, A. (2014). Experimental Study and Numerical Reproduction of Self-Weight Consolidation Behavior of Thickened Tailings. *Journal of Geotechnical and Geoenvironmental Engineering*, Vol 140.

Cargill, K. W. (1986). *The Large Strain Consolidation Controlled Rate of Strain (LSCRS) Device for Consolidation Testing of Soft Fine-grained Soils.* Vicksburg, Mississippi: U.S. Army Engineer Waterways Experiment Staion Report.

Carrier, W. D., Bromwell, L. G., & Somogyi, F. (1983). Design Capacity of Slurried Mineral Waste Ponds. *Journal of Geotechnical Eningeering*, Vol 109, 699-716.

Erten, M. B., Gilbert, R. B., El-Mohtar, C. S., & Reible, D. (2011). Developement of Laboratory Procedure to Evaluate the Consolidation Potential of Soft Contaminated Sediments. *Geotechnical Testing Journal*, Vol 34, 1-9.

Estepho, M. (2014, January). Seepage Induces Consolidation Test; Characterization of Mature Fine Tailings. *Master Thesis*. Univeristy of British Columbia.

Gibson, R. E., England, G. L., & Hussey, M. J. (1967). The Theory of One-dimensional Consolidation of Saturated Clays, I. Finite Nonlinear Consolidation of Thin Homogenous Layers. *Geotechnique*, Vol 17, 261-273.

Gjerapic, G., & Znidarcic, D. (2007). A Mass-conservative Numerical Solution for Finite-strain Conoslidation During Continous Soil Deposition. *Proceeding Geo-Denver: Computer Application in Geotechnical Engineering*, (pp. 1-10). Reston, VA.

Huerta, A., Kriegsmann, G. A., & Krizek, R. J. (1988). Permeability and Compressibility of Slurries from Seepage-induced Consolidation. *Journal of Geotechnical Engineering*, Vol 114, 614-627.

Imai, G. (1979). Developement of a New Consolidation Test Procedure Using Seepage Force. *Soils and Foundation*, 45-60.

Jeeravipoolvarn, S., Chalaturnyk, R. J., & Scott, J. D. (2009). Sedimentation-Consolidation Modeling with an Interaction Coefficient. *Computer and Geotechnic*, 751-761.

Koppula, S. D., & Morgenstern, N. R. (1982). On the Consolidation of Sedimenting Clays. *Canadian Geotechinal Journal*, Vol 19, 260-268.

Luca, B. (2002). *Determination of Consolidation Parameters of a Sludge Using the Seepage-induced Consolidation Test.* Retrieved from Innovation in Environmental and Energy Technology: www.mipvlaanderen.be/file.aspx?id=135

Maher, A., Douglas, W. S., Jafari, F., & Pecchioli, J. (2013). *The Processing and Beneficial Use of Fine-grained Dredged Material.* Piscataway, NJ: Center for Advanced Infrastructure and Transportation.

McVay, M., Townsend, F., & Bloomquist, D. (1986). Quiescent Consolidation of Phosphatic Waste Clays. *Journal of Geotechnical Engineering, ASCE*, Vol 117, 162-169.

Mesri, G., & Rokhsar, A. (1974). Theory of Consolidation for Clays. *Journal of Geotechnical Engineering Division, ASCE*, 889-904.

Mikasa, M. (1965). The Consolidation of Soft Clay, A New Consolidation Theory and Its Application. *Japanese Society of Civil Engineers*, 21-26.

Mikasa, M. (1982). The Consolidation of Soft Clay - A New Cosnolidation Theory and Its Application. Tokyo, Japan: Kajima Institution Publishing Co.

Monte, J. L., & Krizek, R. (1967). One Dimensional Mathematical Model for Large-strain Consolidation. *Geotechnique*, Vol 26, 495-510.

Pane, V. (1981). *One-dimensional Finite Strain Consolidation.* Boulder, Colorado: Master Thesis, Department of Civil, Environmental, and Architectural Engineering, Univeristy of Colorado.

Pane, V., & Schiffman, R. L. (1981). A Comparison between Two Theories of Finite Strain Consolidation. *Soils and Foundations*, Vol 21, 81-84.

Pane, V., & Schiffman, R. L. (1997). The Permeability of Clay Suspensions. *Geotechnique*, Vol 4, 273-288.

Pedroni, L., & Aubertin, M. (2008). Evaluation of Sludge Consolidation from Hydraulic Gradient Tests Conducted in Large Size Columns. *GeoEdmonton*, (pp. 769-776). Edmonton, Canada.

Raymond, G. P. (1969). Consolidation of Deep Deposits of Homogenous Clay. *Geotechnique*, Vol 19, 478-494.

Scott, J. D., Dusseault, M. B., & Carrier, W. D. (n.d.). Large-scale Self-weight Consolidation Testing. *ASTM Special Technical Publication No.892*, 500-515.

Shrestha, P. L., Su, S. H., James, S., Shaller, P. J., Doroudian, M., Firstenberg, C. E., & Thompson, C. T. (2014). Conceptual Site Model for Newark Bay-Hydrodynamics and Sediment Transport. *Journal of Marine Sciences and Engineering*, Vol 2, 123-139.

Smith, R. E., & Wahls, H. E. (1969). Consolidation Under Constant Rates of Strain. *Journal of the Soil Mechanics and Foundations Division, ASCE*, Vol 95, 519-539.

Somogyi, F. (1979). Large Strain Consolidation of Fine-grained Slurries. *Canadian Society for Civil Engineering.* Winnipeg, Manitoba: Canada.

Somogyi, F., Keshian, B., & Bromwell, L. (1981). Consolidation Behavior of Impounded Slurries. *American Society of Civil Engineers Spirng Convention.* New York.

Sridharan, A., & Prakash, K. (2001). Consolidation and Permeability Behavior of Segregated and Homogeneous Sediments. *Geotechnical Testing Journal*, Vol 24, 109-120.

Terzaghi, K. (1923). Die berechnung der durchlassigkeitsziffer des tones aus dem verlauf der hydrodynamischen spannungserscheinungen. Akademie der Wissenschaften in Wien, Sitzungsberichte. *Mathematisch Naturwissenschaftliche Klasse*, 125-138.

Wissa, A. E., Christian, J. T., Davis, E. H., & Heiberg, S. (1971). Analysis of Consolidation at Constant Strain Rate. *Journal of the Soil Mechanics and Foundation Division, ASCE*, 1393-1413.

Znidarcic, D., & Liu, J. C. (1989). Consolidation Characteristics Determination for Dredges Materials. *Center for Dredging Studies* (pp. 45-65). College Station, Texas: Texas A&M University.

Znidarcic, D., & Schiffman, R. L. (1982). On Terzaghi's Concept of Consolidation. *Geotechnique*, Vol 32, 387-389.

Znidarcic, D., Miller, R., VanZyl, D., Fredlund, M., & Wells, S. (2011). Consolidation Testing of Oil Sand Fine Tailings. *Proceedings Tailing and Mine Waste.* Vancouver, British Columbia.